

Physiological Chemistry and Physics and Medical NMR Volume 41, 2011

Addresses of Chief Editor and Editorial College

Chief Editor

Gilbert N. Ling
P.O. Box 1452
Melville, New York 11747

Editorial College

O. D. Bonner
Department of Chemistry
University of South Carolina
Columbia, South Carolina 29208

Harris Busch
Department of Pharmacology
Baylor College of Medicine
Houston, Texas 77030

Ivan L. Cameron
Department of Anatomy
University of Texas Health Science Center
San Antonio, Texas 78284

Doriano Cavallini
Institute of Biological Chemistry
University of Rome
00185 Rome, Italy

James S. Clegg
Bodega Marine Laboratory
University of California
Bodega Bay, California 94923

George H. Czerlinski
Leibnitz Foundation Institute
P.O. Box 20091
Sedona, Arizona 86341-0091

W. Drost-Hansen
Laboratorium Drost
Williamsburg, Virginia 23188-9415

Ludwig Edelmann
Anatomie und Zellbiologie
Universitdt des Saarlandes
D-66421 Homburg (Saar), Germany

Carlton F. Hazlewood
Research Consultants International
P.O. Box 130282
The Woodlands, Texas 77393

Ferdinand Heinmets
Technology Incorporated
P.O. Box 790644
San Antonio, Texas 78279-0644

S.R. Kasturi
Tata Institute of Fundamental Research
Mumbai 400 005, India

Miklós Kellermayer
Department of Clinical Chemistry
University Medical School
Pécs, 7624 Hungary

Janos Ladik
Institute of Physics and Theoretical Chemistry
University of Erlangen-Nurnberg
D-8520 Erlangen
Germany

George M. Mrevlishvili
Department of Physics
Tbilisi State University
380028 Tbilisi
Republic of Georgia

Toshihiko Ubuka
Department of Clinical Nutrition
Kawasaki University of Medical Welfare
Kurashiki, Okayama, 701-0193, Japan

Denys Wheatley
BioMedES
Leggat House, Keithhall
Inverurie
Aberdeen AB51 OLX
United Kingdom

EDITORIAL AND BUSINESS OFFICE

Physiological Chemistry and Physics
and Medical NMR
P.O. Box 1452
Melville, New York 11747

Editor In Chief, Dr. Gilbert N. Ling
Managing Editor, Margaret M. Ochsenfeld

SCOPE: PCP provides a forum for the review and publication of reports of original research in a broad range of subjects in biophysics, biochemistry and cellular physiology. Reports of direct applications of basic knowledge to human studies are invited; examples would include the measurements of relaxation times as part of NMR imaging. Single experiments, conclusions based on inadequate statistics, purely speculative papers, and clinical case reports are not accepted.

POLICY: The pages of PCP are accessible to competing viewpoints, interpretations, theories and opinions. Debate is invited via Editorial Comments and Letters to the Editor. Criteria for evaluating submissions include soundness of the study and clarity of presentation, and papers are not rejected on the basis of interpretation or theory, however controversial. PCP believes that scientific issues should be settled by investigation and open debate, not by an appeal to anonymous authority.

PCP attempts to achieve a balance between freedom of expression and constructive peer review. All papers are refereed by reviewers who may remain anonymous, but the Chief Editors make all final decisions, and will handle appeals from authors who feel their papers are unfairly reviewed.

The Editors endeavor to make decisions regarding acceptance or rejection of manuscripts quickly, and have set self-imposed deadlines for doing so. Referees also are given deadlines.

TYPES OF PAPERS: *Regular papers* may be experimental or theoretical. *Short notes*, *Priority notes* and *Letters* in response to published papers are invited. *Reviews* are desired, but authors are urged to contact an Editor before sending a finished review manuscript. *Symposia* may be published as regular or supplemental issues.

SUBSCRIPTIONS: Price is US\$160.00 per volume in the United States and US\$170.00 outside the United States. *Physiological Chemistry and Physics and Medical NMR* is published annually, the volume numbered yearly. New subscriptions will start with the first issue of the volume in progress, unless the subscriber directs otherwise. Most back issues are available

Contributions appearing herein do not necessarily reflect views of the publisher, staff or Editorial College.

Instructions to Authors

SUBMISSIONS: An original and two copies of all material are requested. The original must be typewritten on one side only. Papers should be sent to Dr. Gilbert N. Ling, Editor, P.O. Box 1452, Melville, New York 11747 U.S.A. Manuscripts should be submitted only to this journal and not have been published in part or whole in another publication, except as short preliminary notes, abstracts, or as unpublished work in reviews or symposia. Be sure to keep a copy of your manuscript.

NOTE: Referees will be instructed to destroy their copies of the manuscript after reviewing them. We will return only the original manuscript to you for revision or if rejected.

MANUSCRIPTS: All material should be typed double-spaced with margins at least one inch wide and pages numbered consecutively beginning with the title page. In addition to a paper copy, send an IBM- or Macintosh-compatible file on a CD, in Word or Wordperfect. *Title Page* should include title (of at most 100 characters and spaces), full names of authors as you wish them to be published, names and cities of institutional affiliation(s) of authors and of institution(s) where the studies were performed, and name, full address, telephone number, fax number and e-mail address of the person to whom correspondence, proofs, and reprint requests are to be sent. Four to six *key words* should be listed on the title page. These words will assist indexers. Also, at bottom of title page include a short running title of 40 characters or less.

Abstract should be concise and no longer than 225 words. *Body* may or may not be divided into Introduction, Materials and Methods, Results and Discussion, depending on the length and nature of the paper. Introductory remarks should indicate clearly the significance of the work presented. *References* may be indicated in the text and listed in the reference list in whatever style the author prefers, but we prefer that titles of articles be omitted.

TABLES: Tables should be typewritten on separate sheets and identified by roman numerals (eg. Table III) and titles. Table notes should be keyed by superscript italic lower-case letters (eg. ^aControl). The approximate locations of *tables* and *figures* should be indicated in the margins of the manuscript.

ILLUSTRATIONS: Original artwork or glossy photostatic prints, together with two photocopies (like Xerox copies) should be provided. Each illustration should be numbered on the back in pencil, along with the authors' names. It is preferred that line drawings be made on paper that is not larger than 8 1/2 by 13 inches, and that the drawing be its intended size in the printed paper. Most figures will occupy 1/2 to full column, that is 5 inches wide. Lines and lettering should be thick enough to allow reduction. A drawing of overall dimension of 8 by 10 inches that will be reduced to 1/4 of its original size should be lettered with 18-point (capitals 6 mm high, lower-case 4 mm high) or larger lettering. Glossy photostatic prints are acceptable, and should be attached firmly to a sheet of paper the same size as the manuscript. Postacceptance: If possible send figures as an image file using TIFF or JPEG formatting scanned at a resolution of 600 dpi.

PHOTOGRAPHS: High-quality black and white glossy prints should be provided in triplicate, and may be provided as one print plus two photocopies if the photocopies are sufficiently clear to portray the original to referees. Photographs should be attached firmly to a sheet of paper the same size as the manuscript. Photographs that have been scanned and stored as a TIFF file with a resolution of 300 dpi may also be submitted.

REFEREES: Two anonymous referees will be sought for each paper. Authors are encouraged to suggest names and addresses of suitable referees. Referees will be given deadlines for mailing manuscripts back or phoning reviews in, and will be invited to provide editorial statements or Letters that deal with issues raised by submitted papers.

REPRINTS: An order form is enclosed with proofs sent to authors.

PAGE CHARGES: Page charge is \$20.00 per published page. It may be waived in the case of severe international exchange difficulties. An additional charge of \$15.00 will be levied for photographs that require screening (eg., E.M's, chromatograms, scans).

The Possible Role of Cranio-Cervical Trauma and Abnormal CSF Hydrodynamics in the Genesis of Multiple Sclerosis

Raymond V. Damadian and David Chu

*FONAR Corporation
110 Marcus Drive, Melville, NY 11747
E-mail: rvdamadian@fonar.com*

Abstract: UPRIGHT® Multi-Position™ MR scanning has uncovered a key set of new observations regarding Multiple Sclerosis (MS), which observations are likely to provide a new understanding of the origin of MS. The new findings may also lead to new forms of treatment for MS. The UPRIGHT® MRI has demonstrated pronounced anatomic pathology of the cervical spine in five of the MS patients studied and definitive cervical pathology in the other three. The pathology was the result of prior head and neck trauma. All eight MS patients entered the study on a first come first serve basis without priority, and all but one were found to have a history of serious prior cervical trauma which resulted in significant cervical pathology. The cervical pathology was visualized by UPRIGHT® MRI. Upright cerebrospinal fluid (CSF) cinematography and quantitative measurements of CSF velocity, CSF flow and CSF pressure gradients in the upright patient revealed that significant obstructions to CSF flow were present in all MS patients. The obstructions are believed to be responsible for CSF “leakages” of CSF from the ventricles into the surrounding brain parenchyma which “leakages” can be the source of the MS lesions in the brain that give rise to MS symptomatology. The CSF flow obstructions are believed to result in increases in intracranial pressure (ICP) that generate “leakages” of the CSF into the surrounding brain parenchyma. In all but one MS patient, anatomic pathologies were found to be more severe in the upright position than in the recumbent position. Similarly, CSF flow abnormalities were found to be more severe in the upright position than in the recumbent position in all but one MS patient. Images of the MS patient anatomic pathologies and CSF flow abnormalities are provided with comparison images from normal examinees in Figures 1–16.

KEY WORDS: Multiple Sclerosis, Cranio-Cervical Trauma, CSF Hydrodynamics, CSF Leaks, Intracranial Pressure, CSF Peak Velocity, CSF Pressure Gradient, CSF Flow

THE ADVENT of MRI and its unique abilities to generate the tissue contrasts needed to see detail in the body's soft tissues was an important step forward in medical imaging. A particularly important example was the ability to visualize the plaque lesions of Multiple Sclerosis (1). Traditionally the symptom-generating lesions in the brain and spinal cord of Multiple Sclerosis (MS) patients are ascribed to tissue specific autoimmune interactions. These are believed to generate the parenchymal lesions of MS. More recently the advent of phase coded MR imaging has made it possible to visualize and quantify the dynamic *flow** of the cerebrospinal fluid (CSF) within the cranial vault and spinal canal.

The present inquiry originated in the course of performing UPRIGHT® MR images on a patient (patient #1, Figure 1a) with an established diagnosis of MS. It was noted that one of the MS brain lesions conspicuously appeared to be arising directly from the CSF within the lateral ventricle (Figure 1a arrow #1). An MS lesion, appearing to arise from the ventricular CSF, brought to our attention the unexplained tendency for MS lesions to be *peri-ventricular* in their distribution (2) (Figure I, Figure II). Considered conjointly, an MS lesion appearing to arise directly from ventricular CSF (Figure 1a) and the tendency of MS lesions to be *peri-ventricular* in their distribution (Figure I, Figure II) engendered the question whether abnormal CSF hydrodynamics (e.g., elevated intracranial pressure [ICP] or abnormal flow dynamics) was playing a role in the genesis of MS lesions. To address the question, eight patients with an established diagnosis of MS and seven normal examinees were studied in the FONAR UPRIGHT® Multi-Position™ MRI.

Materials and Methods

The first eight MS patients who volunteered for the study were scanned. There was no selection among MS patients. They were all scanned in the order in which they volunteered.

MRI scans were performed on a 0.6 T UPRIGHT® scanner (FONAR Corporation, Melville, NY) with a quadrature head-neck combination coil. The patient bed can be rotated to any angle between the horizontal and vertical position in the space between the two poles of the upright magnet.

Regular clinical anatomical scans of the head and neck were acquired. Ciné phase contrast scans of CSF flow were imaged using a phase contrast RF-spoiled gradient echo sequence with TR = 19-22 ms, TE = 9-12 ms, slice thickness = 8 mm, flip angle = 20-25°, matrix = 256x128 zero filled to 256x256, and NEX = 2. Data acquisition was retrospectively gated using ECG or pulse oximeter covering the entire cardiac cycle.

Thirty-two (32) uniformly spaced time frames were obtained by linear interpolation in post-processing.

To visualize the overall CSF flow pattern, a single slice of FOV = 26 cm was imaged in the midline sagittal plane. In order to quantify the CSF *flow*, an axial slice of FOV = 16 cm at the mid C-2 level and perpendicular to the spinal canal was imaged (velocity encoding along the slice-select direction, $v_{enc} = 3-11$ cm/s).

Quantification of CSF *flow* was accomplished by manually drawing the Region of Interest (ROI) around the spinal canal and spinal cord in the axial mid C-2 phase contrast

* flow in the absence of italics is generic, the presence of italics specifies cc/sec

scan. Phase offset was corrected by requiring the spinal cord to have zero net phase change over the whole cardiac cycle.

MR examinations of MS patients (Figures 1–8) and normal examinees (Figures 9-15) in the study were performed in both the *upright* and *recumbent* positions using the FONAR UPRIGHT® Multi-Position™ MRI. Examinees were deemed normal if they exhibited uninterrupted dorsal and ventral CSF flow on *upright* sagittal CSF flow images (e.g., Figure 15c). MS patients #7 and #8 could not be scanned recumbent. Lower limb paralysis prevented MS patient #7. Severe vertigo and emesis in the recumbent position prevented MS patient #8. CSF cinematography (ciné) was obtained both in the sagittal and axial planes. Quantitative MR measurements of CSF *flow* (cc/sec) through the spinal canal annulus obtained from axial MR images were calculated from the phase coded CSF *flow* image data. The *flow* data were obtained from axial images taken at the mid C-2 level, unless specified otherwise. The CSF velocity (cm/sec) was measured as the average annular proton velocity for each of the 32 imaging annuli acquired throughout the cardiac cycle. The peak CSF velocity was determined as the highest proton annular velocity measurement obtained for each phase (systole and diastole) of the cardiac cycle. The pressure gradient was derived from the measured CSF velocity data using the Navier-Stokes equation, with negligible contribution from the viscous term. There were three notable findings.

Results

CSF Flow Imaging and Quantification in Multiple Sclerosis Patients

The *first*, and partially expected result stemming from the MR images of MS patient #1 (Figure 1a) and the known *peri-ventricular distribution* of MS lesions (Figure I, II), was the finding of abnormal CSF flows in all eight MS patients (Figures 1–8, Table 2A, col. 10). The abnormal CSF flows corresponded with the cranio-cervical structural abnormalities found on the patients' MR images. The *second* finding was a history of severe cervical trauma prior to the patient's MS diagnosis in six of the eight MS patients and a significant possibility of cervical trauma in a seventh patient (Table 1, MS patient #8). The *third* finding was the discovery that CSF **inflow** (cc/sec) and **inflow** velocity (cm/sec) in the *upright* position is about half (53–56%) (Table 3) of what it was in the *recumbent* position in both the MS patients and normal examinees. Alperin *et al.* have shown that the average (oscillatory) CSF volume (cc) in the upright position was less than half the oscillatory volume (cc) in the supine position, but neither a reduction of CSF **inflow** velocity (cm/sec) nor of CSF **inflow** (cc/sec) in the upright position have been previously reported (3).

The first important observation of this study of eight MS patients was that *every MS patient* exhibited *obstructions to their CSF flow* when examined by phase coded CSF cinematography (ciné) in the *upright* position (Table 2A, col. 10 & 13). *All MS patients* exhibited CSF flow abnormalities that were manifest on MR cinematography as interruptions to flow or outright flow obstructions somewhere in the cervical spinal canal, depending on the location and extent of their cervical spine pathology (Table 2A, col. 10, 11 & 13). Normal examinees did not display these flow obstructions (Table 2B, col. 10 & 11).

TABLE 1. Clinical History and Symptomatology of MS Patients

1	2	3	
Patient #	History of Cranio-Cervical Trauma	Nature of Trauma	
Patient #1 (MVA #1)	Motor vehicle accident 1978 — Rear-ended by pickup truck. Patient sustained whiplash. Wore neck brace for 2 months thereafter. Passenger seat occupant hospitalized.	Whiplash injury. Cervical collar worn 2 months after accident.	
Patient #2	(1992) While patient was standing on top of a 20-ft. extension ladder repairing his home rooftop, the extension link decoupled. Ladder extension section slid groundward with patient on board. 16-oz. hammer fell 3 ft. and landed on top of patient’s head. Ladder extension section then further slid to ground. Patient fell to ground hitting back of head. Patient semi-conscious and dizzy after ground impact.	Hammer hit to top of patient’s head. Ladder fell backward when extension link decoupled. Patient landed hitting back of head. Semi-conscious and dizzy following impact.	
Patient #3 (MVA #2)	Major car accident 30 years ago. Rear ended by pickup truck. Car trunk collapsed to level of rear car window. Patient believes head whiplashed during accident. 2 years later second car accident, hit tree. Thrown forward on impact.	Neck and head trauma from rear-ending by pickup truck. Patient described accident as “whiplash”.	
Patient #4	17 years old today – Patient age 6 years old was picked up by angry parent and shaken back and forth by shoulders. Head was caused to shake back and forth and against a wall. 8 years later (2007 age 14), hit in face by teenager which caused his right arm to go limp. Taken to Schneider’s Children’s Hospital, Great Neck L.I. (NSUH). Diagnosed as MS from MRI images.	Severe parental shaking age 6 (11 years prior to MS diagnosis). Exacerbating incident immediately prior to MS diagnosis (2007). Patient hit in face by teenager. Right eye bruised and right arm went limp. MRI taken immediately following injury showed multiple periventricular MS lesions.	
Patient #5	No accident trauma. Ballroom ballerina/tap/ modern dance since age 3. 4–5 hours dancing/day from ages 12 to 17.	Possible dance head neck trauma. Intense dancing 1990 to 1995. MS symptoms started in 2004.	
Patient #6 (MVA #3)	Motor vehicle accident 1998 at age 19. 11 years prior to MS hit a post while driving in parking lot. Head went forward then back (reverse whiplash). Could not move neck after accident. Fractured left clavicle. Wore neck collar more than 2 weeks. Unable to move left arm. Second accident playing baseball. Hit back of neck. Blurred vision (optic neuritis) followed plus numbness in left shoulder and tingling.	Modified whiplash — head forward then back. Neck injury 11 years prior and 6 months prior. Second incident provoked symptoms.	
Patient #7 (MVA #4)	Severe car accident 1995. “Black ice”. Car spun, hit divider, wrapped around tree. 2 months after accident developed spasms in each leg and impaired locomotion. Neck surgery 2003. Deteriorated markedly following surgery. Lost control of both legs. Currently wheelchair bound.	Seat belt came across left side of neck. Bruises to left neck.	
Patient #8 (MVA #5)	Age 2-3 involved in a severe motor vehicle accident that totalled the car. Patient believes she was in the customary sitting position (no seat belt or infant seat).	Possible neck injury from motor vehicle accident.	
Avg. # years trauma preceded MS diagnosis			

4	5	6
Years Physical Trauma Preceded Diagnosis	Description of MS Image Pathology	Current Symptoms
8	Two peri-ventricular MS lesions penetrating corpus callosum from lateral ventricle into adjacent brain parenchyma. Lateral ventricle swollen mid-line (Sag T2).	Loss of vision left eye — optic atrophy left eye. Loss of muscle strength both legs. Wheelchair bound.
2	Occipital horn hydrocephalus plus peri-ventricular edema i.e. "interstitial edema", MS lesions predominantly adjacent to enlarged occipital horns on both right and left.	Memory problems, sleep apnea, bladder and bowel incontinence, impotence, visual difficulties, fatigue.
21	Solitary MS lesion adjacent to left occipital horn and peri-ventricular interstitial edema anterior horns.	Transient episodes of kaleidoscopic vision, numbness left hand, frequent falling. Wears leg brace to diminish falling. Severe foot drop right foot. Severe right hand weakness. Loss of bladder control. Loss of fine motor control.
8	Multiple peri-ventricular MS lesions radiating off lateral ventricle. Multiple peri-ventricular lesions. Also pronounced interstitial edema lesions both anterior and occipital horns.	Backaches, headaches, numbness in the face. Lack of energy for 17 year old. Sleeps a lot. Gets many canker sores in mouth.
9	One lesion posterior to left occipital horn. Interstitial edema around entire ventricle. Peri-ventricular lesions.	Right arm numbness, sternal numbness. Numbness from mid-sternum to right shoulder extending to right fingertips.
11	Solitary lesion Flair Axial midway up left lateral border left ventricle, peri-ventricular interstitial edema. Possible second MS lesion adjacent occipital horn.	Tingling numbness left shoulder. Blurred vision left eye. Visual blurring after exercise.
1	Parenchymal MS appearing lesion superior to right occipital horn. Couple small peri-ventricular lesions. MS lesions adjacent to left lateral ventricle midway in AP direction. Peri-ventricular interstitial edema.	Loss of motor control lower legs. Wheelchair bound. Fatigue.
27	Multiple peri-ventricular lesions, pronounced hydrocephalus of the occipital horns of the lateral ventricles with accompanying peri-ventricular lesions and edema, prominent peri-ventricular interstitial edema and hydrocephalus in the main body of the lateral ventricles anteriorly.	Optic neuritis, severe vertigo, nausea and vomiting when supine, stumbling when walking.
11		

TABLE 2A. Anatomic Images, CSF Flow Images and CSF Flow Quantification of MS Patients

1	2	3	4	5	6	7	8	9
Patient #	Up. Peak Sys. CSF Vel. (outflow) cm/sec	Rec. Peak Sys. CSF Vel. (outflow) cm/sec	Up. Peak Dias. CSF Vel. (inflow) cm/sec	Rec. Peak Dias. CSF Vel. (inflow) cm/sec	Up. Press. Grad. Peak to mmHg/cm	Rec. Press. Grad. Peak to mmHg/cm	Upright MRI Image Analysis ←----- see glossary -----→	Recumbent MRI Image Analysis
Patient #1 (MVA #1)	.67	1.52 P<.05	.40	.745	.012	.024	1)C2 c.clock rot. 16°, 2)C6/7 cd.c., c.sten.	1)C2 c.clock rot. 5.7° 2)no c.sten., no cd.c.
Patient #2	2.58 P<.05	1.39 P<.05	1.047 P<.05	1.033	.054 P<.05	.031 P<.05	1)r.lis. C5, 2)cd.c., c.sten. C5/6 3)ligfl. cd.c. C6/7, ligfl. can. obst. C6/7 4)c.sten. C6/7	1)vent. can.obs., 2)r.lis., c.sten. red. 3)ligfl. obst. absent
Patient #3 (MVA #2)	1.14	.336	.394	.702	.016	.011	1)r.lis. C4, C5, 2)cd.c., c.sten. C4/5,	1)r.lis. red., 2)no sp.cd. abut. C5/6
Patient #4	1.80 P<.05	2.71 P<.05	.464	1.36 P<.05	.036 P<.05	.063 P<.05	1)sp.cd. post. 2)C3/4 dors. can.obs., 3)CTE 2mm 4)sp.cd. abut. post. wall sp.can. C3/4	1)sp.cd. more ant., 2)dors. can. pat., 3)CTE 1mm
Patient #5	2.03 P<.05	2.14 P<.05	.731 P<.05	1.55 P<.05	.050 P<.05	.046 P<.05	1)dsc. hrn. at C3/4, C4/5, C5/6 2)dsc. bulges at C2/3, C6/7	1)C2/3, C5/6 dsc. hrn. 2)C3/4 hrn. absent 3)C4/5less dsc. bulge 4)C6/7 dsc. bulge not present
Patient #6 (MVA #3)	.79	.94	.32	.80	.014	.020	1)CTE 2mm	1)CTE 2mm
Patient #7 (MVA #4).	.865	—	.51	—	.024	—	1)cd.c. C2/3 to C5/6 2)r.lis C5	1)cd.c. red. C2 to C6 2)C5 r.lis. red. (2003 conventional recumbent MRI)
Patient #8 (MVA #5)	.818	—	.380	—	.020	—	1)post. disp. sp.cd. at C2/3, obst. dors. CSFfl. at C2/3 2)markedly enlarged occipital horns lat. ventcls. 3)peri-ventcl. ed. occipital horns 4)CTE – T2 axials 5)rot. C3 c. wise	
Mean Value (MS patients)	1.34 (8 pat.)	1.51 (6 pat.)	.531 (8 pat.)	1.03 (6 pat.)	.028 (8 pat.)	.033 (6 pat.)		

a-ant., anterior; abut., abutment; b-bel., below; c-c.clock, counter clockwise; c.sten., spinal canal stenosis; c.wise, clockwise; can., canal; can.obs., spinal dors., dorsal; dsc., disc; e-ed., edema; g-grad., gradient; h-hrn., herniation; i-inter., interruption; inta., intact; l-lat., lateral; ligfl., ligamentum flavum; red., reduced; rot., rotation; s-sp., spinal; sp.cd., spinal cord; sys., systolic; u-unobst., unobstructed; Up., upright; v-vel., velocity; vent., ventral; — **BOLDED numbers Col. 2-7** (P<.05)

10	11	12	13	
UPRIGHT MRI Ciné CSF Flow Analysis	Recumbent MRI Ciné CSF Flow Analysis	MRI Image Differences Up./Rec.	CSF Ciné Differences Up./Rec.	
←----- see glossary -----→				
1)dors. CSFfl. obst. at C2/3 2)vent. CSFfl. obst. C3 to C5/6, 3)vent. CSFfl. not obst. by C6/7 dsc. hrn. when Up.	1)dors. CSFfl. faint but inta., 2)vent. CSFfl. inta. to C6/7, 3)vent. CSFfl. obst. at C6/7 by disc. hrn.	1)C2 rotated 16° Up., 5.7° Rec.	1)vent. CSFfl. obst. Up. but not Rec.	1
1)dors. CSFfl. obst. top C2 to C3/4, 2)dors. CSFfl. obst. C5/6, 3)vent. CSFfl. obst. bel. C3/4	1)vent. CSFfl. obst. C3/4 & bel.	1)no infolding ligfl. Rec., 2)less c.sten. Rec.	1)CSFfl. obst. Up., 2)full circumspinal CSFfl. Rec.	2
1)dors. CSFfl. obst. C2/3 to C5/6, 2)vent. CSFfl. obst. C2/3 & bel.	1)vent. & dors. CSFfl. inta.	1)C4, C5 listhesis, much less Rec.	1)CSFfl. obst. Up., 2)CSFfl. unobst. Rec.	3
1)dors. CSFfl. obst. bel. C2/3, 2)vent. CSFfl. inta.	1)dors. CSFfl. obst. bel. C2/3, 2)vent. CSFfl. inta.	1)cord more ant. Rec.	1)same CSFfl. obst. Up. & Rec.	4
1)dors. CSFfl. obst. C2/3 to C5, 2)vent. CSFfl. obst. at C2/3, C3/4, C4/5, C5/6	1)vent. CSFfl. int. less when patient Rec.	1)C5/6 hrn. less Rec.	1)vent. CSFfl. less inter. Rec.	5
1)vent. CSFfl. obst. C2/3 to C6	1)no CSFfl. int. when patient Rec.	1)no difference	1)vent. CSFfl. obst. C2/3 to C6 Up. 2)no CSFfl. inter. Rec.	6
1)dors. CSFfl. obst. C2/3 to C4/5, 2)vent. CSFfl. obst. at C5	1)dors. CSFfl. obst. C2/3 & bel. (2003 conventional recumbent MRI)	1)less cd.c. C2 to C6, 2)r.lis. red. Rec.	1)CSFfl. obst. at C2/3 but restored at C4/5 Up. 2)not restored bel. C4/5 Rec. (2003 conventional recumbent)	7
1)dors. CSFfl. obst. C2/3				8

canal obstruction; cd.c., cord compression; cent., central; CSFfl., CSF flow; CTE, cerebellar tonsil ectopia; d-dias., diastolic; disp., displaced; m-MVA, motor vehicle accident; o-obst., obstructed, obstruction; p-pat., patent; post., posterior; press., pressure; r-r.lis., retrolisthesis; Rec., recumbent; ventcls., ventricles

TABLE 2B. Anatomic Images, CSF Flow Images and CSF Flow Quantification of Normal Examinees

1	2	3	4	5	6	7	8	9	
Patient #	Up. Peak Sys. CSF Vel. (outflow) cm/sec	Rec. Peak Sys. CSF Vel. (outflow) cm/sec	Up. Peak Dias. CSF Vel. (inflow) cm/sec	Rec. Peak Dias. CSF Vel. (inflow) cm/sec	Up. Press. Grad. Peak to Peak mmHg/cm	Rec. Press. Grad. Peak to Peak mmHg/cm	Upright MRI Image Analysis ←----- see glossary -----→	Recumbent MRI Image Analysis	
Normal #1	1.07	.751	.414	.457	.021	.017			
Normal #2	.613	1.03	.332	.825	.0114	.023			
Normal #3	.752	1.05	.321	.746	.0181	.023			
Normal #4	.640	.976	.301	.626	.0135	.0135			
Normal #5	1.27	.595	.526	.488	.0227	.0126			
Normal #6	.586	.849	.325	.786	.018	.016			
Normal #7	1.32	1.022	.583	1.08	.020	.019			
Mean Value (normal examinees) (n = 7)	.893	.896	.4004	.715	.0177	.018			
+/-	.319	.172	.1124	.215	.0040	.004			

a-ant., anterior; **abut.**, abutment; **b**-bel., below; **c**-c.clock, counter clockwise; **c.sten.**, spinal canal stenosis; **c.wise**, clockwise; **can.**, canal; **can.obs.**, spinal dors., dorsal; **dsc.**, disc; **e-ed.**, edema; **g-grad.**, gradient; **h-hrn.**, herniation; **i-inter.**, interruption; **inta.**, intact; **l-lat.**, lateral; **ligfl.**, ligamentum flavum; **red.**, reduced; **rot.**, rotation; **s-sp.**, spinal; **sp.cd.**, spinal cord; **sys.**, systolic; **u-unobst.**, unobstructed; **Up.**, upright; **v-vel.**, velocity; **vent.**, ventral;

10	11	12	13	
UPRIGHT MRI Ciné CSF Flow Analysis	Recumbent MRI Ciné CSF Flow Analysis	MRI Image Differences Up./Rec.	CSF Ciné Differences Up./Rec.	
←----- see glossary -----→				
CSFfl. inta. vent. & dors.	CSFfl. inta. vent. & dors.			
CSFfl. inta. vent. & dors.	CSFfl. inta. vent. & dors.			
CSFfl. inta. vent. & dors.	CSFfl. inta. vent. & dors.			
CSFfl. inta. vent. & dors.	CSFfl. inta. vent. & dors.			
CSFfl. inta. vent. & dors.	CSFfl. inta. vent. & dors.			
CSFfl. inta. vent. & dors.	CSFfl. inta. vent. & dors.			
CSFfl. inta. vent. & dors.	CSFfl. inta. vent. & dors.			

canal obstruction; cd.c., cord compression; cent., central; CSFfl., CSF flow; CTE, cerebellar tonsil ectopia; **d**-dias., diastolic; disp., displaced; **m**-MVA, motor vehicle accident; **o**-obst., obstructed, obstruction; **p**-pat., patent; post., posterior; press., pressure; **r**-r.lis., retrolisthesis; Rec., recumbent; ventcls., ventricles

Significant differences in MS patient CSF flow cinematography (ciné) in the sagittal midplane were observed between the *upright* and *recumbent* positions, while no positional differences in ciné flow were observed in normal examinees (Table 2B, col. 10, 11 & 13). CSF flow differences between the two positions were found in the six MS patients that were scanned both upright and recumbent (Table 2A, col. 10, 11 & 13). Obstructions of spinal CSF flow in *both* the dorsal and ventral spinal canals, when viewed sagittally, were found by cinematography in five of the eight MS patients when they were examined in the *upright* position (Table 2A, patients #1, #2, #3, #5 and #7, col. 10). Patient #3 exhibited *both* dorsal and ventral CSF flow obstruction *only* in the *upright* position (Table 2A, col. 10). Dorsal and ventral CSF flows in patient #3 were unobstructed in the *recumbent* position (Table 2A, col. 11).

Regarding the quantitation of CSF flow (cc/sec) abnormalities, determinations of peak CSF velocities (cm/sec) produced the most pronounced differences between the MS patients and normal examinees (Table 2A, col. 2, 3, 4, & 5). While the peak velocity measurements in our study were measured differently than the peak velocities by Haughton *et al.* [Haughton *et al.* (4) determined the peak velocity to be the highest voxel velocity measured in the scan as compared to the highest annular velocity measured in the scan in our determination], both peak velocity methods found the peak velocity determination to be the most sensitive measure for detecting CSF flow abnormalities.

Among the MS patients, three of the eight patients had significantly ($P < .05$) elevated peak CSF **outflow** (systolic) velocities (cm/sec) from the brain (2.58, 1.80, 2.03 cm/sec) in the *upright* position (Table 2A, col. 2, patients #2, #4 and #5) compared to the mean value for the normal examinees in the *upright* position ($.893 \pm .32$ cm/sec, Table 2B, col. 2). **Outflow** velocities for all three of these MS patients were more than twice the upright **outflow** peak velocities for the normal examinees. Four (patients #1, #2, #4, and #5) had significantly elevated peak CSF **outflow** velocities (cm/sec) (1.52, 1.39, 2.71 and 2.14 cm/sec, Table 2A, col. 3) in the *recumbent* position, two of which (2.71 and 2.14 cm/sec) were more than twice the normal value ($.896 \pm .17$ cm/sec, Table 2B, col. 3). A fifth MS patient (patient #3) had a *recumbent* CSF **outflow** velocity of .336 cm/sec that was significantly reduced relative to normal ($.896 \pm .17$ cm/sec).

In addition, two of the eight MS patients (Table 2A, col. 4, patients #2 and #5) exhibited significantly elevated peak **inflow** velocities in the *upright* position (Table 2A, col. 4, 1.047, and .731 cm/sec) relative to the peak **inflow** velocities of normal examinees (.400 cm/sec) in the *upright* position (Table 2B, col. 4). Importantly, therefore, five of the eight MS patients had at least one significantly abnormal peak CSF velocity measurement in three of the parameters measured (*upright outflow*, *recumbent outflow*, and *upright inflow*), and three of the MS patients exhibited elevated peak velocities in *both* the *upright* and *recumbent* positions (patients #2, #4, and #5, Table 2A, col. 2 & 3).

Sharply Reduced CSF Inflow Velocity in the Upright Position

Additionally it was found that peak CSF **inflow** (1.023 cc/sec) and peak CSF **inflow** velocity (0.400 cm/sec) (Table 3) were sharply reduced in normal examinees in the *upright* position when compared to **inflow** and **inflow** velocity in the *recumbent* position. Both peak **inflow** (cc/sec) and peak **inflow** velocity (cm/sec) in the *upright* position were found to be about half (53%–56% respectively), of what they were in the *recumbent* position (Table 3) in the normal examinees. Except for patient #2 and normal examinee #5, both

MS patients *and* the normal examinees exhibited reduced **inflow velocity** in the *upright* position (Table 2A, col. 4 & 5; Table 2B, col. 4 & 5). In the case of patient #2, the anticipated velocity reduction arising from the *upright* position was offset by the peak velocity acceleration arising from the patient's pathology (Table 2A, col. 4 & 8).

This *striking reduction* of CSF **inflow** into the brain in the *upright* position in both MS patients (Table 2A) and normals (Table 2B, Table 3) was unexpected, inasmuch as cerebral blood flow in normal subjects is unaffected by position (5). The observed reduction in CSF **inflow** in the *upright* position apparently constitutes normal physiology. The unexpected observation that CSF *flow* is significantly reduced in the *upright* position (or significantly increased in the *recumbent* position) raises interesting questions regarding the physiological significance of the increased CSF *flow* of recumbency.

The High Percentage of “Normal” Examinees That Did Not Qualify as Normal

Another unexpected finding was the high percentage of “normal” adults that did not qualify as **normal**. It was found that a large percentage of normal examinees (as high as 75%) did not qualify as normal with respect to their cervical spine anatomy, e.g., exhibiting localized disc herniations (or significant bulges) at C5/6 or elsewhere, or localized interruptions of CSF flow. Such examinees were entirely asymptomatic currently and historically, but were nonetheless unable to meet a standard for normal cervical spine anatomy. With the cervical spine being the most active segment of the spine, the finding, though unexpected, is not inconsistent with the cervical spine's high degree of bio-mechanical activity.

A Possible Physiologic Role of Nocturnal Sleep Enabled By Enhanced CSF Flow Into the Brain in Recumbency

Since one of the physiological roles attributed to the CSF is the delivery of nutrients to the brain and the removal of toxic metabolic waste, the increase in CSF *flow* facilitated by recumbency engenders the consideration that the normal nocturnal sleep process may in fact be playing an active role in facilitating the removal of metabolic waste from the brain and delivering nutrients. Recumbent sleep may be enabling increased CSF **inflow** into the brain for the physiologic purpose of delivering nutrients to the brain and cleansing

TABLE 3: Change of CSF Inflow With Position in Normal Examinees
(see Tables 2A and 2B for velocities)

1 Peak <u>INFLOW</u> (cc/sec) UPRIGHT	2 Peak <u>INFLOW</u> (cc/sec) RECUMBENT	3 Peak <u>INFLOW</u> <u>Velocity</u> (cm/sec) UPRIGHT	4 Peak <u>INFLOW</u> <u>Velocity</u> (cm/sec) RECUMBENT
1.023	1.935	.400	.715
% Difference Up/Rec 53%		% Difference Up/Rec 56%	

it of toxic metabolic by-products*. Similarly, it may account, in some measure, for the benefits of recumbent sleep in the medical healing process.

Prior Histories of Significant and Severe Trauma

The most unexpected finding in this MR study of MS patients was the revelation that when carefully questioned, six of the eight Multiple Sclerosis patients had a prior history of severe trauma to the neck (Table 1, col. 2) with one patient (patient #2) having sustained *both* neck and head trauma. In addition, there is a significant likelihood that trauma had a role in the genesis of a seventh patient's MS (Table 1, patient #8, col. 2). The finding is consistent with prior reports that trauma may have a causative role in the onset of MS (6,7,8). All seven patients had distinct cervical anatomic pathology on their current MR images that corresponded with their trauma histories, thereby establishing that the historical trauma events contributed directly to their permanent pathologies of the cervical spine (Table 2A, col. 8 & 9) and that their cervical trauma histories *were not immaterial*. Four had received neck injuries in motor vehicle accidents, three of which were whiplash injuries, and the fourth a "reverse whiplash" (neck flexion preceding neck extension) injury (patient #7). A fifth, patient #8, was involved in a severe motor vehicle accident at age 2–3 that "totalled" the car in which she was riding without a seat belt or infant seat.

Noteworthy was the fact that the trauma and particularly motor vehicle trauma, notwithstanding its severity, was never correlated by either the patients or their physicians with the onset of their MS symptomatology. The symptoms of head and neck trauma, however, can be long lasting (e.g., 17 yrs.) (9). In all but two of the patients (patients #2 and #7, Table 1, col. 4) the trauma preceded the onset of MS symptoms by more than 8 years. When the mean value was calculated for all eight MS patients, the average number of years patient trauma preceded the patient's MS diagnosis, was 11 years. In addition, the abnormal CSF *flow* dynamics found in the MS patients of this study corresponded to the MR cervical pathology that was visualized (Table 2A, col. 2–9).

In the UPRIGHT® MRI examination of the eight MS patients, four of the eight exhibited severe cervical anatomic pathology (patients #1, #2, #3 and #7, Table 2A, col. 8). The remaining four patients had less severe but still serious cervical anatomic pathology (Table 2A, col. 8) and two (MS patients #2 [Figure 2] and #8 [Figure 8]) exhibited conspicuous swelling of the body of the cerebral lateral ventricles or of the occipital horns of the lateral ventricles.

Anatomic Pathology and CSF Flow Obstruction More Severe With the Patient Upright

In all but one (patient #6) of the seven MS patients that were imaged in both the upright and recumbent positions, the visualized anatomic pathology was more severe in the *upright* position than in the *recumbent* position (Table 2A, col. 8 & 9). Patient #1, for example, exhibited a 16° mal-rotation of C-2 on the patient's *upright* axial image (Figure 1e)

* The authors thank Charles Green, FONAR Corporation scientist and engineer, for his proposal that the increased CSF *flow* into the brain of recumbency might have the beneficial effect of enhancing CSF cleansing of the brain.

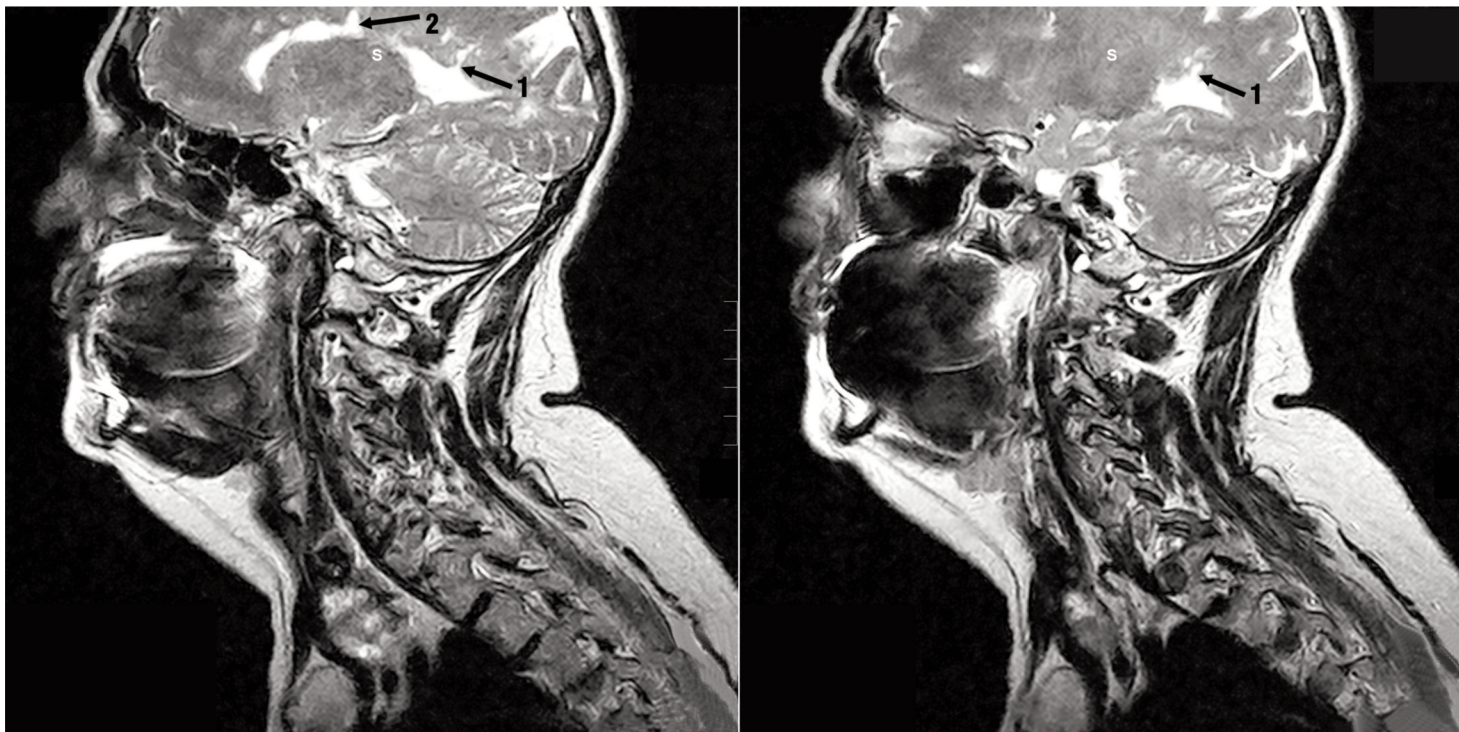


FIGURE 1a. Sagittal T2-weighted image of a Multiple Sclerosis patient (patient #1) showing two peri-ventricular MS plaques (arrows 1 & 2) perpendicular to the ventricular wall. Lesion 1 (arrow 1) exhibits an explicit connection between ventricular CSF and an MS plaque. Lesion 2 exhibits a similar connection to ventricular CSF but in a less striking manner. The images visualizing the CSF “leaks” of Figure 1a were obtained on March 11, 2010 with the patient upright in the FONAR UPRIGHT® Multi-Position™ MRI.

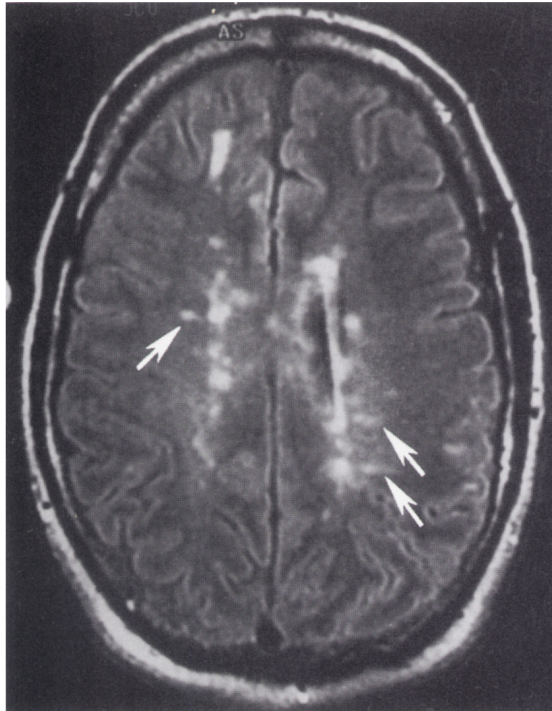
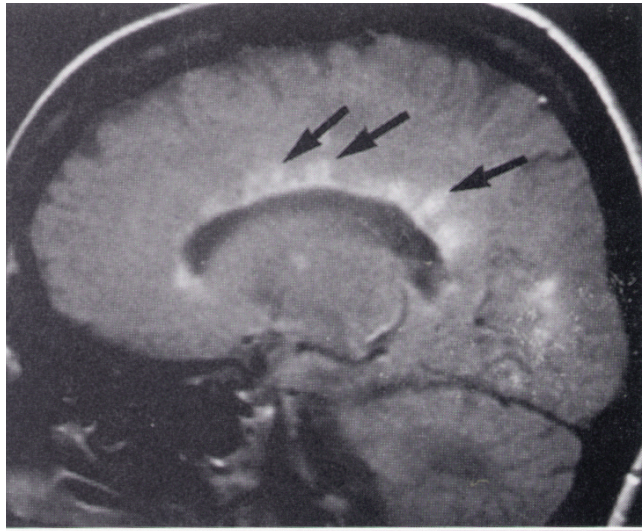
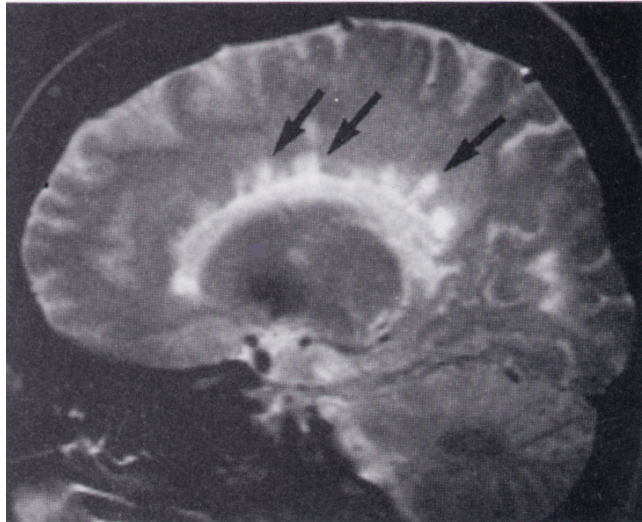


FIGURE I. (Figure 61-2, Stark, D. B., Bradley, W. B. Jr., Eds. Magnetic Resonance Imaging, Ed. III Vol. III, 1999, S. K. Laxhanpal, K. R. Maravilla, "Multiple Sclerosis", ch. 61, p. 1381, Mosby, Inc.) Axial fluid-attenuated inversion recovery (FLAIR) image at the level of the corona radiata shows multiple hyperintense MS plaques in the periventricular and subcortical white matter. Several plaques with the corona radiata demonstrate a characteristic appearance, with the long axis of the plaque oriented perpendicular to the axis of the lateral ventricles (*parallel with the white matter fibers within the corona radiata*), known as Dawson's fingers (arrows). *Noteworthy is the author's description of the plaque axis being parallel to the white matter fibers within the corona, a natural pathway for "leaking" CSF. (Author's additions to the original published legends of Figure 61-2 appear in italics.)*



A



B

FIGURE IIA and IIB. (Figure 61-3A and 61-3B, Stark, D. B., Bradley, W. B. Jr., Eds. Magnetic Resonance Imaging, Ed. III Vol. III, 1999, S. K. Lakhanpal, K. R. Maravilla, "Multiple Sclerosis", ch. 61, p. 1381, Mosby, Inc.) Sagittal spin-density-weighted (A) and T2-weighted (B) images in a patient with MS show multiple periventricular plaques, again demonstrating the characteristic elongated appearance of the plaques oriented perpendicular to the ventricular wall (arrows). This appearance is often best demonstrated on sagittal T2-weighted images such as these. *Image B exhibits contiguity between the peri-ventricular MS plaques (arrows) and ventricular CSF. The MS plaque at the right most arrow when carefully examined exhibits a stem, similar to Figure 1a, connecting the MS plaque to ventricular CSF. (Author's additions to the original published legends of Figure 61-3A and 61-3B appear in italics.)*

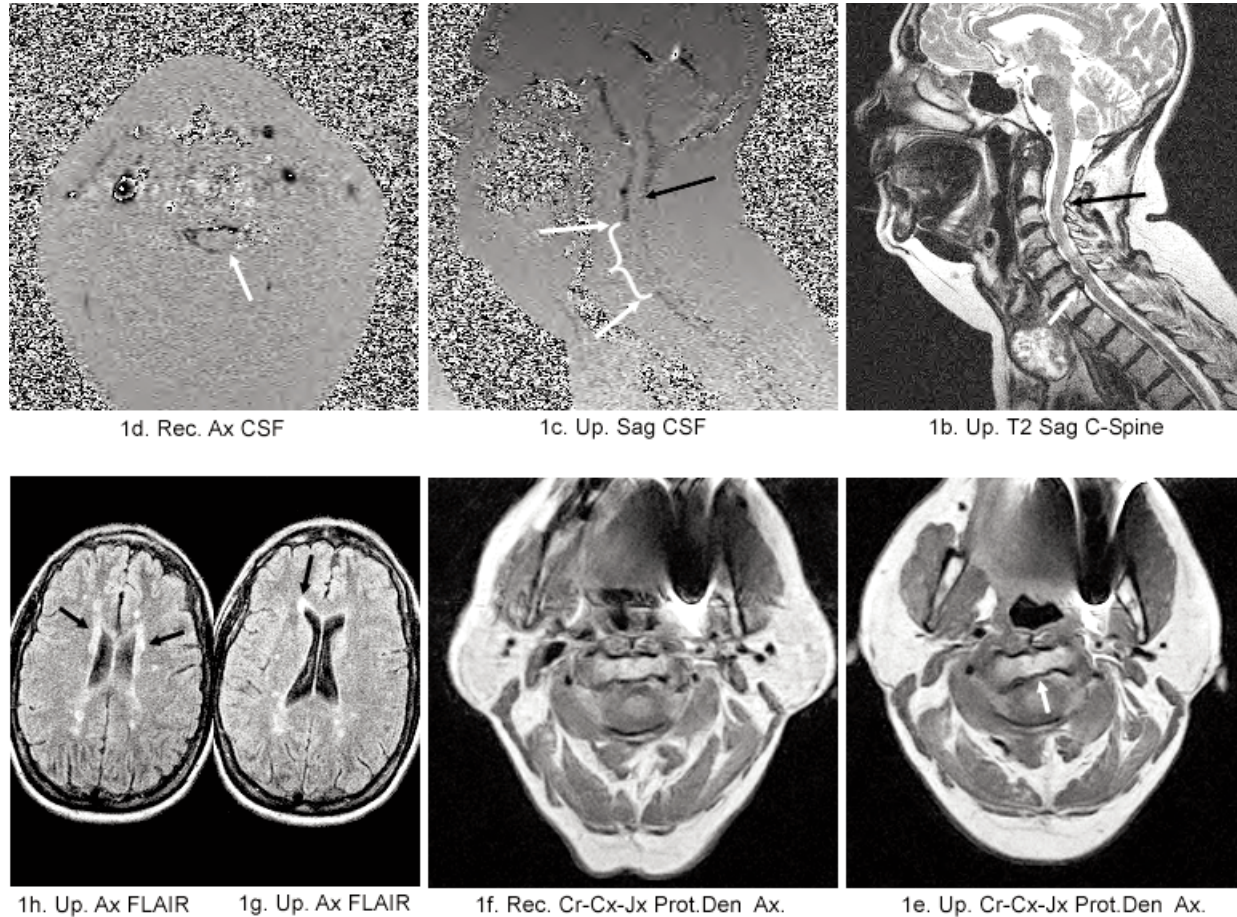


FIGURE 1b–1h. The first MS patient (patient #1) exhibited peri-ventricular MS lesions (Figures 1g & 1h) that were adjacent to the occipital horns of the lateral ventricles as well as to the anterior horns. Additionally, MS patient #1 exhibited a non-uniform distribution of peri-ventricular interstitial edema (PVIE). Peri-ventricular interstitial edema suggestive of CSF leakage was present anterolaterally in both right and left lateral ventricles in the axial image of Figure 1h (black arrows) and was most pronounced adjacent to the anterior horn of the right lateral ventricle (Figure 1g black arrow). The patient also exhibited a sixteen degree (16°) counter-clockwise rotation of C2 in the upright position (Figure 1e white arrow) which reduced to a five degree (5°) rotation in the recumbent position (Figure 1f). Additionally, disc herniations and disc protrusions were observed to be present in the upright position at all cervical levels from C2/3 to C6/7 (Figure 1b) with the most prominent protrusions/herniations occurring at C4/5, C5/6, and C6/7 abutting the spinal cord and obstructing the ventral spinal canal. The disc herniation and cord abutment at C6/7 was the most pronounced (Figure 1b white arrow). An impediment to dorsal CSF flow manifest as hypertrophy and infolding of the ligamentum flava at C2/3 and C3/4 dorsally (Figure 1b black arrow) was also visualized.

The visualized anatomic obstructions of the dorsal and ventral spinal canals resulted in corresponding dorsal and ventral interruptions of CSF flow in the spinal canal (Figure 1c). Axial CSF flow measured in the recumbent position at C4 was interrupted from 1 o'clock to 6 o'clock in the left lateral spinal canal (Figure 1d white arrow).

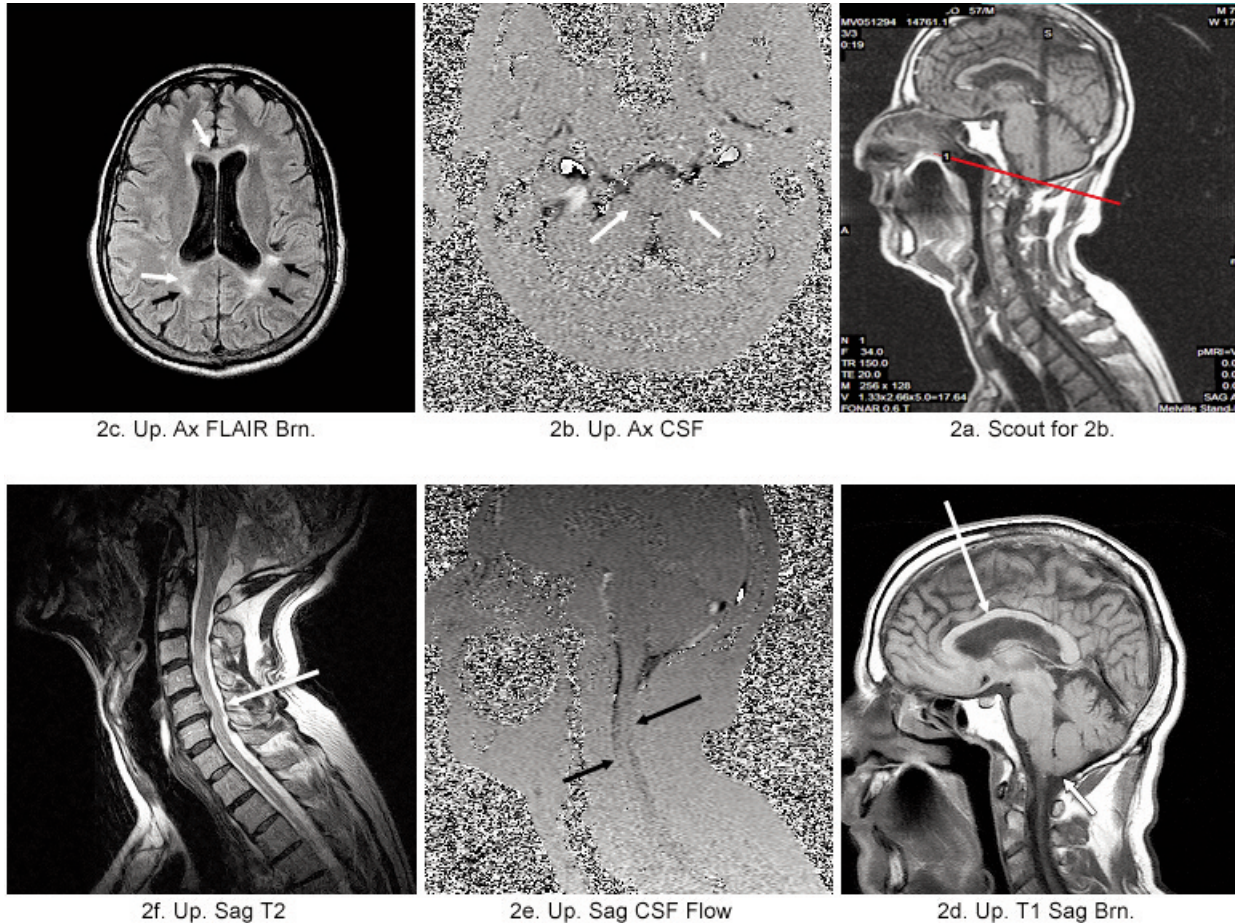


FIGURE 2a–2f. MS patient #2 exhibited MS lesions adjacent to both occipital horns of the lateral ventricles (Figure 2c black arrows), MS lesions adjacent to both anterior horns (Figure 2c) and hydrocephalus of the lateral ventricles (Figure 2c) and (Figure 2d white arrow). The presence of non-uniform peri-ventricular interstitial edema at the anterior horns was also evident (Figure 2c white arrow). Anatomically, cerebellar tonsil ectopia (CTE) was seen abutting the brainstem (Figure 2b white arrows) and was manifest as incomplete and dorsally obstructed CSF flow in the posterior foramen magnum secondary to cerebellar tonsil obstruction (Figure 2b white arrows).

Additionally, anatomic impedance and obstruction of CSF in the ventral spinal canal (Figure 2f opposite white arrow) was visualized at C5 and C4 secondary to a posterolisthesis of C5 and a disc herniation abutting and posteriorly displacing the spinal cord at C5/6. The anatomic CSF obstruction of the ventral spinal canal visualized in the patient's upright sagittal image of the cervical spine (Figure 2f opposite white arrow) was manifest as corresponding impairments of CSF flow ventrally and dorsally from C4 to C5 (Figure 2e black arrows).

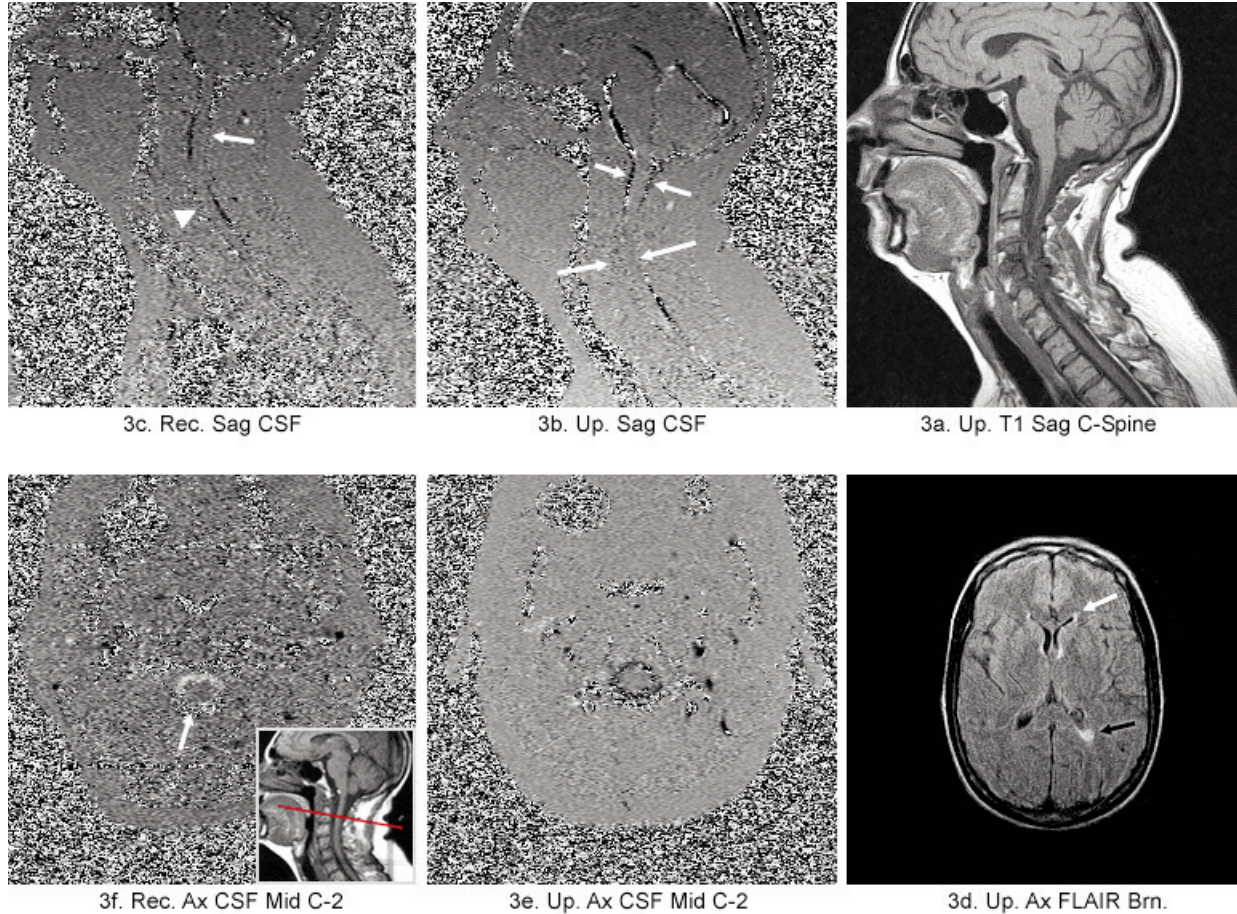
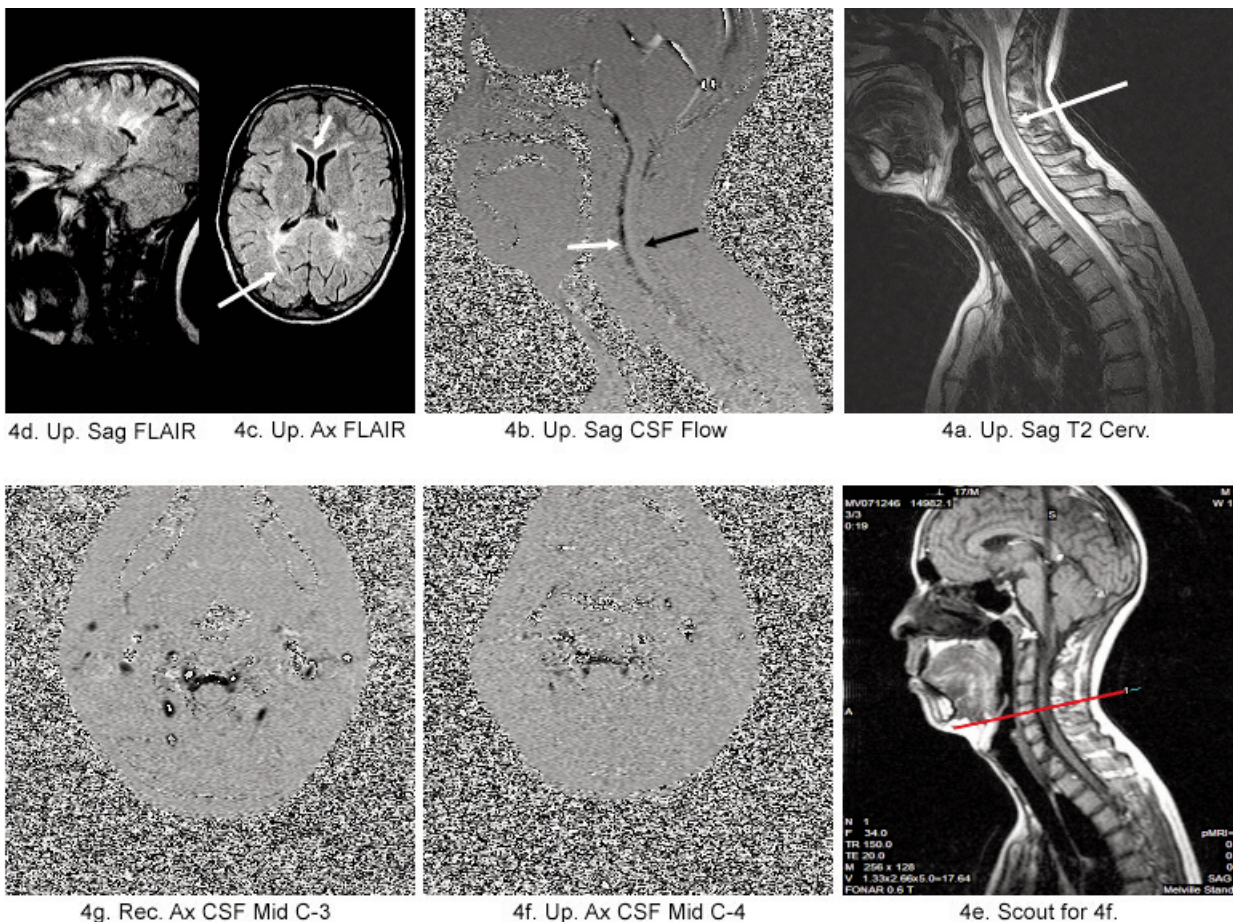


FIGURE 3a–3f. MS patient #3 exhibited an MS lesion adjacent to the occipital horn of the left lateral ventricle (Figure 3d black arrow) and enhanced peri-ventricular interstitial edema at the anterior horns (white arrow). Anatomical degradation of cervical vertebra C4 and C5 and obstructive disruption of the spinal canal at this level is visualized in the upright image of the cervical spine (Figure 3a). Dorsal and ventral CSF flow is likewise interrupted at C4 and C5 (Figure 3b long white arrows). Dorsal and ventral CSF flow is unobstructed anatomically at C2 (Figure 3a) in the upright position and unobstructed both sagittally (Figure 3b short white arrows) and axially (Figure 3e) with respect to CSF flow in the upright position. In the recumbent position, however, CSF flow is obstructed dorsally at C2 (Figure 3f white arrow), in contrast to unobstructed dorsal CSF flow at C2 when the patient is upright (Figure 3e). CSF flow in the recumbent position (Figure 3c white arrowhead), however, is also obstructed ventrally at the same C4 and C5 cervical levels that exhibit the anatomic disintegration visible in the upright MR images of the patient’s cervical spine (Figure 3a).



4d. Up. Sag FLAIR 4c. Up. Ax FLAIR

4b. Up. Sag CSF Flow

4a. Up. Sag T2 Cerv.

4g. Rec. Ax CSF Mid C-3

4f. Up. Ax CSF Mid C-4

4e. Scout for 4f.

FIGURE 4a–4g. MS patient #4 exhibited a pronounced aggregate of MS lesions in peri-ventricular distribution around the lateral ventricles (Figure 4d and 4c) increasing in frequency in the direction of the occipital horns (Figure 4d black arrow). Irregular peri-ventricular interstitial edema is pronounced at the anterior horns (Figure 4c short white arrow). The density of MS lesions is most pronounced adjacent to the occipital horns (Figure 4c) where, in addition, what appears to be a CSF “leakage” striation (Figure 4c) arising from the right occipital horn (white arrow) is conspicuous and suggestive of an increase in ventricular CSF pressure within the lateral ventricle. Patient #4 also exhibits a posterior displacement of the spinal cord within the spinal canal abutting the posterior wall of the spinal canal (Figure 4a) at the level of cervical disc C3/4 (white arrow). The anatomic obstruction of the dorsal spinal canal resulting from the posterior displacement of the spinal cord and its abutment of the posterior wall of the canal (Figure 4a), is accompanied by an obstruction of dorsal CSF flow in the spinal canal (Figure 4b black arrow). Axial MR images of the spinal canal taken in both the upright position (Figure 4f) and in the recumbent position (Figure 4g) exhibit a corresponding absence of dorsal CSF flow in the upright position (Figure 4f) at the mid C-4 level (Figure 4e and 4f) and also at the mid C-3 level in the recumbent position (Figure 4g).

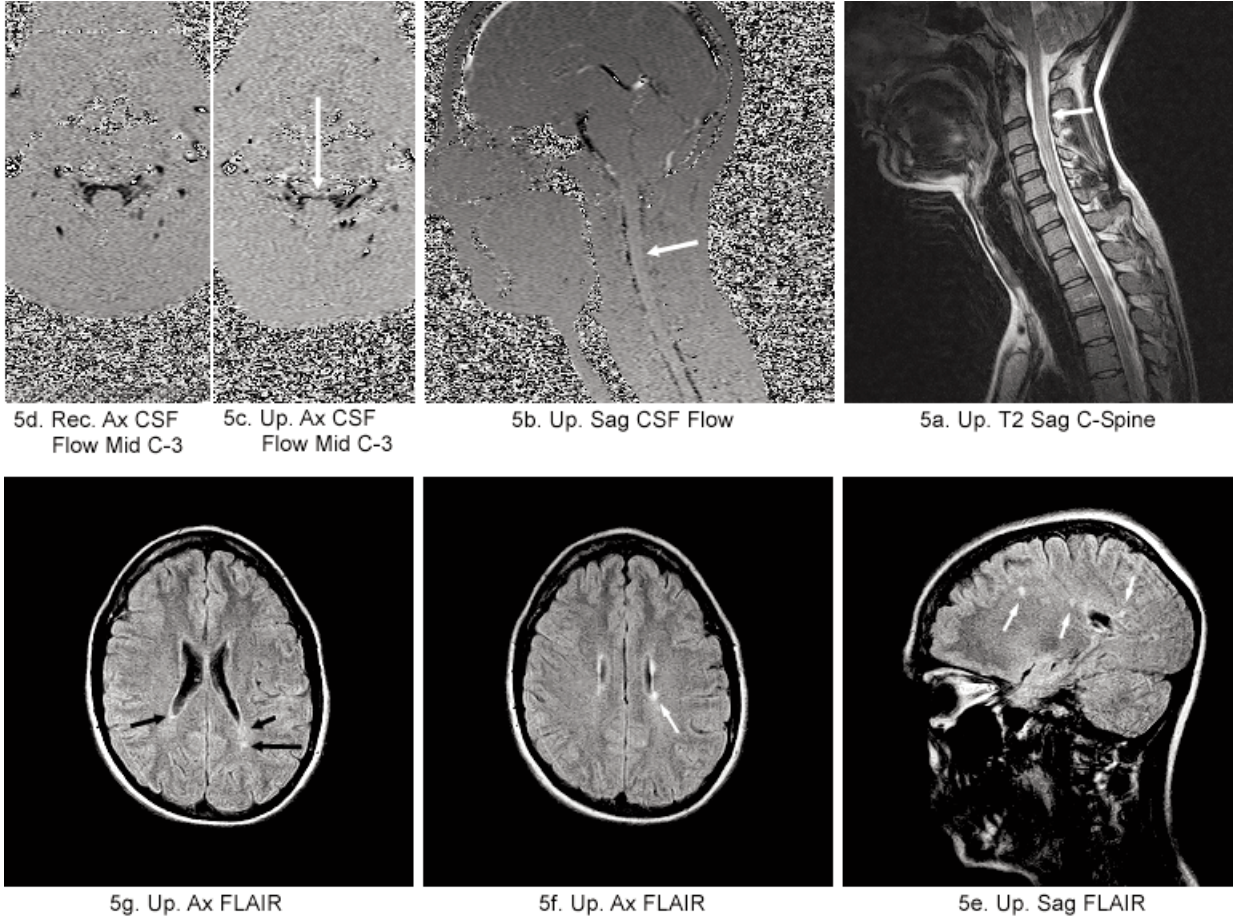


FIGURE 5a–5g. MS patient #5 exhibited peri-ventricular MS lesions (Figure 5e white arrows) on the upright sagittal FLAIR images of the brain. The upright axial FLAIR images (Figures 5g and 5f) show MS lesions adjacent to the left occipital horn of the lateral ventricle (Figure 5g black arrow) and lesions attached to the lateral wall of the left ventricle (Figure 5f white arrow). Additionally, irregular peri-ventricular interstitial edema is present most pronounced in the right occipital horn (Figure 5g black arrow), with the additional suggestion of CSF “leakage” (Figure 5g small black arrow) suggestive of an increase in intraventricular CSF pressure connecting the left occipital horn to the MS lesion. Anatomically, MS patient #5 exhibited cervical disc bulges indenting the thecal sac and anatomically interfering with CSF flow at C4/5, C5/6 and C6/7 (Figure 5a). Direct cervical disc abutment of the spinal cord is exhibited at C5/6. Correspondingly, CSF flow is interrupted ventrally at C2/3, C3/4, C4/5, C5/6 and C6/7 in the upright sagittal images of CSF flow (Figure 5b). Additionally, significant compromise of the dorsal spinal canal at C2/3 (Figure 5a white arrow) that appears obstructive of CSF is manifest as an obstruction and absence of CSF flow dorsally from C2/3 to C6/7 (Figure 5b white arrow). The axial image of CSF flow obtained at mid C-3 (Figure 5c) exhibits an absence of CSF flow dorsally but satisfactory ventral flow (Figure 5c white arrow) corresponding with the upright CSF flow imaging of the sagittal plane that exhibits disc interrupted ventral CSF flow but absent dorsal CSF flow (Figure 5b white arrow). The recumbent axial imaging of CSF flow (Figure 5d) exhibits increased annular flow compared to CSF flow in the upright position at C3 (Figure 5c) but the same annular distribution of CSF flow that shows intact ventral flow but absent dorsal flow.

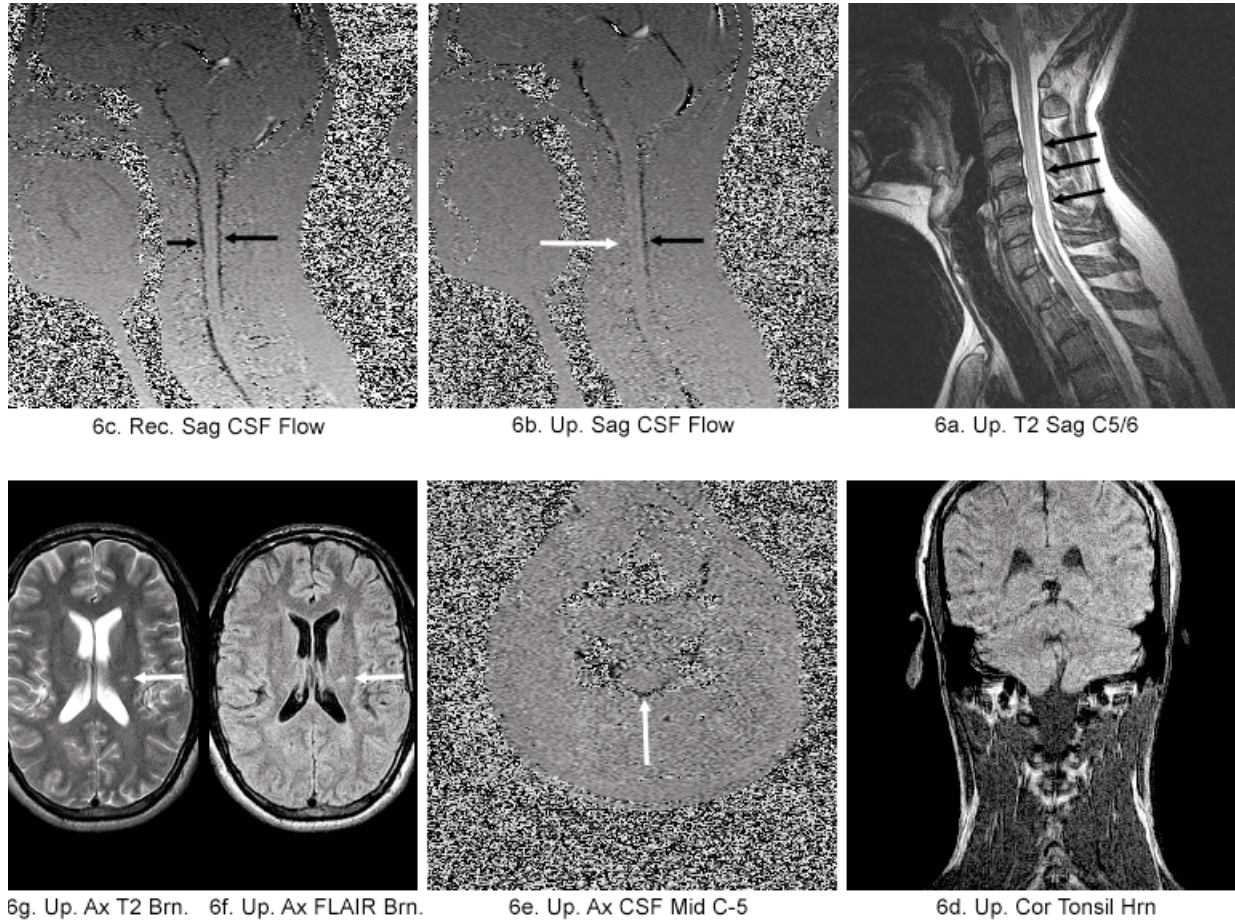
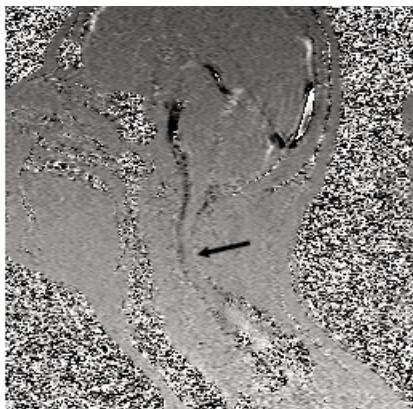


FIGURE 6a–6g. MS patient #6 exhibited an MS lesion proximate to the wall of the left lateral ventricle (Figure 6f & 6g white arrows). CSF flow in the dorsal spinal canal is unobstructed anatomically in the upright position (Figure 6a) and correspondingly unobstructed in the dynamic images of dorsal CSF flow (Figure 6b black arrow). Obstruction of ventral CSF flow (Figure 6b white arrow) in the upright position corresponding to the cervical disc herniations (Figure 6a) that obstruct the ventral spinal canal and abut the spinal cord is evident in Figure 6b. The cervical disc herniations at C3/4, C4/5 and C5/6 responsible for the obstruction are visualized in the upright T2 image of the cervical spine (Figure 6a black arrows) where they are seen indenting the thecal sac abutting the cord and anatomically obstructing the CSF ventrally (Figure 6a). The ventral CSF flow obstruction of MS patient #6 is visible only with the patient upright. When weight loading of the C-spine is removed with the patient in the recumbent position (Figure 6c), CSF flow is restored ventrally and both normal dorsal and ventral CSF flow are simultaneously visualized (Figure 6c black arrows).



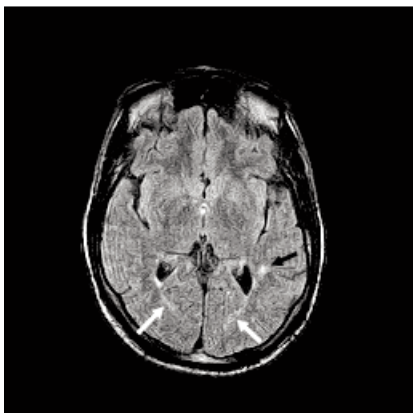
7c. Up. Sag CSF Flow



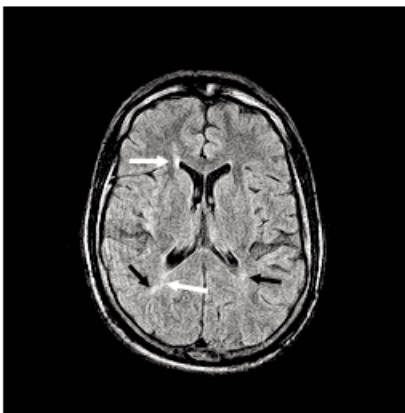
7b. Up. T2 Sag Cerv.



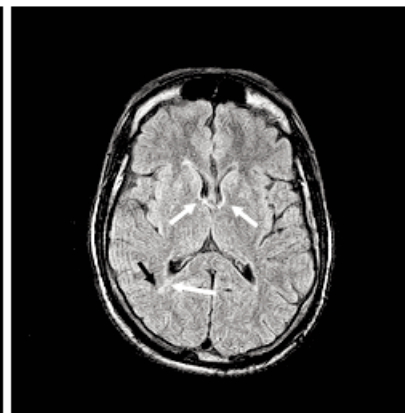
7a. Rec. T2 Sag Cerv.



7f. Up. Ax FLAIR



7e. Up. Ax FLAIR



7d. Up. Ax FLAIR

FIGURE 7a–7f. MS patient #7 exhibited MS lesions adjacent to the left occipital horn (Figure 7f & 7e black arrows) and proximate to the right occipital horn (Figure 7d & 7e small black arrow). Additionally, striations suggestive of CSF “leakages” appear in the upright axial FLAIR images of patient #7 (Figure 7f, 7e and 7d white arrows). Also present is an irregular peri-ventricular interstitial edema suggestive of increased intracranial pressure that is exhibited as hyperintensities contiguous with the anterior horns of the lateral ventricle. The hyperintensity is most pronounced contiguous with the right anterior horn of the lateral ventricle (Figure 7e anterior white arrow). The peri-ventricular edema is also visible contiguous with the lateral walls of the left and right anterior horns of the lateral ventricles (Figure 7d anterior white arrows).

Anatomically severe compression of the spinal cord is visible in MS patient #7 from C2/3 to C5/6 obstructing the ventral spinal canal. The disc compressions of the cord (Figure 7a) are further compounded by an additional retrolisthesis of C5 when the patient is upright (Figure 7b) that compresses the cord further and displaces it posteriorly to a greater extent in the upright position (Figure 7b white arrow) under the added weight load. Additionally, hypertrophies of the ligamentum flavum (Figure 7b intersecting white arrows) compress the spinal cord dorsally and obstruct the dorsal canal (Figure 7a).

The dynamic upright imaging of CSF flow (Figure 7c) exhibits a corresponding obstruction of CSF flow dorsally (Figure 7c black arrow) from C2/3 to C4/5 and impairs CSF flow ventrally in the same region.

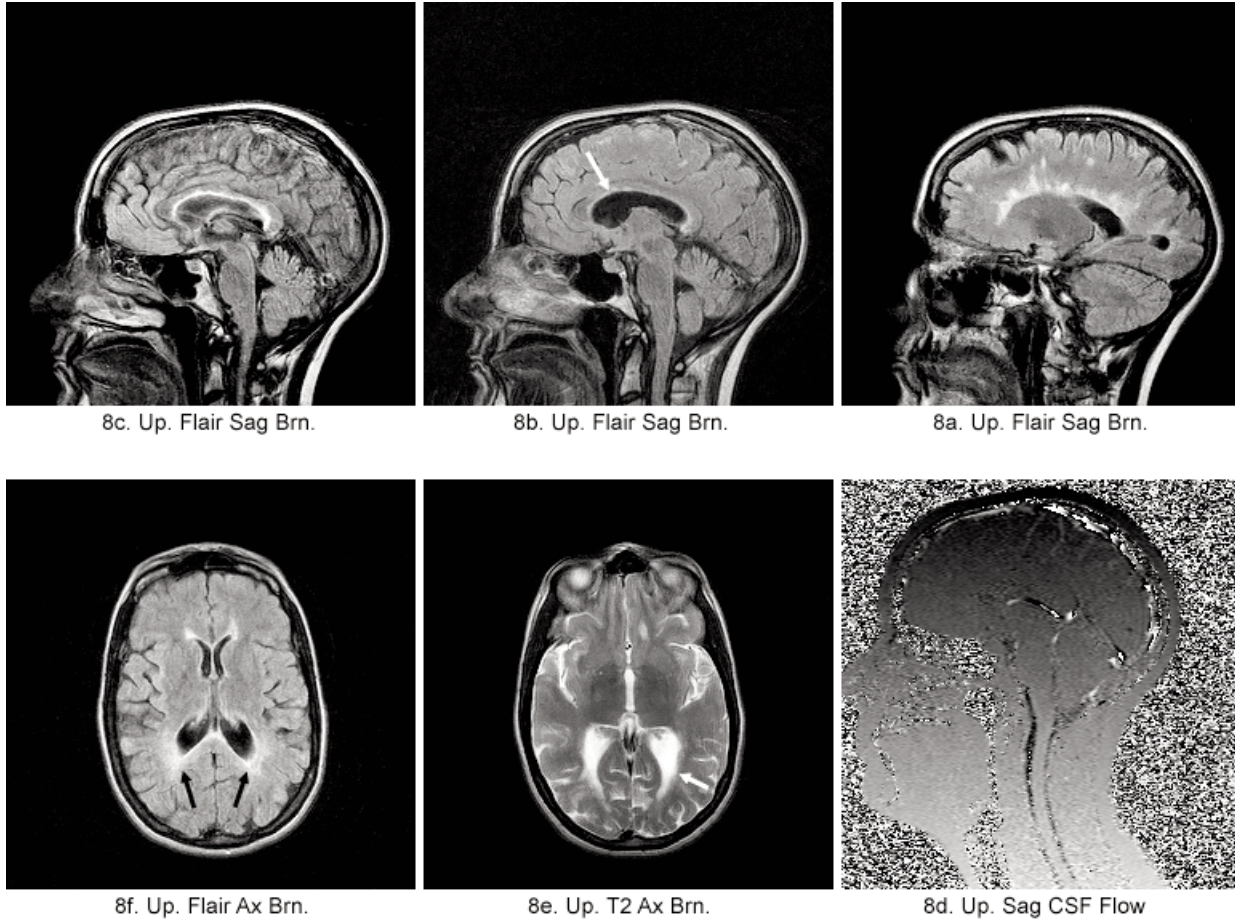
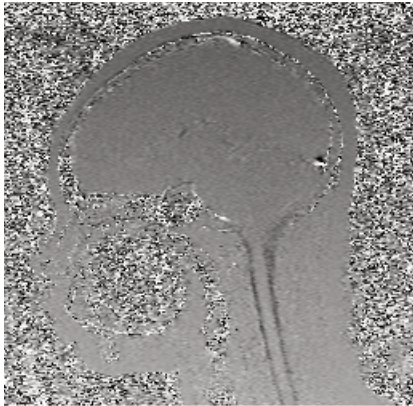


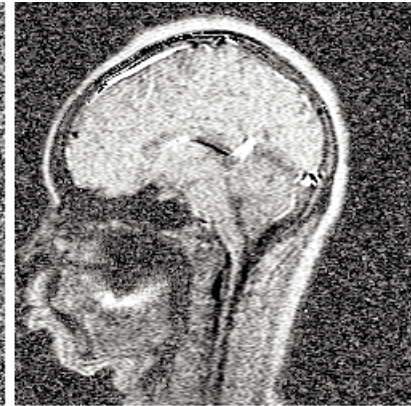
FIGURE 8a–8f. MS patient #8 exhibited a pronounced peri-ventricular distribution of MS lesions (Figure 8a). In addition, multiple cerebral pathologies suggestive of increased intracranial pressure (ICP) were seen. Most conspicuous was the hydrocephalus of the occipital horns of the lateral ventricles visualized in the Upright T2 axial images of the brain (Figure 8e white arrow) and in axial Flair images of the brain (Figure 8f). Particularly prominent was the pronounced edema seen adjacent to the occipital horns of the lateral ventricles (Figure 8f black arrows) strongly suggestive of CSF “leakage”, possibly secondary to an increased ICP, into the surrounding brain parenchyma. Similarly, the conspicuous collar of interstitial edema surrounding the lateral ventricles in the upright Flair sagittal image of the brain (Figure 8c) and the conspicuous ventricular dilatation of the body of the lateral ventricles (Figure 8b white arrow) are further suggestive of an increased intracranial pressure (ICP) being the origin of the CSF “leakage” seen in Figures 8e and 8f.



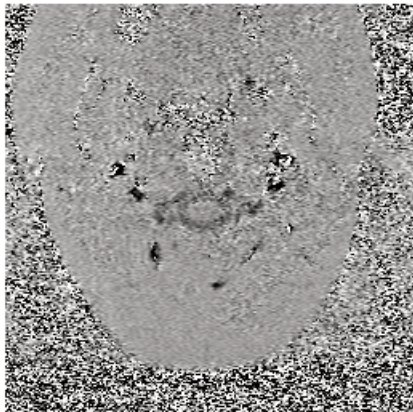
9c. Rec. Sag CSF Brn.



9b. Up. Ax CSF Mid C-2.



9a. Up. Sag CSF Brn.



10c. Up. Ax CSF Mid C-2



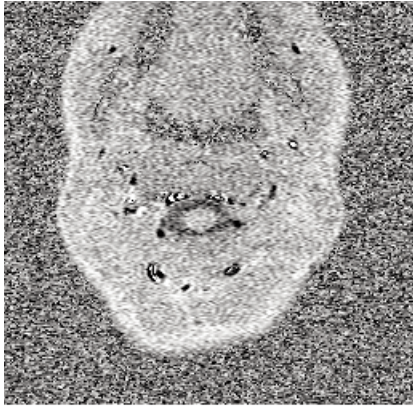
10b. Up. Sag CSF Flow



10a. Up. T2 Sag C-Spine

FIGURE 9a–9c. UPRIGHT® normal examinee #1 exhibits continuous ventral and dorsal sagittal CSF flow (Figure 9a & 9c black channels) as well as uninterrupted 360° annular circumspinal flow (black annulus) visualized in the axial image obtained at mid C-2 (Figure 9b).

FIGURE 10a–10c. UPRIGHT® normal examinee #2 shows full patency of the ventral and dorsal spinal canals (Figure 10a) manifest as uninterrupted ventral and dorsal sagittal CSF flow (Figure 10b black channels) and as uninterrupted 360° annular circumspinal CSF flow in the axial image obtained at mid C-2 (Figure 10c black annulus).



11c. Up. Ax CSF Mid C-2



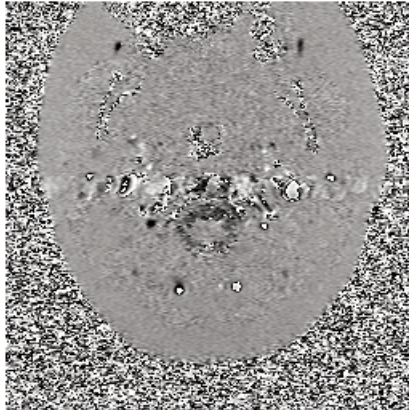
11b. Up. Sag CSF Flow



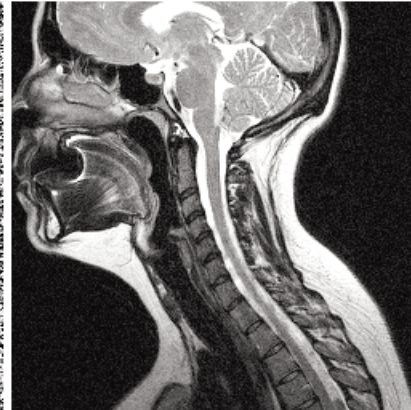
11a. Up. T2 Sag C-Spine



12c. Up. Sag CSF Flow



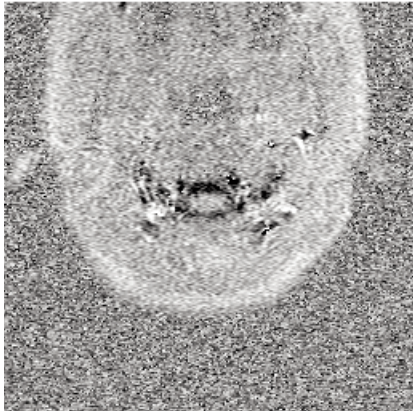
12b. Rec. Ax CSF Flow



12a. Up. T2 Sag C-Spine

FIGURE 11a–11c. UPRIGHT® normal examinee #3 exhibits patent ventral and dorsal spinal canals (Figure 11a) confirmed by intact ventral and dorsal CSF flow in upright sagittal CSF flow (Figure 11b black channels) and full 360° annular circumspinal CSF flow in the axial image obtained at mid C-2 (Figure 11c black annulus).

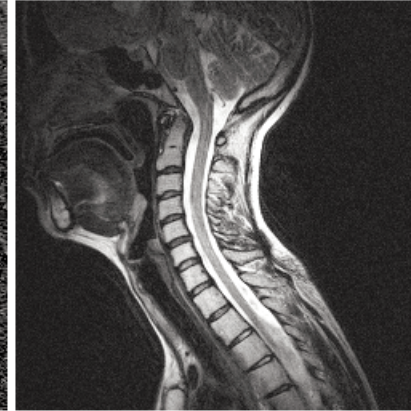
FIGURE 12a–12c. UPRIGHT® normal examinee #4 exhibits patent ventral and dorsal spinal canals (Figure 12a) with full UPRIGHT® ventral and dorsal CSF flow (Figure 12c black channels) and full 360° annular circumspinal recumbent CSF flow in the axial image obtained at mid C-2 (Figure 12b black annulus).



13c. Up. Ax CSF Mid C-2



13b. Up. Sag CSF Flow



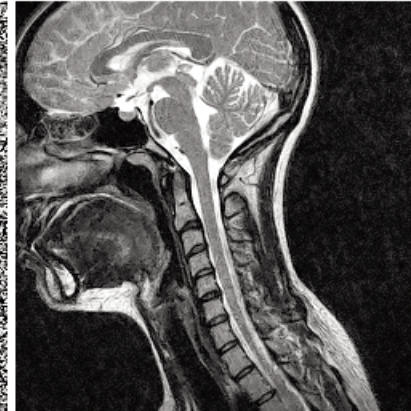
13a. Up. T2 Sag C-Spine



14c. Up. Sag CSF Flow



14b. Rec. Ax CSF Flow



14a. Up. T2 Sag C-Spine

FIGURE 13a–13c. UPRIGHT[®] normal examinee #5 exhibits patent ventral and dorsal spinal canals (Figure 13a) visualized as uninterrupted UPRIGHT[®] CSF flow ventrally and dorsally in the sagittal CSF image (Figure 13b black channels) as well as in full 360° annular circumspinal CSF flow in the UPRIGHT[®] axial image obtained at mid C-2 (Figure 13c black annulus).

FIGURE 14a–14c. UPRIGHT[®] normal examinee #6 exhibits patent ventral and dorsal spinal canals (Figure 14a) confirmed by uninterrupted ventral and dorsal CSF flow in the UPRIGHT[®] sagittal image of CSF flow (Figure 14c black channels) and by full 360° annular circumspinal CSF flow in the axial recumbent image obtained at mid C-2 (Figure 14b black annulus).

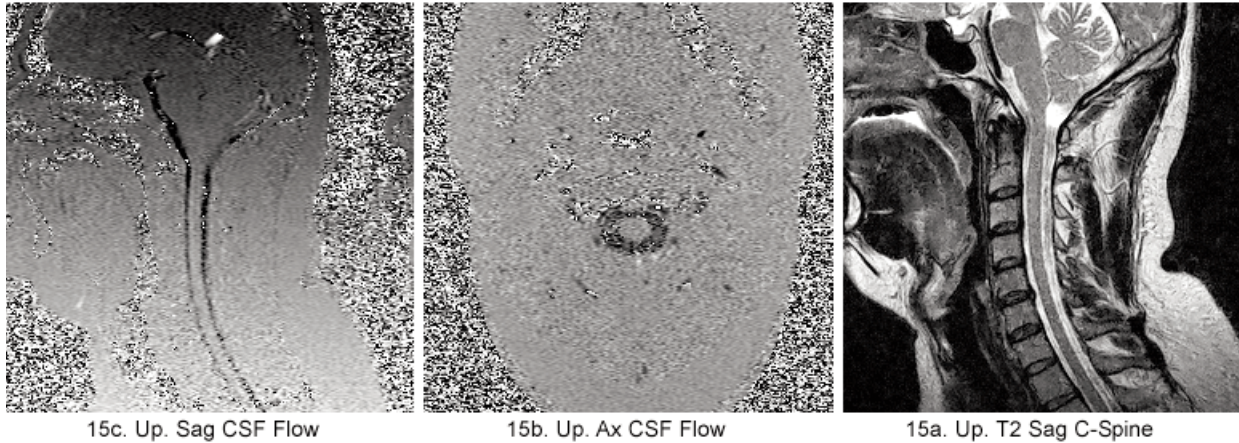
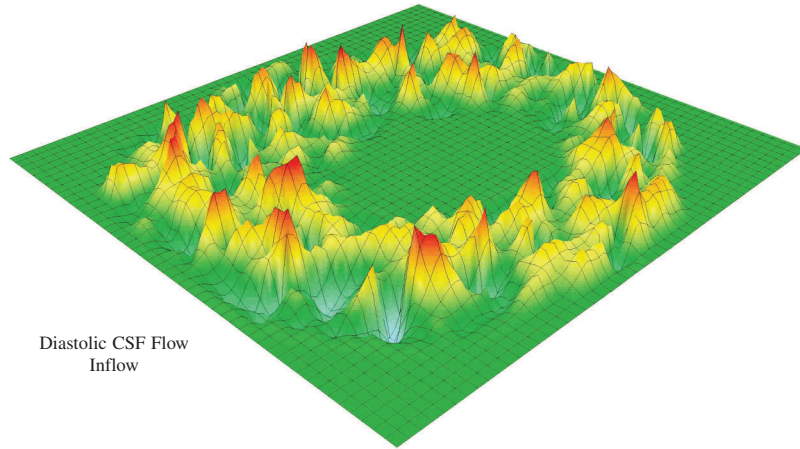
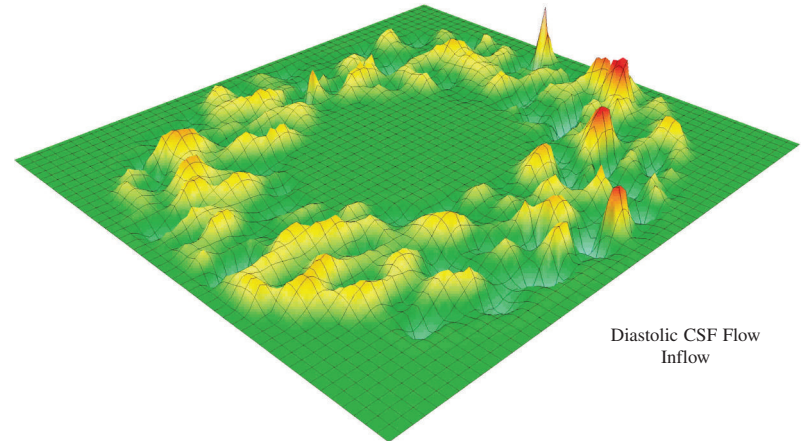


FIGURE 15a–15c. UPRIGHT[®] normal examinee #7 exhibits patent ventral and dorsal CSF channels (Figure 15a) confirmed by full 360° annular circumspinal CSF flow in the UPRIGHT[®] axial image obtained at mid C-2 (Figure 15b black annulus) and by the uninterrupted ventral and dorsal CSF flows exhibited in the UPRIGHT[®] sagittal CSF flow study (Figure 15c black channels).



Diastolic CSF Flow
Inflow

Pre-treatment
Figure 16a



Diastolic CSF Flow
Inflow

Post-treatment
Figure 16b

CSF Pixel* Velocities at mid C-2 in MS Patient #8 Before and After Successful Treatment.

The malalignment of C-1 found by the FONAR UPRIGHT® MRI images of the cervical spine of MS patient #8 in the upright position was successfully treated by Dr. Scott Rosa, using the Atlas Orthogonal (AO) instrumentation. She is the first MS patient of this study of MS patients that has been treated thus far. The patient's symptoms, severe vertigo accompanied by vomiting when recumbent and stumbling from unequal leg length, ceased upon treatment. Figure 16a are the pixel* velocity maps of CSF in the peri-spinal CSF annulus at mid C-2 in the upright symptomatic patient prior to treatment. The CSF void in the center is the spinal cord. Figure 16b are the pixel velocity maps of the upright asymptomatic patient immediately following treatment with the AO instrument. Pixel velocities were obtained from the axial CSF flow MR images obtained at C-2. Figure 16b exhibits an overall reduction in CSF velocity as well as a distinct reduction in the number of CSF flow jets (red), compared to the number of flow jets present in the symptomatic patient prior to treatment (Figure 16a). In addition, average CSF velocity (average peak height) was reduced in the asymptomatic MS patient following treatment as compared to the symptomatic patient prior to treatment. CSF Flow was also more homogeneous (less peak height variation) in the asymptomatic patient than in the symptomatic patient. The CSF pixel velocities of Figure 16 were computed and mapped by FONAR scientists-engineers Michael Boitano and Bob Wolf. The CSF flow measurements obtained immediately following successful AO treatment of the patient and the cessation of her MS symptoms also exhibited a 28.6% reduction of the patient's measured CSF pressure gradient. The patient is currently being maintained free of MS symptoms (vertigo and vomiting on recumbency) by weekly treatments with the AO instrument.

* 3D pixels (voxels)

Dolar, M.T., Haughton, V.M., Iskandar, B.J. and Quigley, M. (2004) Am. J. Neuroradiol., 25:142 reported analogous reductions in CSF pixel velocities in Chiari I patients after surgical decompression.

that reduced to a 5.7° rotation (Figure 1e & 1f) when the patient was *recumbent*. Another example is patient #2. In patient #2, the spinal canal stenosis in the *upright* position at C5/6 (Figure 2f opposite white arrows; Table 2A, col. 8), that was the result of disc herniation, osteophyte compression and retrolisthesis of C-5 obstructing the anterior spinal canal, was further compounded in the upright position by anterior infolding of the ligamentum flavum obstructing the dorsal spinal canal at C5/6 and at C6/7. The canal stenosis in patient #2 was substantially reduced in the *recumbent* position where the ligamentum flavum infolding became non-existent and non-obstructive of the dorsal spinal canal when the patient was *recumbent* (Table 2A, col. 8 & 9). See Table 2A, col. 8 & 9 for the remainder of the important differences in anatomic pathology in the *upright* and *recumbent* positions. Similarly, obstructions of CSF flow were more pronounced in the *upright* position than in the *recumbent* position (Table 2A, col. 10 & 11).

Upright and Recumbent MR Images of Multiple Sclerosis Patients

Upright (and recumbent) MR images of the MS patients and normal examinees are presented in Figures 1–16.

The compared upright and recumbent MR imaging findings of the brain and cervical spine of the Multiple Sclerosis patients are described in Figures 1–8. The MR images of the normal examinees are contained in Figures 9–15.

As described in Figures 1–8, *ALL* MS patients exhibited specific anatomic pathologies of the cervical spine and corresponding obstructions of CSF flow. Four of the MS patients (MS patients #1, #2, #3 and #7) exhibited severe anatomic pathology, while the remaining four (MS patients #4, #5, #6 and #8) exhibited less striking cervical spine anatomic pathology that was nonetheless accompanied by significant obstructions to CSF flow (patient #4, Figures 4b, 4f, 4g; patient #5, Figures 5b, 5c, 5d; patient #6, Figures 6b, 6e) which CSF flow obstructions could result in increases in ventricular intracranial pressure (ICP), CSF leakages and the genesis of Multiple Sclerosis lesions. Additionally, the hydrocephalus of the occipital horns of the lateral ventricles (Figure 8e) and the ventricular dilatation of the body of the lateral ventricles (Figure 8b) are consistent with the likelihood of an increased ICP in patient #8.

The findings raise the possibility that interventions might be considered to restore normal intracranial CSF flow dynamics and intracranial pressure (ICP) as well as surgical procedures to correct the causative anatomy if non-invasive procedures prove insufficient.

Discussion

Struck and Houghton have pointed out in their study of CSF *flow* obstruction in Chiari patients that “the increased CSF flow *velocities* are associated with steeper pressure gradients across the foramen magnum” (10).

Alperin *et al.* have further established that there is a linear correlation between the measured CSF pressure gradient and the measured CSF Intracranial Pressure (ICP) when CSF dynamics are measured *in vivo* (11). As Alperin reported, “A twofold increase in the amplitude of the oscillating pressure (ICP) yielded a twofold increase in the amplitude of the pressure gradient” (11, p. 881).

Accordingly, the elevated peak CSF *velocities* measured in the MS patients of this study would indicate the existence of elevated intracranial pressures (ICP) in these MS patients.

Additionally, three of the eight MS patients (Table 2A, col. 6 & 7, patients #2, #4 and #5) *directly* exhibited elevated peak-to-peak CSF pressure gradients by MRI.

Accordingly, the increases in the peak-to-peak pressure gradients of these MS patients and the accompanying ICP increases can directly be the origin of the CSF “leaks” that appear evident in MS patient images and evident in their *peri-ventricular distribution* (Figure 1a, Figures I, II). Consistent with the findings of Struck and Haughton (10), the MS patients of this study who exhibited elevated CSF peak **inflow velocities** in the *up-right* position (Table 2A, col. 4, patients #2 and #5, 1.047, .731) also exhibited elevated peak-to-peak pressure gradients when upright (Table 2A, col. 6, .054, .050 mmHg/cm) as compared to the normal examinees (Table 2B, col. 6, .0177).

The existence of peri-ventricular interstitial edema, Figure 1–8, in the MR images of the brain of all eight of the MS patients of this study is further consistent with the prospect that an increase in ICP is playing a role in generating MS “plaque” lesions.

The Possible Role of CSF “Leaks” in the Genesis of MS Lesions

The most important finding of this study is that cerebrospinal fluid “leaks” from the ventricles of the brain into surrounding brain parenchyma, possibly secondary to trauma induced blockages of CSF flow and resulting increases in ICP, may be playing an important *etiologic role* in the genesis of Multiple Sclerosis. The existence of such possible CSF “leaks” contributing to MS plaque formation could not be known until MS plaques themselves became readily visible on medical images. The advent of MRI made this a reality (1). Such CSF “leaks” could not have been seen prior to MRI, and a role for CSF “leakage” in the genesis of MS could not have been known prior to the advent of MRI and prior to the availability of phase coded MR imaging. These combined technologies have now made CSF flows directly visible and quantifiable.

The first suggestion of this possibility arose from the T₂ weighted sagittal brain image of a patient with MS (Figure 1a, patient #1) displaying an explicit CSF connection between ventricular CSF and one of the patient’s MS lesions (Figure 1a, arrow #1). Another lesion in the same image exhibits a similar direct connection to ventricular CSF but in a less striking manner (Figure 1a, arrow #2). In addition, the *peri-ventricular distribution* of MS lesions naturally gives rise to the question that if MS lesions are not correlated in any way to CSF hydrodynamics, why are they not randomly distributed *throughout* the white matter of the brain, instead of being clustered around the ventricles of the brain. Further consistent with the possibility that MS plaques originate as CSF “leaks” secondary to trauma, is the existence of Dawson’s fingers (Figure I) where the “long axis of the (MS) plaque” is “*parallel* with the *white matter fibers* in the corona radiata”, i.e., not within the white matter fibers themselves but *parallel* to them. “Dawson’s fingers” might well be the “leak” pathways of cerebrospinal fluid originating in the ventricle and joining the body of the MS plaque within the brain parenchyma. *Parallel* to the white matter fibers would be the path of least resistance for “leaking” CSF to diffuse within the brain parenchyma, i.e., *alongside* the white matter fibers.

Protein is the principal ingredient, other than water, of the cerebrospinal fluid. CSF contains approximately 15 to 40 mg/dL of protein (12). CSF gel electrophoresis has estab-

lished that there are “more than 300 polypeptides in CSF” (13). In addition, “nine antigenic species have been demonstrated in CSF that are absent in serum” (14). The question naturally arises whether the “leakage” of these CSF antigenic proteins, like the antigenic tau proteins they are known to contain (15), could be the source of the antigens generating the autoimmune reactions known to be the origin of MS lesions.

If trauma induced “leakage” of CSF proteins into the surrounding brain parenchyma, and particularly “leakage” of antigenic proteins, is contributing to the formation of MS plaques, then the vascular expansion stenting of the Azygous and Internal Jugular Veins recommended by Zamboni *et al.* (16) could be *monitored after installation* by UP-RIGHT® phase coded MRI *measurements of CSF flow*. Upright phase coded imaging of CSF flow would assure that installed expansion stents are achieving the corrections of CSF flow dynamics and intracranial pressure (ICP) that are needed to terminate plaque generating CSF “leaks”.

It is possible that those patients who currently do not respond to the Zamboni vein expansion stents or those who relapse are relapsing or not responding because the necessary restoration of normal CSF hydrodynamics and normal ICP has not been fully accomplished by the initial venous stenting procedure or is not being maintained.

Schoser *et al.* have reported that an increase in ICP is associated with an increase in blood velocity in the straight sinus (17). One possible explanation, therefore, for the success of the Zamboni *et al.* expansion stent procedure (16) could be that the Zamboni expansion stent is diminishing blood flow velocity in the straight sinus and BVR (Basil Vein of Rosenthal), thereby reducing ICP and diminishing plaque generating CSF “leaks”.

Alperin *et al.* increased the measured ICP in their experimental animal (baboon) by restricting “jugular venous outflow” by “applying pressure over the neck region”. The reduced “jugular venous outflow” resulted in an increase in the animal’s measured intracranial pressure (ICP), demonstrating that reduced “jugular venous outflow can result in increased ICP”. The reduced jugular venous outflow observed by Zamboni to exist in MS patients further suggests the presence of an elevated intracranial pressure in MS patients and that the successful response of MS patients to Zamboni *et al.*’s placement of expansion stents placed in the Internal Jugular Vein is the result of lowering MS patients’ ICP closer to normal.

Noteworthy in this context is the recent report by McKee *et al.* who found abnormal forms of the immunoreactive tau proteins in lesions in the brain and spinal cords of professional athletes who had experienced repetitive head trauma (18). Since the tau proteins are a normal component of CSF (12), the possibility arises that “leaks” of ventricular CSF (Figures 1a, I, II, 1g, 1h, 2c, 3d, 4c, 4d, 5f, 5g, 7d, 7e, and 7f), secondary to trauma, could also be the origin of the antigenic tau proteins found in these repetitive head trauma patients (18).

In addition, the tau proteins have been identified as a significant participant in Alzheimer’s disease. The possibility that they too are originating in the ventricular CSF, possibly secondary to increases in ICP, raises the prospect that Alzheimer’s may also be the result of pathologic CSF hydrodynamics, which if corrected could halt the progress of Alzheimer’s symptoms. Accordingly, while multiple authors (6,7,8) have fruitfully called attention to the correlation between trauma and the onset of MS, perhaps the “missing link” to date has been the inability to directly “see” the CSF “leaks” and CSF flow obstructions that have now been made visible by phase coded MR imaging. This new power

to dynamically visualize CSF hydrodynamics and its abnormalities opens the prospect of medically restoring pathologic CSF flow dynamics to normal under MR image guidance, thereby eliminating pathogenetic CSF leakages and the symptomatology to which they give rise.

Myelogenesis is a normal physiologic process that repairs damaged myelin over time (19). If the myelin injuring process, i.e., “leaked” antigenic CSF proteins, could be terminated, there is the possibility that with the continuing injury from CSF “leakage” terminated, the demyelinated axons of MS lesions could be remyelinated by normal physiologic myelogenesis and the MS lesions repaired.

The findings further suggest that going forward, victims of Motor Vehicle Whiplash injuries with persisting symptoms, e.g., headache, neck pain, should be scanned by UPRIGHT® MRI to assure that their CSF hydrodynamics and cervical anatomy (C1-C7) are normal. Should their CSF hydrodynamics prove abnormal, they should be monitored by UPRIGHT® MRI to assure they are restoring to normal over time, or ultimately decompressed by expansion stenting or cervical realignment if they are not.

Cervical Spine Trauma Pathology and Resulting CSF Flow Obstructions May Increase ICP and Produce Plaque Generating CSF “Leakage”

In conclusion, the results of our investigation suggest that Multiple Sclerosis may be biomechanical in origin wherein traumatic injuries to the cervical spine result in cervical pathologies that impede the normal circulation of CSF to and from the brain. The resulting obstruction of CSF **outflow** from the brain impairs the outflow of CSF from the lateral ventricles of the brain where 500 cc of cerebrospinal fluid is generated daily by the choroid plexuses (20). The obstruction to CSF **outflow** would result in an increase in ventricular CSF pressure (ICP) which in turn could result in “leakage” of cerebrospinal fluid and its content of more than 300 polypeptides and at least six (6) antigenic proteins (e.g., tau proteins) into surrounding brain parenchyma. The attachment of antigenic proteins to surrounding brain nerve fibers would stimulate the antigen-antibody reactions that produce the axon demyelinations characteristic of MS.

The authors wish to thank Scott Rosa, David Harshfield, Francis Smith and Jevan Damadian, *et al.* for initiating the use of the FONAR UPRIGHT® Multi-Position™ MRI technology for visualizing cerebellar tonsil ectopia (CTE) in automobile whiplash injuries (21). Their demonstration of the power of the FONAR UPRIGHT® Multi-Position™ MRI technology for imaging brain injury patients prompted us to enquire about the role of brain injury in Multiple Sclerosis when we observed, for the first time, the ventricular CSF connection to an MS lesion that was seen in patient #1.

References

1. Young, I.R., Hall, A.S., Pallis, C.A., Bydder, G.M., Legg, N. J., Steiner, R.E. (1981) *Lancet*, 318:1063–1066.
2. Laxhanpal, S.K. and Maravilla, K.B. (1999) in *Magnetic Resonance Imaging*, Eds. Stark, David D., Bradley, Jr., William G., Edition III, p. 1381, Figure 61-2, 61-3, Mosby, Inc.
3. Alperin, N., Sivaramakrishnan, A., Hushek, S.G., (2005) *Journal of Magnetic Resonance Imaging*, 22:591–596.

4. Houghton, V.M., Korosec, F.R., Medow, J.E., Dolar, M.T., and Iskandar, B.J. (2004) *AJNR, Am. J. Neuroradiol.*, 24:169.
5. Ouchi, Y., Nobezaawa, S., Yoshikawa, E., Futatsubashi, M., Kanno, T., Okada, H., Torizuka, T., Nakayama, T. and Tanaka, K. (2001) *J. Cerebral Blood Flow and Metabolism*, 21, p. 1058 (1058–1066).
6. Brain, W., Wilkinson, M. (1957) *Brain* 80:456–478.
7. Poser, C.M. (2000) *Arch. Neurol.* 57:1074–1077.
8. Martinelli, V. (2000) *Neurol. Sci.*, 21:5849–5852.
9. Bunketorp, L., Nordholm, L., Carlsson, J. (2002) *Eur. Spine J.* 11:227 (227–234).
10. Struck, A.F and Houghton, V.M. (2009) *Radiology* 253, No. 1, p. 185.
11. Alperin, N., Lee, S., Loth, F., Raskin, P., Lichtor, T. (2000) *Radiology* 217:877–885, Figure 8.
12. Felgenhauer, K. (1974) *Klin. Wochenschr.* 52(24):1158–1164.
13. Merrill, C.R., Goldman, D., Sedman, S.A., Ebert, M.H. (1981) *Science* 211:1437–1438.
14. Laterre, C., Heremans, J., Carbonara, A. (1964) *Clin. Chim. Acta.* 10:197.
Bock E. (1973) *A Manual of Quantitative Immunoelectrophoresis*, Axelen, N.H., Kroll, J., Weeke, B., Eds., *Universitetsforlaget*, Oslo, pp. 119–124.
15. Sjögren, M., Vanderstichele, H., Ågren, H., Zachrisson, O., Edsbacke, M., Wikkelso, C., Skoog, I., Wallin, A., Wahlund, L., Marcusson, J., Nägga, K., Andreasen, N., Davidsson, P., Vanmechelen, E., Blennow, K. (2001) *Clinical Chemistry* 47: 1776–1781.
16. Zamboni, P., Galeotti, R., Menegatti, E., Malagoni, A., Gianesini, S., Bartolomei, I., Mascoli, F., Salvi, F. (2009) *J. Vascular Surgery* 50(6):1348–1358.
17. Schoser, B., Reimenschneider, N., Hansen C. (1999) *J. Neurosurg.* 91:744–749.
18. McKee, A., Gavett, B., Stern, R., Nowinski, C., Cantu, R., Kowall, N., Perl, D., Hedley-Whyte, E., Price, B., Sullivan, C., Morin, P., Lee, H., Kubilus, C., Daneshvar, D., Wulff, M., Budson, A. (2010) *J. Neuropathol. Exp. Neurol.* 69(9):918–929.
19. Xin, M., Yue, T., Ma, Z., Wu, F., Gow, A. and Lu, Q. (2005) *J. Neurosci.* 25(6):1354–1365.
20. Department of Neurological Surgery, Columbia University Medical Center (<http://www.columbianeurosurgery.org/conditions/adult-hydrocephalus>).
21. Freeman, M., Rosa, S., Harshfield, D., Smith, F., Bennett, R., Centeno, C., Kornel, E., Nystrom, A., Heffez, D., Kohles, S. (2010) *Brain Injury*, 24(7–8):988–994.

*Received June 8, 2011;
accepted June 22, 2011.*

Truth in Basic Biomedical Science Will Set Future Mankind Free

Gilbert N. Ling

*Damadian Foundation for Basic and Cancer Research
Tim and Kim Ling Foundation for Basic and Cancer Research
110 Marcus Drive, Melville, NY 11747
E-mail: gilbertling@dobar.org*

Abstract: It is self-evident that continued wellbeing and prosperity of our species in time to come depends upon a steady supply of major scientific and technologic innovations. However, major scientific and technical innovations are rare. As a rule, they grow only in the exceptionally fertile minds of men and women, who have fully mastered the underlying basic sciences. To waken their interest in science at an early critical age and to nurture and enhance that interest afterward, good textbooks at all level of education that accurately portray the relevant up-to-date knowledge are vital. As of now, the field of science that offers by far the greatest promise for the future of humanity is the science of life at the most basic cell and below-cell level. Unfortunately, it is precisely this crucial part of the (standardized) biological textbooks for all high schools and colleges in the US and abroad that have become, so to speak, fossilized. As a result, generation after generation of (educated) young men and women have been and are still being force-fed as established scientific truth an obsolete membrane (pump) theory, which has been categorically disproved half a century ago (see Endnote 1.) To reveal this *Trojan horse* of a theory for what it really is demands the concerted efforts of many courageous individuals especially young biology teachers who take themselves and their career seriously. But even the most courageous and the most resourceful won't find the task easy. To begin with, they would find it hard to access the critical scientific knowledge, with which to convert the skeptic and to rally the friendly. For the wealth of mutually supportive evidence against the membrane (pump) theory are often hidden in inaccessible publications and/or in languages other than English. To overcome this seemingly trivial but in fact formidable obstacle and to reveal the beauty and coherence of the existing but untaught truth, I put together in this small package a collection of the major clenching theoretical and experimental findings. These findings will remove the last trace of uncertainty about the total disproof of the membrane theory. In addition, I have also included an introduction of the association-induction hypothesis, which is the *one and only* unifying theory of the living cell that has survived and unwaveringly grown more comprehensive and powerful after more than half of a century of worldwide testing.

(In Endnote 1 on page 43, I will show: (1) how (one of the postulated membrane pumps,) the sodium pump (alone) would consume at least 15 to 30 times the total available energy of muscle cells; and (2) that, pump or no pump, they are all variants of the membrane theory, and as such long dead.

IN DECEMBER 1910, the Irish physical chemist, Frederick G. Donnan presented at the London Physiological Society, a summary of what was to be known later as the Theory of Donnan Equilibrium. The full version of the theory was written in German, and published in the year following (Donnan 1911). Translated into English, the title of the article reads: *Theory of Membrane Equilibrium and Membrane Potential from the Presence of Non-dialyzable Electrolytes: A Contribution to the Physico-chemical Physiology*.

From this and others closely following publication(s) of Donnan and his coworkers, I summarize the Donnan theory as follows:

A membrane of the right kind separates two solutions named respectively solution 1 and solution 2. Both solutions contain one (or more) permeant (being able to permeate) ionic species, but solution 1 alone contains an ionic species, to which the membrane is impermeable (being unable to permeate). As a result, an electrical potential difference, ψ , would develop at equilibrium between the two solutions. Referred to as a *membrane potential*, ψ equals in magnitude the difference between the electrical potential, P_1 , in solution 1 and the electrical potential, P_2 , in solution 2. This relationship is summarized in Equation 1, where n represents the valence of the permeant ion species and that C_1 and C_2 are respectively their concentrations in the two solutions. R , T and F are the gas constant, the absolute temperature and the Faraday constant respectively.

$$\psi = P_1 - P_2 = (RT/nF) \log (C_1/C_2). \quad (1)$$

Alternatively, we may write

$$\psi = P_1 - P_2 = (RT/F) \log r, \quad (2)$$

where

$$r = (C_1^+ / C_2^+)^{1/x} = (C_2^- / C_1^-)^{1/y}. \quad (3)$$

In Equation 3, C_1^+ and C_2^+ are respectively the concentrations of the *permeant cation* of valency x in solution 1 and 2. C_2^- and C_1^- are respectively the concentrations of the *permeant anion* of valency y in the two solutions. A simplified version of Equation 3 is Equation 4:

$$(C_1^+ / C_2^+)^{1/x} = (C_2^- / C_1^-)^{1/y}. \quad (4)$$

Equation 3 and 4 illustrate the pervasive *connectedness* of the Donnan membrane equilibrium. That is, a change in the concentration of one ionic species invariably alters the equilibrium concentrations of *all* the other ionic species present. However, to gain a deeper insight into the background of Donnan's theory, we need to know something about Donnan's personal history.

Donnan was born in Colombo, Ceylon but returned to Ireland at the age of 3. He was educated in Queen's College in Belfast. In 1893 he went to Leipzig to study under the renowned physical chemist, Wilhelm Ostwald (1853–1932.) In 1896–1897 he moved again — this time to study under another famous physical chemist, Jacobus van't Hoff (1852–1911) in Berlin. For reasons described below, I mention that in 1885 van't Hoff

(rather casually) introduced the concept of *semipermeability* to describe a membrane that is permeable to water but impermeable to (all) ions, molecules and other solutes dissolved in water (van't Hoff 1887).

However, to the best of my knowledge, semipermeable membrane as van't Hoff originally described in these words has not been observed in the real world. Instead, a membrane found permeable to water is invariably permeable also to some solutes. In time, the definition of the term, semipermeability has gradually loosened to denoting permeability to water and some solutes but not to others. As an example, Donnan's one-time teacher, Wilhelm Ostwald showed that a copper-ferrocyanide precipitation membrane is impermeable to sucrose but permeable to water and the positively charged potassium ion, K^+ (Ostwald 1890.)

As a whole, Donnan made an important contribution to general physiology (*algemein Physiologie* — a name first introduced by H. Dutrochet (1776–1847), see Rich 1926, p. 359,) by providing a quantitative physico-chemical framework, on which to erect and to test sundry subsidiary hypotheses of the properties and behaviors of the living cell. In the section immediately following, I shall demonstrate how, at that time, investigators came to believe that Donnan's theory can explain not only (1) cell **membrane permeability** *per se*, but also three other cardinal attributes of the living cell: (2) **solute distribution**, (3) **swelling and shrinkage** and (4) **electric potential**.

1. Membrane permeability

Hugo deVries (1848–1935) was a highly productive and influential botanist. He introduced the term, *Plasmolysis* (and its reversal, *deplasmolysis*) to describe the stepwise shrinkage of water-filled protoplast of a large mature plant cell when immersed in a concentrated solution of sucrose or sodium chloride (NaCl) as illustrated in Figure 1.

deVries gained wide recognition for demonstrating that the protoplast of the root hair cells of red beet, when immersed in a concentrated NaCl solution, stayed shrunken for 7 days (deVries 1871.) This experimental observation convinced many contemporary investigators that the cell membrane of (at least some) plant cells is indeed impermeable to NaCl. Yet in undergoing shrinking, the root cell also clearly shows that the same cell membrane is fully permeable to water.

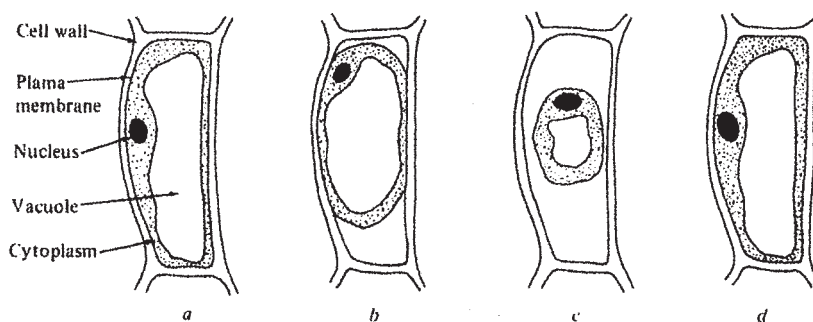


FIGURE 1. Diagrammatic illustration of successive stages in the plasmolysis (b,c) of a mature plant cell (a) and deplasmolysis (d). (From Dowben 1959)

deVries also introduced the so-called *osmotic method* to determine the permeability or impermeability of biological membranes (de Vries 1884.) To wit, solutes like NaCl that cause sustained protoplast shrinkage in large plant cells when added to the bathing solution are considered impermeant. Solute that do not cause protoplast shrinkage at all are considered highly permeant. Solute that cause transient protoplast shrinkage followed by recovery to its initial volume are considered moderately permeant (Ling 2007, p.26.)

Eighteen years after deVries's epochal finding on red beet hair cells, Emil Abderhalden announced another historic discovery of lasting importance (Abderhalden 1898.) He demonstrated that the human red blood cell contains no (or very little as proven later) sodium ion (Na^+) even though the blood plasma, in which the red blood cell spends its life, contains an abundance of Na^+ .

Considered together, the discoveries of deVries and of Abderhalden support the belief that both *plant* and *animal* cells are permeable to water but impermeable to Na^+ , which is, of course, the dissociated (or ionized) cationic component of NaCl. As such, these discoveries offered — or appeared to offer — experimental verification of the (loosened) definition of semipermeability, which provides the conceptual foundation of Donnan's theory of membrane equilibrium.

2. Swelling and shrinkage

Shortly after Donnan introduced his membrane equilibrium theory, Höfler (1918) worked out a method of measuring the (changing) volume of the irregularly shaped protoplast during *plasmolysis* (Figure 1.) Using this method, Höfler showed that mature plant cells do indeed behave like a *perfect osmometer*. That is, the product of the equilibrium volume of the protoplast (v) and the osmotic pressure (π) of the surrounding medium is a constant — as van't Hoff had pointed out in his classical theoretical work (for details, see Ling 2007, pp. 20–21.) In their 1932 review, McCutcheon and Lucké hailed Höfler's finding as offering the ultimate proof of the membrane theory (McCutcheon and Lucké 1932 pp. 86–87.)

3. Cellular electrical potential as membrane potential

Julius Bernstein (1839–1917) was a student of the great physicist-physiologist, Ludwig von Helmholtz (1821–1894) — a member of the *Reductionist Four*, who shared the belief that the laws governing the inanimate world govern the living too (Ling 2001, p. ii.)

Bernstein took seriously Ostwald's earlier suggestion (Ostwald 1890) that the electric potential he (Ostwald) observed across a copper ferrocyanide membrane (separating two K^+ -containing solutions of different strength) might underlie not only the *resting (or injury) potential* of muscle and nerve but also the electric shocks delivered by electric eels.

However, it was not until the year 1902, when Bernstein was already 63 years old, that he finally published what he called the Membrane Theory of cellular electrical potential. He too called the cellular resting potential a *membrane potential* — ten years before Donnan made the same designation (Bernstein 1902, p. 54.)

Bernstein derived his equation for his membrane potential on the basis of an equation for diffusion introduced by W. Nernst (1889, see also Nernst 1892). Representing the membrane potential measured across the resting healthy cell surface as E , the Bernstein equation takes the following form:

$$E = (RT/F) \log ([K^+]_{in} / ([K^+]_{ex})), \quad (5)$$

where R, T and F are as defined for Equation 1 above. $[K^+]_{in}$ and $[K^+]_{ex}$ are the intracellular and extracellular K^+ concentrations respectively.

Donnan's theoretical model of membrane potential as shown in Equation 2 is in fact a more generalized version of what Bernstein suggested earlier in the form of Equation 5. However, there are significant differences between the two models. Bernstein's model requires two essential *a priori* assumptions. That is, the cell membrane must be impermeable to both the major anion in the bathing medium, Cl^- as well as the major cation of the bathing medium (blood plasma), Na^+ . In contrast, Donnan's model requires only one *a priori* assumption. Namely, the cell membrane is impermeable to Na^+ .

The relationship between E (or ψ) and the absolute temperature T and that between E (or ψ) and $\log [K^+]_{ex}$ in both Equation 1 and Equation 5 have been confirmed repeatedly, especially after new techniques were introduced to measure accurately the potential of individual living cells. These new techniques include that of impaling isolated (single) giant axons of squid and cuttlefish (Curtis and Cole 1942, Huxley and Stämpfli 1951.) And the technique of impaling single muscle fiber (and other large and small single cells) with the aid of the Gerard-Graham-Ling (*aka* Ling-Gerard) microelectrode (Ling and Gerard 1949, Ling 2007, pp. 46–49.)

4. Selective ionic accumulation

Membrane permeability is a rate process. As such, it deals with a *transient* event. Abderhalden's discovery that red blood cells contain no Na^+ (or very little Na^+ , as later work showed) was historically important for yet another reason. It shows that the asymmetric ionic composition of living cells persists throughout the entire life of the cell. As a result, a valid theory of the living cell must provide a mechanism for attributes that *endure* in time. On the surface at least, Donnan's theory answers this need. For it is an *equilibrium* theory — meaning it could in theory stay unchanging forever.

In harmony with this agreement, Hans Netter of the University of Kiel suggested that ionic distribution in living muscle, nerve and red blood cells could all be neatly explained in terms of the Donnan theory of membrane equilibrium (Netter 1928.) Mond and Amson from the same university also introduced a set of important ideas in that same year. That is, the permeability of the muscle cell membrane to K^+ and impermeability to Na^+ could be the result of the existence of a limiting membrane pore size that allows the passage of the smaller (hydrated) K^+ but not the larger (hydrated) Na^+ (Mond and Amson 1928.)

However, it was Boyle and Conway in their paper published in the 100th volume of the prestigious (English) Journal of Physiology that had taken Donnan's theory of membrane equilibrium to its full height — on all four of the cardinal attributes of cell physiology mentioned above.

Regrettably, Boyle and Conway did not give due credit to Netter, nor to Mond/Amson, for ideas mentioned above, which these German scientists introduced first. (See Ling 1992, p. 4.) Perhaps it was the on-going War (WWI) with Germany that warped their judgement.

In the Boyle/Conway theory, the living cell membrane acts like an *atomic sieve*, an idea that was suggested 74 years before by Maurice Traube (1867) for his inanimate semipermeable copper-ferrocyanide membrane. Following Mond and Amson, Boyle and Conway

also postulate a limiting pore size permitting the passage of smaller (hydrated) K^+ but not the larger (hydrated) Na^+ . Notwithstanding, Boyle and Conway's theory is far more advanced than the simple but seminal ideas Traube and Mond/Amson introduced respectively. For details, the reader must consult Boyle and Conway's original work. A few high lights are given below:

The Boyle-Conway version of the atomic sieve theory could apparently explain why muscle cell contains an abundance of K^+ at a high Donnan ratio (r) of 40. It could also explain why chloride ion, though proven fully permeant by Boyle and Conway (1941), exists at a very low level. That too could be construed as being equal to the Donnan theoretical value of $1/40$ (Equation 3 and 4.)

On a still broader perspective, Boyle and Conway's theory also offers reasonable explanations of cell swelling and shrinkage (see also Proctor and Wilson 1916) and the cellular electric potential as described by Equation 5 (see Ling 1984, p. 34.)

In summary, Boyle and Conway's theory published in 1941 represents the pinnacle in the application of Donnan's theory of membrane equilibrium to the living cell. As such, it took on the shape of a unifying, all-encompassing membrane theory. For his work on the (Donnan) membrane equilibrium, Donnan received the Davy Medal of the Royal Society of London in 1928.

Then suddenly a chain of unexpected events that would turn the world of cell physiology upside-down made their appearances — even though at that time, many researchers in cell physiology, whose work would be profoundly affected, did not know. In that I was no exception.

A set of dramatic top-to-bottom “turn-arounds” (with their coherence seen only in hind sight many years later)

1. A decisive new tool of unprecedented importance

In the late 1930's, a tool for accurately measuring membrane permeability emerged for the *first time* in history: *radioactive tracer technology*. Almost overnight, studies with the aid of radioactive tracers like ^{24}Na have falsified the widely if not universally-held belief that the cell membrane is impermeable to Na^+ . But that was not all.

In fact, as more and more radioactive tracer studies were performed and reported, it became clear that most if not all the ions and molecules hitherto considered impermeant are in fact permeant (Ling 2007, pp. 43–45, pp. 58–59.)

2. Disproof of the validity of the Osmotic Method itself

In 1937 the Soviet scientists, Nasonov and Aizenberg published an exceedingly simple but critical experiment.

They immersed frog muscles in a concentrated sucrose solution, and observed that the muscle steadily shrank until it reached and stayed at a new constant volume equal to 92% of its initial weight. There is nothing surprising in that. What is surprising is the fact that while the muscle cells were shrinking, they were also steadily taking up sucrose until it too reached a constant level *inside* the cells. The authors concluded that membrane impermeability was not the cause of cell shrinkage caused by sucrose, nor is it the cause of

the low concentration of sucrose in normal resting muscle cells. The essence of this piece of work was repeated and confirmed by Kamnev (1938.)

Now, muscle tissues are, as a rule, made of bundles of parallel-running fiber-like muscle cells. The space between the individual muscle fibers is called the *extracellular space* (ecs), which is filled with whatever the bathing solution contains. In the experiments described above, it is mostly sucrose. Clearly, the validity of their conclusion that sucrose had in fact penetrated and accumulated *within* the muscle cells, depends critically on the correct choice of the volume percentage of the ecs of the frog muscle they used. Kamnev adopted an ecs value of 9%, a figure which is lower than earlier estimates. Thus, Boyle and Conway in the work described earlier used an ecs value of 13%. (For still other high estimated values, see Troshin 1966, Table 56 on p. 224.) Which one is right?

It is therefore fortunate that my coworkers and I, using a total of five independent methods, four of which are totally new, had extensively investigated this problem and reached what seemed to be a reasonable conclusion. That is, the ecs of the most widely used frog muscle (the sartorius muscle) averaged $9.2\% \pm 0.69\%$, which agrees well with Kamnev's figure of 9% (Ling 2001, p.44.)

The three Soviet scientists's simple experiment described above was the first to invalidate incisively the Osmotic Method for determining the membrane permeability of solutes, which deVries introduced and was used in a major share of the experiments that lent support for the membrane theory up to that time.

3. Höfler reversed his earlier stand

On further investigating the protoplasm of mature *Tradescantia* cells, Höfler discovered that his earlier conclusion on the semipermeability of the cell membrane was wrong — and, to his credit, he made his new conclusion known without delay (Höfler 1926, 1932.) That is, it was the inner vesicular membrane (also called tonoplast) in immediate contact with the watery fluid in the central vacuole of the mature plant cell that is semipermeable (See Figure 2.) The outer cell (or plasma) membrane of the protoplast directly in contact with the external bathing solution is freely permeable to sucrose — thereby once more changing an earlier strong support for the impermeability of the living cell membrane to sucrose to evidence against it.

4. Mg^{++} and K^+ distribution in the same living cells are shown to be completely independent, refuting the predicted constancy of the Donnan ratio, r

When the rare radioactive tracer $^{28}Mg^{++}$ became available momentarily in the United States, Ling, Walton and Ling (1979) were in a position to take full advantage and conducted a detailed study of the equilibrium distribution in frog muscle cells of this divalent ion side by side with that of the mono-valent K^+ . The main conclusion from this study is that *the distribution of these two types of ions, one mono-valent and the other divalent, are entirely independent of each other.* In other words, changing the concentration of one kind of ion in the external environment had no detectable influence on the distribution of the other kind.

This finding again irreconcilably contradicts Donnan's theory of membrane equilibrium. As illustrated in Equation 3 and 4, the theory predicts that all ions present in the

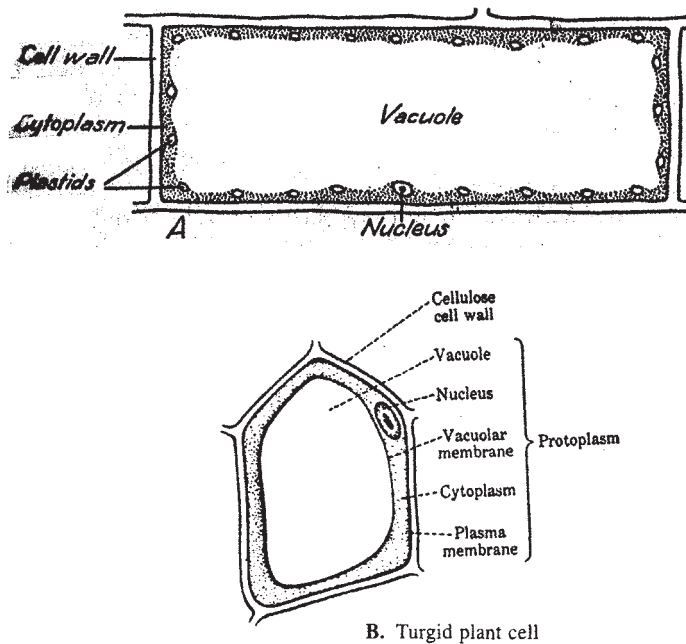


FIGURE 2. Diagrammatic illustration of a mature plant cell. (From Glasstone's Textbook of Physical Chemistry, van Nostrand, 1946.)

same system are “connected”. In other words, all ions present in the system, whatever their valency and charge, should distribute in such a manner as to yield the same Donnan ratio, r (see Equation 4 on p. 20.) When the Donnan ratio of one ion changes, the Donnan ratio of all ions within the whole system change with it to assume the same new value. Our experiments showed just the opposite.

(The equilibrium distribution of both Mg^{++} and of K^+ in fact follow rigorously the two-term Troshin equation, see p. 115 in Troshin 1966 and also p. 163 in Ling 2007 for this equation. See also the puzzling question, Why the two-term equation should contain only two terms at all in such a complex system as a living muscle cell? The answer given on page 220, paragraph 5 in Ling 2007 marks an exciting high point in the evolving history of the AI Hypothesis.)

A simple but fatal mistake made 100 years ago in the original derivation of Donnan's theory of membrane equilibrium — until now, undisclosed

In his admirable Textbook of General Physiology, Sir William Maddox Bayliss pointed out in its Preface that the greatness of a scientist does not lie in his never making a mistake. Rather, it lies in his willingness to admit having made a mistake and promptly publicly correcting it. (Bayliss 1924) For without this willingness of all participating scientists to admit and correct his or her own now-proven mistakes, science as a continuing effort of all Mankind to seek the truth would be paralyzed — as is the case of the fossilization of biology textbooks mentioned in the Abstract of this paper.

By the same token, it is vital for the continued survival and prosperity of science that each member of the scientific community shoulders the duty, no matter how hard, of correcting mistakes made by other scientists as well. In agreement with the spirit of this belief, I want to report something unusual here. That is, in deriving the basic concept of Donnan's theory of membrane equilibrium, a serious mistake had been made and to the best of my knowledge not explicitly described and corrected until now. (But, see below.)

This serious mistake lies in the assumption that there is an electrical potential P_1 or P_2 in each of the two solutions which the semipermeable membrane separates and hence the existence of a membrane potential, Ψ (or E) as their algebraic sum. This assumption is a serious mistake because this it violates the Law of Macroscopic Electroneutrality. (see Nernst 1892, Encyclopedia Britanica 2010; Morikawa 2001, Guggenheim 1950.)

Having made this clear, I ask why someone has not explicitly pointed out this glaring error earlier. After all, 100 years is a long time. In fact, someone else did write about the underlying problem — but not in a straightforward way. That someone was no one else than Edward A. Guggenheim, one of the world's foremost thermodynamicist. And, alas, also a co-author of Donnan in the paper Donnan and Guggenheim published conjointly in 1932 in *Zeitschrift für physikalische Chemie*, vol. 162.

The inclusion of the term, $z_i F \Psi$, in Equation 4.2 and 7.2 in this 1932 article and their explanation, " Ψ ...hat denselben Wert für jede Ionenart" (Ψ ...the symbol for electrical potential...has the same value for each ion species,) left no doubt that the mistake was made (by Donnan alone in 1911; by Guggenheim alone in 1929 and by Donnan and Guggenheim conjointly in 1932.)

My guess is that Guggenheim was not fully aware or certain of this mistake until some time between 1932 and 1950 — then he made great effort in his 1950 advanced treatise on thermodynamics, stressing the importance of not violating the Law of Macroscopic Electric Neutrality (on page 330 to page 331.) Notwithstanding, Guggenheim never did come out and admit that he and Donnan had made the mistake.

This is regrettable. It is relevant to remember that Donnan had earlier written a preface for Guggenheim's 1933 book, *Modern Thermodynamics by the Method of Willard Gibbs*, when Guggenheim was still in his twenties. This fact suggests that Donnan might have been a kind and highly respected scientist to young Guggenheim for Guggenheim to come out and announce that Donnan and Guggenheim together had made a serious mistake and it was Guggenheim and not Donnan that had made this discovery.

Well, so much conjecture on a strange mystery that unfortunately could never be fully explained. In the following section, I turn to experimental discoveries that prove once and for all that no measurable electric potentials exist in (macroscopic) solution 1 and 2. Accordingly, no membrane potential Ψ (or E) could exist in the real world or even in theory. Wide-ranging experimental studies described next bears this out.

Converging disproof of the theory of membrane potential Ψ (or E) in each of all four types of membrane models examined

The following are summaries and conclusions of the experimental findings — as a rule unexpected by the authors who made the observations — on four types of membrane

models. They are the glass membrane, the collodion membrane, the oil membrane and the phospholipid membrane. The glass membrane was the first extensively studied and it was also the first cited by a physiologist (Cremer) as a model of the semipermeable cell membrane.

1. Glass membranes.

In 1881, Ludwig von Helmholtz published his study of the electric potentials measured across two aqueous solutions separated by a thin glass membrane (Helmholtz 1881.) Max Cremer (1865–1935), a professor of physiology at the University of Berlin, cited this work and suggested that the glass membrane is a suitable model for the semipermeable membrane of the living cell (Cremer 1906.) The high sensitivity of the glass membrane electrode to H^+ but not to other mono-valent cations was attributed at the time to the (selective) permeability of the hydrated glass channels in the glass membrane to this very small H^+ ion. Then an unusual discovery was announced, to the astonishment of just about everyone in this field of investigation.

As a rule, a glass electrode has no sensitivity to silver ion (Ag^+ .) Yet, it acquired full sensitivity to this ion after soaking overnight in a solution of silver nitrate (Horovitz 1923, aka Lark-Horovitz 1931.) The author Horovitz believed that it is *surface adsorption* of the ion involved rather than bulk phase *permeability* that determines ion specificity of the electric potential measured. In years following, Horovitz's experimental discovery was repeatedly confirmed by Nicolsky (1937), by Haugaard (1941) and by Ling and Kushnir (in Ling 1960 and in Ling 1967.)

2. Oil membrane

In 1892 Nernst pointed out that in two ion-containing phases in contact, the Law of Electric Neutrality does not allow the accumulation of significant electric charges inside each phases. Accordingly it is only at the phase boundaries that ions accumulate and generate electric potential differences (Nernst 1892.) (The question arose, Would Donnan go ahead with publishing his theory if he had discovered and fully understood before 1911 what Nernst wrote in 1892.)

In 1913 Baur again pointed out that the electric potential measured across two aqueous solutions separated by a thin layer of oil, does not arise from the permeability of ions through the oil layer but is due to the adsorption of these ions on the two oil surfaces (Baur 1913.) Four years later, Baur and Kronmann provided additional evidence in support of Baur's adsorption theory. In still later years, Ehrensverd and Sillen (1938) and Colacicco (1965) further confirmed the work of Baur and of Baur and Kronmann.

Colacicco's study was particularly interesting and enlightening. He introduced different concentrations of KCl into the two aqueous solutions that an oil layer separates but found no measurable electric potential difference across the oil layer if the oil layer is just that, a plain layer of neutral oil.

However, if a negatively charged anionic detergent, say, sodium dodecyl sulfate is added to one solution, a dramatic change follows. Now, the side of the oil layer containing the anionic detergent becomes a cation-sensitive electrode. As such, this side of the oil layer gives rise to an electric potential sensitive only to the concentration of the cation,

K^+ in the bathing medium but not to that of the anion, Cl^- also present. However, if instead an anionic detergent, a cationic detergent like cetyltrimethylammonium bromide is added, that side of the oil layer becomes an anion-sensitive electrode responsive only to Cl^- but not to K^+ . Colacicco's finding was in turn confirmed and extended recently by Tamagawa and Nogata (2004.)

3. *Collodion membrane*

In the commercially available form called collodion, nitrocellulose is soluble in mixtures of ether and ethyl alcohol. When the closed end of a glass test tube is dipped into such a collodion solution and allowed to dry in a moist environment, a collodion thimble electrode could be slipped off the test tube and used as model for electric potential studies. As an example, if different concentrations of KCl are added to the solutions bathing two sides of the thimble, a K^+ -sensitive electric potential difference — following more or less the dictate of Equation 5 — will be measured.

In the 1920's, Leonor Michaelis and his coworkers conducted extensive investigations of the collodion membrane electrode as a model of the cell membrane. When Horovitz's iconoclastic discovery became known, the question was raised, Could there be electric charges on the surface of the collodion membrane too? This, Michaelis and Perlzweig (1927) categorically rejected on the ground that nitrocellulose is a neutral substance and devoid of net electric charges. Little could they imagine how the advent of World War II could profoundly change the foundation of their reasoning at the time.

World War II cut off the import from Germany of the Schering brand of collodion, which up to that time, Michaelis's laboratory routinely purchased and used. As a result, Michaelis's students, most importantly, Carl Sollner, had to prepare their own collodion from scratch. To their amazement, the purer the collodion they manufactured, the worse it became as building material for their cell membrane model. In fact, the purest collodion they made generated no electric potential at all.

Then they discovered something few expected. It was an impurity in the Schering brand of collodion that made it a good model-building material. And that impurity was soon identified as carboxyl groups, which can be added at will onto the collodion by merely exposing it to an oxidizing agent like sodium hydroxide or sodium bromide. The oxidized collodion thimble electrode thus prepared behaves very well as a model of the cell membrane: it is fully sensitive to K^+ like the living cell in accordance with the prediction of Equation 5. (For additional evidence that it is the carboxyl groups on the two surfaces of the collodion membrane electrode, see below.)

4. *Phospholipid bilayer membrane*

Measurement of the electric potential difference across phospholipid bilayer membranes yielded equally convincing evidence that it is not the ionic permeability through the membrane but the algebraic sum of two surface potentials on each side of the phospholipid bilayer. Thus, when negatively charged phosphotidic acid was used to make the bilayer, the potential measured is cation-sensitive. When positively charged lysyl phosphotidyl glycerol was used, the bilayer is anion-sensitive. When electrically neutral phosphotidyl choline or diglycolsyl diglyceride was used, the bilayer demonstrates no (or very weak)

sensitivity to cations or anions (Colacicco 1965; Hopfer *et al* 1970; Ohki 1972; McDonald and Bangham 1972.)

Not one of the four types of inanimate models generates an electric potential difference in the way that Donnan's theory predicts. In retrospect, the perfection of this (and other similar) kind of converging experimental evidence provide insight on what a scientific truth really portends.

We now conclude that Donnan's theory of membrane equilibrium and membrane potential has been invalidated because in its theoretical derivation, a key assumption violating the Law of Macroscopic Electric Neutrality has been made. Experimentally, the theory has also been thoroughly disproved. In both inanimate model studies and in the studies of living cells, the predicted behaviors of ions have all been unequivocally falsified. *It is entirely safe to say that Donnan's theory of membrane equilibrium and membrane potential have proven totally erroneous.*

Historically speaking, Donnan's theory of membrane equilibrium though eventually proven erroneous, nonetheless played a positive role in the development of cell physiological science — like Stahl's phlogiston theory did in the development of the modern theory of chemistry

In the late seventeenth and early eighteenth century, there lived in Germany a talented and famous scientist-physician by the name of Georg Ernst Stahl (1660–1734.) Stahl inherited from his teacher, Johann Becher, the idea that combustible materials contain an ignitable matter, which Stahl gave the name, *phlogiston*. Although the phlogiston theory eventually was found erroneous, it has, nonetheless, provided a basis for the many experiments that contributed to the birth of the new chemistry under the influence of Antoine Lavoisier (1743–1794.) (For another idea of Stahl, see Endnote 1 on p. 43.)

In my opinion, Donnan's theory of membrane equilibrium and membrane potential also provided the basis for the many experiments that contribute to the birth and development of a new theory of the living cell like the *association-induction (AI) hypothesis* — to be described below after a brief introduction to a revolutionary change in the development of physics itself.

From the world one can see to the microscopic world of atoms, electrons one cannot see

Before entering into the history and substance of the association-induction (AI) Hypothesis itself, I would like to describe the background of another more subtle historic relationship between Donnan's theory and the AI Hypothesis. Namely, the transition in physics from the investigation of the *macroscopic* world, which one can see to the new *microscopic* world of atoms, electrons etc., which as a rule, one cannot see (even with the best light microscopes.)

As pointed out earlier, Donnan's theory of membrane equilibrium is by and large a play on van't Hoff's concept of semipermeability. In introducing this concept, van't Hoff had in fact divided the world of solutes into two categories. Permeant solutes can traverse these semipermeable membranes, whereas impermeant solutes are unable to do so, not in hours, nor in days nor even in years, but forever.

The question arose, is such an idea of eternal impermeability compatible with our more modern knowledge of the world we know today? The answer is No. That being the case, Why did an exceptionally gifted scientist like van't Hoff make such a terrible blunder?

The answer is, van't Hoff, like his student, Donnan, lived in a world before physicists and chemists finally understood and accepted the new *microscopic* physics that the Austrian mathematician-physicist, Ludwig Boltzmann (1844–1906) had almost single-handedly invented. It is a new way of interpreting *macroscopic* phenomena and objects (measured in micra or 10^{-4} cm or larger) in terms of the properties and behaviors of *microscopic* atoms, electrons etc., (measured in Ångstrom units or 10^{-8} cm and/or in nano-meters or 10^{-6} cm) — known now as *Statistical Mechanics*.

Similarly, *permeability* and *impermeability* spoken at van't Hoff's and Donnan's time were *macroscopic* properties. How they can be re-interpreted in *microscopic* statistical mechanical terms is a central theme of the association-induction hypothesis to be briefly summarized below.

The Association-Induction (AI) Hypothesis

More than half of a century has passed since the embryonic version of the association-induction hypothesis was published in 1952 and known as Ling's Fixed Charge Hypothesis (Ling 1952.) The main theme of the AI hypothesis was presented in 1962 in a 680-page volume entitled *A Physical Theory of the Living State; the Association-Induction Hypothesis* (Ling 1962.) However, it was not until 1965 when the *Polarized (Oriented) Multilayer (PM or POM) Theory* of cell water was added (Ling 1965) that the association-induction hypothesis became complete.

Since 1952 and even before, the hypothesis has been extensively tested here and abroad. Over 200 original articles and reviews have been published from my laboratory alone. Throughout this whole lengthy period of time, there has been no major reverse in the steady growth and evolvement of the AI Hypothesis. Notwithstanding, the association-induction hypothesis is virtually unknown and just as bad, untaught.

Historic background of the association-induction hypothesis

So far, I have discussed how the AI Hypothesis may be seen as an (opposing) sequel of the membrane theory in the same way that Lavoisier's modern chemistry is an opposing sequel to Stahl's Phlogiston theory. I must now point out the more obvious. That is, the AI Hypothesis is the heir to a theory that was introduced in 1835 by the French zoologist, Felix Dujardin (1801–1860.)

Dujardin described in 1835 a water-insoluble, translucent and gelatinous material that oozes out from within a crushed protozoon — called infusoria then — and gave this “living jelly” the name of *sarcode* (meaning fleshy) (Dujardin 1835.) Later this name was replaced by the term, protoplasm, a name introduced by the German botanist, Hugo von Mohl (1846) who described a similar material that lies under the cell wall of plant cells.

The protoplasmic concept became widely adopted for decades, highlighted by two historic events that occurred in the 1860's. They are respectively Max Schultze's pronouncement in 1861 of the “protoplasmic doctrine” that “living cells are lumps of protoplasm with a nucleus” (Schultze 1861) and second, Thomas Huxley's 1868 Sunday

evening lecture in an Edinburgh church, in which he announced that *protoplasm is the physical basis of life* (Huxley 1869.)

Unfortunately but perhaps inevitably, the protoplasmic theory steadily lost ground as time wore on. The main reason for this decline of popular interest was the discoveries of more and more intracellular structures or organelles in addition to the cell nucleus. None of these inclusions could be seen as being made of the same colorless, translucent material that Dujardin and von Mohl saw and described as sarcode or protoplasm.

This decline in popularity can be put in the words of Encyclopedia Britannica Online, “as the cell has been fractionated into its component parts, protoplasm as a term no longer has meaning.” (“Cell” Encyclopedia Britannica 2009.)

The truth is, once more, the protoplasm of Dujardin, von Mohl, Schultze and Huxley is like van’t Hoff’s semipermeability, and Donnan’s theory of membrane equilibrium, an example of *macroscopic* objects or concepts. And to move forward again, it too must await for the arrival of *microscopic* interpretations like that introduced by the AI Hypothesis.

As I have pointed out in preceding pages, the AI Hypothesis has been described in four full-length books (Ling 1962, 1984, 1992 and 2001.). To these volumes, the reader will have to turn to as the sources of information on the history of the evolving theory and results of experimental testing up to the current year. However, for those looking for a bird’s eye view of the theory (up to the year 1998), I would recommend the two-tier summary given online, one very brief and the other somewhat longer in www.gilbertling.org/lp6c.html.

For those interested in more detailed accounts of the progress made mostly in the last two decades, he and she can go to my website: www.gilbertling.org “*Science Cannot Conquer Cancer and AID without Your Help*” (Ling 1998) and find on its front page a list of ten titles. Each title introduces a detailed review on one of the special subdivision of cell physiology, including the (1) sodium pump, (2) selective K⁺ accumulation, (3) oxidative phosphorylation, (4) multilayer polarization-orientation of cell water etc. Each is written in pdf format and can be downloaded free (and printed out) by merely clicking the title on the front page.

The remainder of the present article briefly describes the concept of “nano-protoplasm,” a term I first introduced only two years ago in 2008 as the ultimate unit of life. And how *association* and *induction* play in not only determining the chemical makeup of nano-protoplasm but also in how they work in making nano-protoplasm *alive*. Then, in the briefest manner, I will also describe how the nano-protoplasms and the cells and organ they compose, perform the four cardinal cell physiological *attributes*: (1) selective solute distribution, (2) permeability, (3) cellular resting potential and (4) cell swelling and shrinkage.

Nano-protoplasm defined by what it is and what it does

The red blood cell is the first animal cell discovered and recognized as a living cell. Finding the low level of Na⁺ in human red cells was another landmark event in cell physiology. Indeed, as I have pointed out recently (Ling and Ochsenfeld 2008, abstract) all the major theories of the living cell are built around this discovery of Abderhalden reported over a century ago. For this and other reasons, we will continue to use the human red blood cell to illustrate what is the chemical makeup of nano-protoplasm and what nano-protoplasm does in making *life* and *life activity* what they are.

(I hasten to add that although the underlying concept has been the central theme of the AI Hypothesis from its beginning, the name, nano-protoplasm was a relatively new addition. Indeed, it was first introduced in the year 2008 in the publication bearing its name in the title: *Nano-protoplasm, the Ultimate Unit of Life*. (Ling 2007b, I regret that the publication of the journal, *Physiological Chemistry Physics and Medical NMR* has fallen behind schedule, hence the year disparity.)

Now, mature human red blood cells — to be subsequently referred to as rbc — have no nucleus nor any other sub-cellular organelle or structures. Indeed, seen through the best light microscope or even electron microscope (see Figure 3) the entire cell is a homogeneous biconcave disk.

64% of the weight of a rbc is water. 97% of the remaining (36%) solid belongs to a single protein, hemoglobin. Therefore water and hemoglobin together make up more than 98% of the rbc. Note that all the non-hemoglobin solids including non-hemoglobin proteins (e.g., enzymes) and phospholipids that partially make up the enclosing cell membrane are, according to the best source available, less than 2% of the weight of the rbc (Ponder 1948, 1971.) Indeed, that less than 2% weight also includes 100 mmoles per kg of K^+ and 2 mM of ATP, which is, of course, the end-product of all energy metabolism.

Thus, in theory we can use a magic scalpel to cut up a rbc into smaller and smaller pieces until each piece contains just one hemoglobin molecule. And with this hemoglobin molecule also are about 7000 water molecules, 20 K^+ and one ATP molecule. Through specific *association* mechanisms of one kind or another, all these entities are bound together into one coherent nano-protoplasmic unit described by the formula:



(For a more general formula for all kinds of nano-protoplasms, see Ling 2007b, p.121.) Assumed spherical in shape, *this specific nano-protoplasmic unit would measure 6.8 nano-meters in diameter.*

Having completed a short description of what a nano-protoplasm unit is, we now proceed to describe what nano-protoplasm can do in *life* and *life activity*.

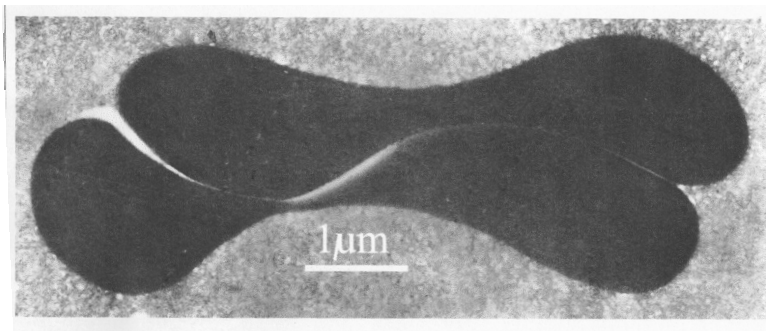


FIGURE 3. Electron micrograph of the cross-section of two mature human red blood cells in blood plasma. (Cryofixed, freeze-dried and embedded in Lowicryl.) (Gift of Dr. Ludwig Edelmann.)

As a rule, each nano-protoplasm existing in its natural environment can exist in just two alternative conformations as illustrated in Figure 4. They are respectively the α -helical state (left) and the fully extended state (right.)

A nano-protoplasm unit would exist in the fully extended state when ATP is adsorbed on the ATP-specific *cardinal site* also shown in the diagram of Figure 4. There, *all the components shown in the molecular formula are in the associated state*. In this (auto-cooperative) assembly, ATP functions as an *electron-withdrawing cardinal adsorbent* (EWC); its adsorption brings about a falling-domino like chain reaction that was once called *Indirect F-effect* (Ling 1962, pp. 92–102.) Since 2007, this term has been replaced by the new name, *AI-cascade mechanism*. (For a detailed step-by-step description of the AI cascade mechanism, see Ling 2001, pp. 170–178 or Ling 2007b, pp. 137–140.)

The adsorption of ATP on its cardinal site induces an *AI-cascade mechanism*. As a result, all the K^+ , as shown in the illustration, become engaged in *close-contact, one-on-one adsorption* on the β -, and γ -carboxyl groups of the hemoglobin molecule. And in addition, the bulk-phase water molecules are adsorbed (directly or indirectly) as *polarized-oriented multilayers* on the exposed imino (NH) and carbonyl (CO) groups of the fully extended polypeptide chains of the hemoglobin molecules.

Removal of ATP from its specific cardinal site on the hemoglobin molecule causes the reverse change. The operation of the *AI-cascade mechanism* would now lead to an all-or-none (auto-cooperative) desorption of both the K^+ and water molecules and the assumption of the hemoglobin molecule in its folded state, in which the backbone NH and CO groups are now locked in H-bonds with other backbone CO and NH groups and the β -, and γ -carboxyl groups form salt-linkages with fixed cations in the form of ϵ -amino groups on lysine residues and guanidyl groups of arginine residues.

The nano-protoplasm containing the fully extended protein as shown on the right-hand side of the Figure 4 represents the *resting living state*. On the other hand, the nano-protoplasm containing the protein in the folded state shown on the left-hand side of the figure corresponds to either the *active living state* (if the change is reversible) or the *death state* (if the change is irreversible.)

To illustrate how the *dead state* of nano-protoplasm differs from one in the *active living state*, let us consider muscle contraction. A normal muscle at rest is in the *resting living*

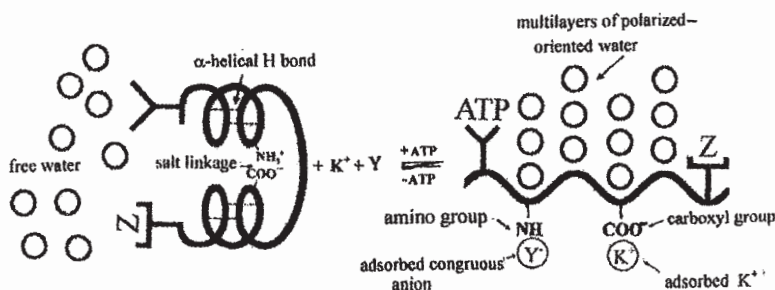


FIGURE 4. Diagrammatic illustration of the all-or-none auto-cooperative transition between the folded (left) and fully-extended (right) state of the a nano-protoplasm unit.

state. When it is stimulated say by a single electric shock, it would momentarily lose its ATP and transiently go into a shortened *active living state*. But with replenishment of ATP, it will return to its *relaxed resting living state*. However, if the muscle were poisoned say with the drug iodoacetate, it would not be able fully to regenerate its lost ATP after each contraction. Eventually, it would have lost all its ATP and with that, the muscle would enter a permanently shortened *death state*, which in conventional terms is also known as *rigor mortis*.

In summary, *being alive* means the existence of the nano-protoplasm in the resting living state. Reversible shifts between the resting and active living state constitutes *life activities*.

Having understood what is alive and what is dead in general terms, we are now in a position to discuss two sets of highly important quantitative parameters that play key roles in the all-or-none auto-cooperative transitions between the resting and active living (or dead) state we just mentioned. These parameters are called respectively *c-value* (and *c'-value*) and *c-value analogue* (and *c'-value analogue*.)

These values are all electronic parameters and hence broadly speaking, *inductive* — of the association-*induction* thesis — in their functions. Rigorously defined elsewhere (Ling 1962, pp. 57–60, Ling 2006a, Appendix I on p.118) the *c-value* and *c'-value* may be regarded as describing the effective electron and positive charge density of the β -, and γ -carboxyl groups and fixed cations respectively. On the other hand, *c-value analogue* and *c'-value analogue* measure the electron and positive-charge density of dipolar backbone carbonyl (CO) and imino (NH) groups respectively.

Results of theoretical computations, shown in Figure 4.11 on p. 77 in Ling (1962) or in Figure 7 on p. 131 in Ling (2007b) affirmed by experimental data, revealed that at low *c-value*, the β -, and γ -carboxyl groups prefer to adsorb K^+ over both Na^+ and fixed cations. In contrast, at high *c-value*, the converse is true. They then prefer Na^+ and fixed cations over K^+ . In a parallel manner, at low *c-value analogue*, the backbone carbonyl groups prefer to adsorb water molecules (as polarized-oriented multilayers) while at high *c-value analogue*, they prefer to form α -helical bonds with other backbone sites.

The amazing thing about the AI cascade mechanism is that it allows the binding of an *electron-withdrawing cardinal adsorbent* (EWC) like ATP to bring about a uniform change of both the *c-* and *c'-value* as well as the *c-* and *c'-value analogue* of all the sites far and near in the nano-protoplasm at once. To understand how this is done, you must consult the fuller description given earlier (Ling 2001, pp. 170–78 and Ling 2007b, pp. 137–40.)

Indeed, it is on this keyboard of *c-value*, *c-value analogue* etc. that *electron-withdrawing cardinal adsorbents* (EWC) like ATP and *electron-donating cardinal adsorbents* (EDC) like the cardiac glycoside drug, ouabain play their living melodies.

Having disclosed how electronic polarization or *induction* plays a key role in all life activities, we are now in a position to look deeper into the concept of *association* (of the *association-induction* hypothesis) and how it plays its key part in life phenomena.

First, let us begin with the opposite. The Donnan theory of membrane equilibrium is based on the concept of ionic *dissociation*. Van't Hoff's famous equation, $\pi v = inRT$, where n is the number or moles of the osmotically active electrolyte in the system of volume v . " i " is the dimensionless *van't Hoff factor*. For a dilute solution of an electrolyte like NaCl, van't Hoff demonstrated that i is not unity but close to 2, showing that the Na^+

and Cl^- are not associated but are *nearly fully dissociated*. Van't Hoff's Swedish student, S. Arrhenius—and later, Paul Debye all become famous elaborating on the *dissociated state of ions* in dilute solutions (For more details on this subject, see Ling 2005.)

By this time, the reader must be fully aware of the great importance of the pair of alkali metal ions, K^+ and Na^+ in living phenomena. Yet as a singly-charged cation, this pair of chemically highly similar alkali metal ions are identical as far as long range attributes are concerned. There is no secret here. We all know that sight and sound, for example, are long-range attributes. One can see and hear from close and far. However, touch is a short-range attribute. To find out how an object feels, you have to touch and thus be in direct contact with the object.

Now, the only difference between K^+ and Na^+ are in their short-range attributes, notably their size. Naked K^+ is larger than naked Na^+ . But dissolved in water, each ion takes on a more or less permanent coat of water of hydration. The hydrated K^+ is now smaller than the hydrated Na^+ . Indeed, the atomic sieve theory of Mond and Amson and that of Boyle and Conway had utilized these short-range attributes already to sort them apart. But as the reader knows by now, that theory does not work.

In contrast, the AI Hypothesis also used the short range attributes to set this pair of ions apart — when they are engaged in *close-contact, one-on-one* adsorption on β^- , and γ -carboxyl groups. But that is not all. It is this *close-contact, one-on-one adsorption* that creates the reversal of preference with c-value changes of the β^- , and γ -carboxyl groups. Indeed, it is no exaggeration to say that without this close contact, one-on-one adsorption, life and living activity, as we know them, would not be possible.

This conjecture will become clearer by seeing how the AI Hypothesis offers its interpretations on the four cardinal cell physiological attributes to be discussed next in the order: (1) solute distribution, (2) solute permeability, (3) electric potential and (4) swelling-shrinkage.

One recalls that at one time, Boyle and Conway felt that their atomic sieve theory based on Donnan's theory of membrane equilibrium could offer a similar unifying interpretation — before their theory collapsed.

The new unifying interpretations of the quartet of cardinal cell physiological attributes

1. Distribution of ions and other solutes in intact living cells (and in isolated parts thereof)

The general principle that a solute can exist as a free solute dissolved in cell water and also bound to some fixed element like intracellular proteins can be traced to Martin Fischer (1921) and others like Moore and Roaf (1908.) (See also Ling 2005.) Later, it was elaborated further by Troshin (1966), who also introduced a two-term (Troshin) equation (see Ling 2001, p. 163.) But it was not until 1952, that Ling offered a *microscopic* (or *statistical mechanical*) mechanism as to why K^+ and Cl^- are almost fully *dissociated* in an aqueous solution of similar strength, while K^+ and fixed anions like the β^- , and γ -carboxyl groups are almost completely *associated*.

The underlying cause of full association was given the name, the *Principle of Enhanced Ionic Association due to Site Fixation*. The more up-to-date and complete statistical mechanical derivation was given in detail 43 years later (Ling 2005 pp. 12–18) but in 1952,

Ling gave the following explanation, which is a lot simpler but informative enough for our present purpose today as in 1952.):

(i) "The force of attraction between ions of opposite sign in solution is opposed by the kinetic energy of the ions themselves. If one of the ions is rigidly fixed, half of this energy is abolished, so that the ions stay on the average closer together than they would be able to do when both are free..."

(ii) "Fixation allows the close juxtaposition of a number of similarly charged ions, for the repulsive forces between them are less strong than the covalent bonds of fixation. Their individual fields thus overlap, and sum with respect to the force exerted collectively upon a free ion of opposite sign." (Ling 1952, p. 769.)

It was then shown how the *Boltzmann distribution law* (see Boltzmann 1904) would predict theoretically a 7-to-1 preferential adsorption of K^+ over Na^+ on the β -, and γ -carboxyl groups of mostly myosin in frog muscle cells. It is true that a 7-to-1 preference was not as high as observed (40-to-1) but it is also without question headed in the right direction. This then offered a partial semi-quantitative explanation how K^+ is preferentially accumulated over Na^+ in almost all living cells but it is not the full answer.

The full answer would have to address why the concentration of Na^+ does not match that in the external bathing solution. A qualitative theoretical explanation was provided for the first time in 1965 with the introduction of the polarized/oriented multilayer theory of cell water (Ling 1965.)

Again using basic statistical mechanical theory, Ling introduced in 1993 a quantitative equation for the (true) equilibrium distribution coefficient or *q-value* of a solute (entirely) in the cell water, comprising a linear combination of two terms, a *volume factor* and a *surface factor* (Ling 1993.) In contrast, a *ρ -value* or *apparent equilibrium distribution coefficient* owes an additional part of its origin to adsorbed solute also present inside the cell. *q-values* never exceed unity. *ρ -value* can exceed unity by a large factor sometimes. When it does that, most of the intracellular solute involved is in an adsorbed state.

And it is largely the volume factor of the *q-value* mentioned above that gives rise to the so-called "size rule" (Ling and Hu 1988.) Namely, the larger the solute molecule or ion, the lower is the *q-value*. As an example, the *q-value* of sucrose in frog muscle is about 0.15 due largely to the large size of the sucrose molecule. Na^+ (as chloride), on the other hand, has a *ρ -value* of between 0.3-0.4 when a small portion of the intracellular Na^+ is adsorbed on the β -, and γ -carboxyl groups that are not occupied by K^+ and fixed cations. The true equilibrium distribution coefficient or *q-value* of the Na^+ is in the range 0.2 to 0.3 due to its large hydrated size. (As mentioned in the *Abstract*, see Ling 1997, also Endnote 1 of this article on the fate of the postulated sodium and other membrane pumps.)

2. Cell permeability

While the large aggregates of nano-protoplasm that make up the cytoplasm provide both the β -, and γ -carboxyl groups that selectively adsorb K^+ (over Na^+) and the polarized-oriented multilayers of cell water that effectively exclude Na^+ (as Cl^-), I pointed out that a similar collection of various nano-protoplasm at the cell surface determines the ionic permeability of the cell (Ling 1960.) A diagram by Ling and Ochsenfeld of a portion of a nano-protoplasmic unit containing just four β -, and γ -carboxyl groups is illustrated in Figure 5. The cell surface nano-protoplasmic water provides the pathway for the entry (or

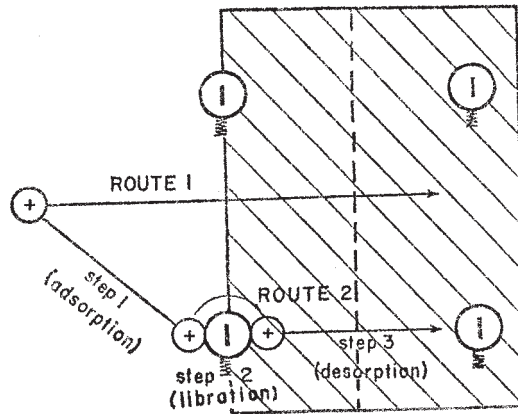


FIGURE 5. Alternative routes of permeation for an external cation into the surface nano-protoplasmic units carrying exclusively fixed anionic sites. Saltatory route (route 1) entails leaping through multilayers of polarized-oriented water molecules. Adsorption-desorption route (route 2) involves three consequent steps shown in the figure. (Ling and Ochsenfeld 1965.)

exit) of a neutral solute molecule like sucrose *via* the so-called *saltatory route* (labeled as Route 1 in the figure.) On the other hand, the β - and γ -carboxyl groups carried on surface nano-protoplasmic units provide a second pathway for cation entry (or exit). Known as the *adsorption-desorption route*, this route is labeled Route 2 in the figure. The low c -value of these β - and γ -carboxyl groups maintained by an adequate amount of adsorbed ATP on the controlling cardinal sites, makes K^+ entry much preferred over that of Na^+ by the adsorption-desorption route.

However, as a rule, due to its high concentration in the bathing medium, there would always be some highly energized Na^+ that would be able to enter *via* the polarized-oriented surface water. This would then account for the much faster rate of Na^+ exchange than K^+ , notwithstanding that the total number of K^+ entering a cell during a given time period is much higher than that of Na^+ .

This relationship bears resemblance to what happens at a tollgate. Like the highly energized Na^+ at the cell surface, the tag-carrying cars going through the tollgate in a given time is faster but also much smaller in number than the total number of non-tag carrying cars (like K^+) which enter or exit *via* the more abundant but slower non-EZPASS gates.

Theory also shows that the degree of electric polarization-orientation of the surface water can exercise powerful influence on the rate of solute permeation (Ling 1993.) An effective control of the state of surface water polarization-orientation thus provides the means for a highly important physiological dimension that was as a rule completely overlooked in conventional cell physiological discourses: *diversity in the rate of permeation for a given solute*.

Thus in order to survive, a frog cannot have just a single fixed rate of permeability for glucose. It needs the glucose to be *rapidly transported* across the cell barriers of the digestive tract as well as the muscle cells in order to provide energy speedily to rapidly contracting muscle cells of a frog escaping from danger. Yet at the same time, the frog must

also offer a leak-proof surface skin cell barrier to prevent a steady loss of glucose to the external pond water. In fact, cell (membrane) barriers to glucose *three orders of magnitude apart*, have been demonstrated in the same North-American leopard frogs, *Rana pipiens pipiens*, Shreber. (See Ling 2007, pp. 187–90.)

I conclude this section by raising another critical question. Does the cell surface contain only *fixed anions* in the form of β -, and γ -carboxyl groups? Or does it also have *fixed cations* as well? According to the AI hypothesis, the surface of excitable cells like muscle and nerve is populated only by β -, and γ -carboxyl groups. In a way, this is to be expected from what physicists call the Faraday Cage Effect. That is, excess electrical charges of a macroscopic object collect at the surface only. In the following section on cellular resting potentials, we offer additional evidence in support of this conclusion. (For examples of cells that do not follow this rule, see Ling 1984, section 14.4.4 on p. 488.)

3. *The cellular resting (and action) potential*

This subject is of particular interest to me because I started my career in cell physiology on this subject. Indeed, both my Ph.D. thesis at the University of Chicago (Ling 1948) and the first four full-length papers I co-authored with my beloved professor and teacher, Prof. Ralph W. Gerard (Ling and Gerard 1949) bear the words, *membrane potential* — which I later found out to be wrong.

In 1955 and again in 1959 I first suggested briefly that the resting potentials of living cells is not a membrane potential at all but essentially similar to the electric potentials of glass electrodes (Ling 1955, 1959.) At that time, I did not know that Cremer already had made a similar suggestion many years before (Cremer 1906.) Indeed, I did not find out about this page in history until the 1980's when I was gathering materials for writing my second book, "In Search of the Physical Basis of Life" (Ling 1984 p. 22.)

However, I did more than just point out an analogy between the electrical potential of glass electrode and of the living cell in 1955 and 1959. I was also presenting a new theoretical fundamental mechanism that I suspected to underlie the electrical potentials in both systems. Since the history of this search has been described repeatedly before (Ling 1992, Chapter 11; Ling 2001 pp. 209–24), I shall go straight to our final conclusion here.

That is, the cellular resting potential is a *close-contact, surface adsorption potential* on the β -, and γ -carboxyl groups of nano-protoplasm occupying the cell surface. It is in this research conducted by myself (and my associate, Leo Kushnir) that I reached the conclusion that for typical living cells like muscle and nerve, the cell surface is essentially *anionic* due to the presence of β -, and γ -carboxyl groups only.

The reader will recall that when carboxyl groups are attached to (electrically neutral) nitrocellulose of the collodion used to make collodion thimble electrodes, these carboxyl groups endow the thimble electrode the ability to respond electrically to external K^+ concentration like the living cell. Glass tubing made with Corning 015 glass is designed for making good pH electrodes as it does not show sensitivity to "interfering ions" like K^+ for example. Ling and Kushnir showed that if such a Corning 015 glass electrode is coated with a very thin layer of oxidized collodion, it then acquires full sensitivity to K^+ as the oxidized collodion thimble electrode does. The characteristic *insensitivity* of the underlying glass electrode to K^+ has now entirely vanished (see Ling 1960 and Ling 1967.)

This specific experiment was undertaken to test the theory that it is something on a very thin surface layer of the electrode that exclusively determines the specificity of ion sensitivity (See earlier theories of Nernst and Baur mentioned on p. 28 above.) Our finding that the collodion-coated glass (CG) electrode behaves indeed like an oxidized collodion thimble electrode has fully confirmed our expectation (Ling 1967.) Then we went one step further.

We exposed the (oxidized) collodion coated glass electrode to a solution of poly-lysine, which carries a great abundance of positive electric charges on the ϵ -amino groups at the end of the lysine side chains. Whereas the oxidized collodion-coated glass electrode shows no sensitivity to chloride ions in the test solution, this poly-lysine-treated, collodion-coated glass (PCG) electrode develops anion sensitivity at low pH — when the carboxyl groups are neutralized and thus have lost its sensitivity to K^+ as illustrated in Figure 6. Since living cells like frog muscle also show no sensitivity to chloride ion and their sensitivity to K^+ is insensitive to pH between pH 5 and 10 (Ling and Gerard 1949), one can conclude that muscle and nerve cell surfaces are primarily anionic. This exclusively anionic surface of excitable cells like muscle and nerve also plays a key role in the creation of what is known as the *action potential*. For full details, the interested reader can have a full review of this in Ling 2007, p. 205. Here, it suffices to give a very short description.

If the muscle cell surface contains both anionic (β -, and γ -carboxyl groups) and cationic (ϵ -amino and guanidyl) groups like that in the cytoplasmic nano-protoplasm described earlier, a rise of the c-value of the surface β -, and γ -carboxyl groups would cause the formation of salt linkages as illustrated in Figure 4. Instead, the absence of fixed cationic groups on the cell surface leaves the surface β -, and γ -carboxyl groups no alternative but to adsorb Na^+ , thereby creating one major component of the action potential called the “overshoot” (Ling 1984, p. 73, Ling 2007, pp. 204–07.)

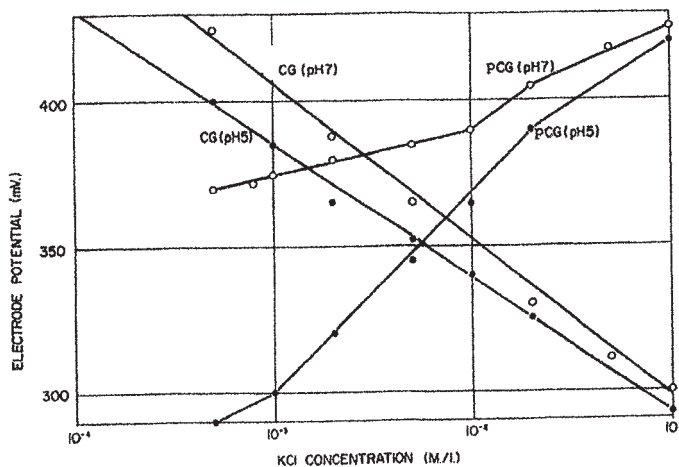


FIGURE 6. Cation and anion sensitivity of a collodion-coated glass (CG) electrode and of a poly-lysine treated collodion-coated glass (PCG) electrode at two different pH's as indicated. (From Ling 1967.)

I finish this section with a reference to the uncannily close correspondence of the electrode behavior of the CG electrode and the living frog muscle: (i) They both exhibit the same rank order of relative preference for the alkali-metal ions: $Rb^+ > K^+$, $Cs^+ > Na^+$. (ii) Both are indifferent to Cl^- . (iii) Both demonstrate a H^+ over K^+ selectivity of about 150. (iv) Both are totally indifferent to external Mg^{++} (Ling 1992, pp. 287–89; Ling 2001, pp. 218–19; Ling 2007, pp. 198–200.)

And this close resemblance is no accident. There is a very good and enlightening reason behind it. Cellulose, like proteins has the inherent capability of existing in two conformations: folded and fully-extended (see Ling 2007, p.189.) In preparing collodion, electron-withdrawing nitro groups are introduced, thereby lowering by the inductive effect (or more precisely, the *direct F-effect*) the c-value of the carboxyl groups introduced. This c-value lowering makes these carboxyl groups not only qualitatively, but quantitatively like the β -, and γ -carboxyl groups of muscle and nerve cell surface nano-protoplasm under the domination of the *electron-withdrawing (cardinal adsorbent) ATP* (For the most recent dramatic verification of this theoretical prediction, see Ling and Ochsenfeld 2008.)

4. Cellular swelling and shrinkage

There are very few scientists as admirable to many including myself as Jacobus van't Hoff — not only for his science but also for his love of classical music and of Nature. But he was a scientist of his time. Although a contemporary of Ludwig Boltzmann, the microscopic interpretation of macroscopic phenomena introduced by Boltzmann was still not yet widely accepted. Indeed, van't Hoff was much closer intellectually to Wilhelm Ostwald, who was a major opponent of Boltzmann and Boltzmann's belief that atoms exist as part of the microscopic units of which macroscopic objects are made.

Along with his concept of semipermeability, van't Hoff also introduced his *bombardment theory of the osmotic pressure*, in which the impermeant solutes produce the (osmotic) pressure in the same way gas molecules produce pressure by bombarding the container wall. That the bombardment theory is wrong has been widely recognized for quite some time now. In 1970 Ling and Negendank published further evidence against the bombardment concept (Ling and Negendank 1970.) They demonstrated that sucrose can cause shrinkage of surviving muscle cells without being in direct contact with (and bombarding) the muscle cell surfaces — but by vapor sorption from a solution containing water at a reduced activity or vapor pressure.

Next, I shall answer the question why a muscle cell swells intensively in isotonic KCl solution but not in isotonic NaCl solution (von Korösy 1914.) The once popular answer was based on the then-widely held but incorrect belief that the cell membrane is permeable to KCl but not to NaCl and the dictate of de Vries's osmotic method working in reverse: permeant solutes cause swelling; impermeant solutes cause shrinkage. As mentioned earlier, radioactive tracer studies completely disproved that once popular interpretation.

Then the pump-leak model was introduced in which the incessant activity of countless postulated membrane pumps located in the cell membrane renders the cell membrane *effectively impermeable to Na^+* (Wilson 1954, Leaf 1956.) However, extensive evidence cited in Endnote 1 rules that out too.

An altogether different mechanism for the ability of isotonic KCl induced swelling of frog muscle cells is the offspring of the marriage of two sets of theoretical concepts. One

set was published in 1969 and already illustrated in Figure 4 (Ling 1969, p. 47) and a new set of theoretical concept 34 years later in a paper entitled: "A new theoretical foundation for polarized-oriented multilayer theory of cell water and for inanimate systems, demonstrating long-range dynamic water structuring of water molecules" (Ling 2003.)

In this 2003 paper, I have shown on theoretical grounds that, under ideal conditions, water molecules can be polarized and oriented *ad infinitum* by an idealized checkerboard of alternately positive and negative sites called an *idealized NP system*. And that a matrix of fully-extended protein chains can function in a way resembling the idealized NP system and produce far deeper layers of water molecules than the average distance maintained primarily by salt linkages between nearest neighboring protein chains in normal living cells (see Figure 4.) It follows that when the size-limiting salt linkages are somehow disengaged, more water molecules will enter the muscle cells and assume the state of polarized-oriented multilayers like water molecules found in normal living cells.

Next I shall demonstrate why an isotonic KCl solution would break open the size-limiting salt linkages as first briefly suggested in 1962 (Ling 1962 pp. 247–50.)

Maintained by an adequate supply of the *electron withdrawing cardinal adsorbent* (EWC), ATP, the β -, and γ -carboxyl groups in a frog muscle that are normally engaged in the size-maintaining salt linkages (see left-hand side figure in Figure 4) assume a low *c*-value. As a result, these β -, and γ -carboxyl groups show a strong preference for K^+ over (Na^+ and) fixed cations. Since the normal frog blood plasma and tissue fluids contain only a very low level of K^+ (2.5 mM), the normal muscle size is maintained.

However, when the muscle is artificially immersed in a solution containing a much higher concentration of KCl (e.g., 118 mM), many of these size-maintaining salt-linkages would be split apart. More water molecules then rush into the muscle cells causing swelling.

I shall next describe a pathological phenomenon that is at once a theoretical variant of the phenomenon of KCl-induced cell swelling but also a familiar subject to all of us since our childhood. Namely, a bump on a hard object may cause your damaged arm or leg to swell up.

As just mentioned, isotonic KCl causes tissue swelling. Yet, the near-isotonic (100 mM) NaCl normally present in the blood plasma and tissue fluid does not cause tissue swelling. According to the AI Hypothesis, this seeming contradiction arises from the theoretically deduced fact that the β -, and γ -carboxyl groups engaged in the size-maintaining salt linkages have very low affinity for Na^+ .

However, this low affinity for Na^+ is true as long as a normal level of adsorbed ATP is maintained — as it is the case for most frog or human muscle and other cells most of the time.

However, when an injury strikes, it may cause local loss of ATP by interrupting its regeneration. Such a loss of ATP would in theory bring about a rise of the *c*-value of the β -, and γ -carboxyl groups engaged in the size-maintaining salt linkages, and cause them to increase their preference for Na^+ . That injury-induced increase of Na^+ preference then ushers in the salt-linkage splitting and water entry sequence. Tissue swelling follows as a result.

Thus, in theory it is the injury-induced loss of ATP that makes the normally harmless, indeed indispensable 100 mM NaCl in the blood plasma to become as harmful as 118 mM KCl and the local damaged tissue now undergoes strong swelling.

Conclusion

In the better part of this communication, I have presented a broad collection of widely different and yet mutually supportive clenching evidence that further enhance the cardinal conclusion presented 49 years ago disproving the membrane (pump) theory (Ling 1962, Chapter 8.) Indeed, at this moment, one can unhesitatingly conclude that there is not even a trace of theoretical and experimental evidence that supports this theory in a positive way uniquely. In contrast and just as sweepingly, one cannot find any evidence that significantly contradicts the alternative association-induction (AI) hypothesis. Indeed, with each passing day, the AI Hypothesis has grown ever simpler (see Ling and Ochsenfeld 2008) while at the same time, it can explain an ever widening range of the living phenomenon (see Ling 2007b.)

The separation of the two contending theories is razor-sharp with virtually no shared common ground. Yet to this very day it is the membrane (pump) theory that is taught as established scientific truth in all high-school and college biology textbooks — not only in the United States but in all other countries worldwide.

Since the 1970's I have been trying everything I could think of to help in correcting this absurd situation (Ling 1997, 1998, 2007 p.62, 2007a) but, so far, to no avail. Nor is this surprising — in retrospect, I have been asking the older generation of people in power to make the necessary change and they refuse to do so.

Now I realize that I should address myself to the young generation of men and women, especially young biology teachers who take themselves and their work seriously. This is indeed why I wrote this article. After all, it is these young teachers that have the power to teach their students the truth rather than a disproved theory masquerading as truth. And by teaching the coming generations truth, they will unshackle and free the future Mankind to innovate, to survive and to prosper in the countless years to come.

Endnote 1.

Georg Stahl famous for his introduction of the concept of *phlogiston*, was also the author of another idea known as Stahl's *animism*. In this doctrine, an immaterial soul or vital principle distinct from matter, produces all phenomena peculiar to the animal world.

In the *Abstract* at the beginning of this communication, I mentioned that to this day, high school and colleges still teach as established truth the membrane pump theory. Who really introduced this membrane pump theory was itself an intriguing story. Many teachers and investigators especially in the botanical fields believe that it was Wilhelm Pfeffer who introduced the membrane theory. This is not true. In his "Osmotic Untersuchungen." (Pfeffer 1877), he did not even mention once the words, membrane theory. Others attributed the introduction of the sodium pump to Robert Dean. This too was a mistake (Ling 1997 p.123.) After a great deal of searching I finally realized that the introduction of the *membrane pump theory* actually predated the introduction of the simpler membrane theory.

The reader knows well by now that the first paper bearing the term, membrane theory was written by Julius Bernstein. But this was only a theory of limited scope, dealing with a specific subject, the cell electric potential. The membrane theory that covers the entire

field of cell physiology was in fact first introduced by no other than Frederick Donnan under the title of membrane equilibrium and membrane potential. And that was in the year 1911.

In contrast, the membrane pump theory was introduced inostensibly by two investigators: Dutrochet and Schwann. Though a few years earlier, Dutrochet's membrane pump theory was an extrapolation from macroscopic membranes like pig's bladder and rabbit intestine. He never claimed to have seen the cell membrane. Theodor Schwann, on the other hand, believed that he actually saw the cell membrane and he also believed that there were what we now call membrane pumps in his cell membrane. True, Schwann did not explicitly introduce the membrane pump theory as such; it came as an integral part of his Cell Theory, which he published in 1839 and thus 72 years ahead of the publication of Donnan's membrane theory.

Theodor Schwann in his Cell Theory (Schwann 1839, p. 184) adopted explicitly Stahl's *animism* in explaining the working of what became known later as the membrane-pump (theory.) This is not surprising because Schwann's professor and sponsor, Johannes Müller was also an outspoken believer in vitalism (Ling 2007, p. 6.)

My first contact with the membrane pump theory, or more specifically, the sodium pump hypothesis began with a departmental seminar on the subject of "The Sodium Pump" based entirely on what I found in my library research (Ling 1997, p. 124.) It culminated in my publication as Chapter 8 of my first book (Ling 1962,) in which I presented the details of the definitive critical experimental data disproving the sodium pump hypothesis. (*In the bulk of the remainder of the book, I also introduced the main theme of the association-induction hypothesis.*) The result of my study shows that in frog muscle, the minimum energy need of the sodium pump is at least 15 to 30 times the total energy available — on the assumption that the frog muscle needs energy to do just one thing, pump sodium. The last paper I wrote on the subject was a 75-page long review I published in 1997 under the title "Debunking the Alleged Resurrection of the Sodium Pump Hypothesis." (Ling 1997.) A pdf version of this article can be downloaded and printed by clicking the title listed on the front page of my website, www.gilbertling.org.

References

- Abderhalden, E. (1898) Zur quantitativen vergleichenden Analyse des Blutes. *Z. physiol. Chem.* 25: 65–115.
- Baur, E. (1913) *Zeitschr. Elektrochem.* 19: 590.
- Baur, E. and Kronmann, S. (1917) *Zeitschr. phys. Chem.* 92: 81.
- Bayliss, W.M. (1924) *Principles of General Physiology*, 4th ed., Longmans, Green and Co., London and New York.
- Bernstein, J. (1902) Untersuchungen zur Thermodynamik der bioelektrischen Ströme. *Pflügers Arch. ges. Physiol.* 92: 521–636.
- Boltzmann, L. (1904) On Statistical Mechanics. In *Theor. Phys. & Philos. Problems* 1974: 164–165.
- Boyle, P.J. and Conway, E.J. (1941) Potassium accumulation in muscle and related changes. *J. Physiol. (London)*. 100: 1–63.
- "Cell" Encyclopedia Britannica. 2009 Encyclopedia Online. 10 March. (2009) <<http://search.eb.com/article/37477>>

- Colacicco, G. (1965) Electrical potential at an oil-water interface. *Nature* 207: 936–938.
- Conway, E.J. and Cruess-Callaghan, G. (1937) Magnesium and chloride “permeations” in muscle. *Biochem. J.* 3: 828–836.
- Cremer, G. (1906) *Z. Biol.* 47: 502.
- Curtis, H. J and Cole, K.S. (1942) Membrane resting and action potentials from the squid giant axon. *J. Cell. Comp. Physiol.* 19: 135–143.
- Donnan, F.G. (1911) Theorie der Membrangleichgewichte und membranpotentiale bei Vorhandensein von nicht dialysierenden Elektrolyten. Ein Betrag zur physikalischen Physiologie. *Z. Elektrochem.* 17: 572–581.
- Donnan, F.G. and Allmand, A.J. (1914) Ionic equilibrium across semipermeable membranes. *J. Chem. Soc.* 105: 1941–1963.
- Donnan, F.G. and Garner, W.E. (1919) Equilibrium across a copper-ferrocyanide or an amyl alcohol membrane. *J. Chem. Soc.* 115: 1313–1328.
- Donnan, F.G. and Guggenheim, W. E. (1932) Die genaue Thermodynamik der Membrangleichgewichte. *Z. physik. Chem.* 162: 346–360.
- Dowben, R.M. (1959) *General Physiology: A Molecular Approach*, Harper-Row, New York
- Dujardin, F. (1835) *Annales des sciences naturelles partie zoologique*, 2nd Sèr., 4: 364.
- Ehrensvar, G. and Sillen, L.G. (1938) *Nature* 141: 788.
- Encyclopedia Britannica 2010, Encyclopedia Britannica Online, 25 Nov. 2010. <http://www.britannica.com/EBchecked/topic/183734/law-of-electroneutrality>
- Fischer, M. H. (1921) *Oedema and Nephritis: A Critical Experimental and Clinical Study of the Physiology and Pathology of Water Absorption by the Living Organism*. 3rd Ed., Wiley, New York.
- Glasstone, S. (1946) *Textbook of Physical Chemistry*, 2nd ed., D. van Nostrand, New York.
- Guggenheim, W.E. (1929) The conception of electric potential difference between two phases and the individual activities of ion. *J. Phys. Chem.* 33: 842–849.
- Guggenheim, E.A. (1950) *Thermodynamics; An Advanced Treatment for Chemists and Physicists*. North Holland Publ. Co. Amsterdam; Interscience Publishers, Inc., New York.
- Hall, T.S. (1951) *A Source Book in Animal Biology*, McGraw-Hill, New York.
- Haugaard, G. (1941) *J. Phys. Chem.* 45: 148.
- Helmholtz, Ludwig von (1881) in *Vorträge und Reden, Volume II: Die Neue Entwicklung von Faraday über Elektrizität, Vortrag zu Faradays Gedächtnisfeier vor den Chemische Gesellschaft zu London*, 5 April.
- Hoff, J. H. van't (1887) Die rolle des osmotische druckes in der Analogie zwischen Lösungen und Gasen. *Z. physik. Chem.* 1: 481–503.
- Höfler, K. (1918) Permeabilitätsbestimmung nach der plasmometrischen Methode. *Ber. dtsh. Bot. Ges.* 36: 414–422.
- Höfler, K (1926) Über die Zuckerpermeabilität plasmolysierter Protoplaste. *Planta.* 2: 454–475.
- Höfler, K (1932) Zur Tonoplastenfrage. *Protoplasma* 15: 462–477.
- Hopfer, U., Lehninger, A.L. and Lenarz, W. J. (1970) *J. Biol. Med.* 2: 41.
- Horovitz, K. (1923) Der Ionenaustausch am Dielektrikum I. Die Elektrodenfunktion der Glaser. *Zeitsch. f. Physik.* 15: 369–398.
- Huxley, T. (1869) On the physical basis of life. *Fortnightly Review* 5: 129.
- Huxley, A.F. and Stämpfli (1951) Direct determination of membrane resting potential and action potential in single myelinated nerve fibres. *J. Physiol. (Lodon)* 112: 476–495.
- Kamnev, I. Ye. (1938) The permeability for sugars of striated frog muscle. *Arkh. anat., gistol. i embr.* 19: 145–160.
- Korösy, K. von. (1914) *Z. Physiol. Chem.* 93: 154.
- Lark-Horovitz, K. (1931) Electromotive Force of Dielectrics. *Nature* 127: 440–440.
- Leaf, A (1956) On the mechanism of fluid exchange in tissues *in vitro*. *Biochem. J.* 62: 241–248.
- Ling, G. N. (1948) “Metabolism and Membrane Potential of Single Muscle Cell” Ph. D. thesis, University of Chicago.

- Ling, G. N. (1952) The role of phosphate in the maintenance of the resting potential and selective ionic accumulation in frog muscle cells. In *Phosphorus Metabolism* (edited by W.D. McElroy and B. Glass), Johns Hopkins University Press, Baltimore. Vol. 2, pp. 748–797.
- Ling, G.N. (1955) New hypothesis for the mechanism of the cellular resting potential. *Fed. Proc.* 14:93.
- Ling, G.N. (1959) On the mechanism of cell potential. *Fed. Proc.* 18: 371.
- Ling, G. N. (1960) The interpretation of selective ionic permeability and cellular potentials in terms of the fixed charge-induction hypothesis. *J. Gen Physiol.* 43: 148–174.
- Ling, G.N. (1962) *A Physical Theory of the Living State: the Association-Induction Hypothesis*. Blaisdell Publ., Waltham, Mass.
- Ling, G.N. (1965) The physical state of water in living cells and model systems. *Ann. N. Y. Acad. Sci.* 125: 401.
- Ling, G.N. (1967) Anion-specific and cation-specific properties of the collodion-coated glass electrode and a modification. in *Glass Electrodes for Hydrogen and Other Cations; Principles and Practice* (ed. G. Eisenmann) Marcel Dekker, Inc., New York.
- Ling, G. N. (1969) A new model of the living cell: a summary of the theory and recent experimental evidence in its support. *Intern. Rev. Cyto.* 26: 1–61.
- Ling, G. N. (1984) *In Search of the Physical Basis of Life*. Plenum Publ. Co., New York.
- Ling, G. N. (1992) *A Revolution in the Physiology of the Living Cell*. Krieger Publ. Co., Malabar, Florida.
- Ling, G.N. (1993) A quantitative theory of solute distribution in cell water according to molecular size. *Physiol. Chem. Phys. & Med. NMR* 25: 145–175. Also available via: http://www.physiologicalchemistryandphysics.com/pdf/PCP25-145_ling.pdf Or, go to www.gilbertling.com, choose volume and article from the drop-down list and click.
- Ling, G.N. (1997) Debunking the alleged resurrection of the sodium pump hypothesis. *Physiol. Chem. Phys. & Med. NMR* 29: 123–198. Also available via: http://www.physiologicalchemistryandphysics.com/pdf/PCP29-123_ling.pdf Or, go to www.gilbertling.com, choose volume and article from the drop-down list and click.
- Ling, G. N. (1998) Science cannot conquer cancer and AIDS without your help. Website online. <<http://www.gilbertling.org>>
- Ling, G.N. (2001) *Life at the Cell and Below-Cell Level: The Hidden History of a Fundamental Revolution in Biology*. Pacific Press, New York.
- Ling, G.N. (2003) A new theoretical foundation for the polarized-oriented multilayer theory of cell water and for inanimate systems demonstrating long-range dynamic structuring of water molecules. *Physiol. Chem. Phys. & Med. NMR* 35: 91–130. Also available via: <http://www.physiologicalchemistryandphysics.com/pdf/PCP35-91_ling.pdf > Or, go to www.gilbertling.com, choose volume and article from the drop-down list and click.
- Ling, G.N. (2005) A convergence of experimental and theoretical breakthroughs affirms the PM theory of dynamically structured cell water on the theory's 40th birthday. In *Water in Cell Biology* (G. Pollack, I. Cameron and D. Wheatley, eds.) Springer, New York.
- Ling, G.N. (2006) In response to an open invitation for comments on AAAS Project 2061's benchmark books on science. *Physiol. Chem. Phys. & Med. NMR* 38: 55–76. Also available via: http://www.physiologicalchemistryandphysics.com/pdf/PCP38-55_ling.pdf Or, go to www.gilbertling.com, choose volume and article from the drop-down list and click.
- Ling, G.N. (2006a) An ultra simple model of protoplasm to test the theory of long-range coherence and control so far tested (and affirmed) mostly on intact cell(s). *Physiol. Chem. Phys. & Med. NMR* 38:105–145. Also available via: http://www.physiologicalchemistryandphysics.com/pdf/PCP38-105_ling.pdf Or, go to www.gilbertling.com, choose volume and article from the drop-down list and click.
- Ling, G.N. (2007) History of the membrane (pump) theory of the living cell from its beginning in mid-19th century to its disproof 45 years ago — though still taught as worldwide today as established truth. *Physiol. Chem. Phys. & Med. NMR* 39: 1–67.

- Also available via: <http://www.physiologicalchemistryandphysics.com/pdf/PCP39-1_ling.pdf>
Or, go to <www.gilbertling.com>, choose volume and article from the drop-down list and click.
- Ling, G.N. (2007a) An unanswered 2003 letter appealing on behalf of all mankind to Nobel laureate Roderick McKinnon to use his newfound fame and visibility to begin restoring honesty and integrity to basic biomedical science by rebutting or correcting suspected plagiarism in his Nobel-Prize-winning work. *Physiol. Chem. Phys. & Med. NMR* 39:89–106. Also available via: http://www.physiologicalchemistryandphysics.com/pdf/PCP39-89_ling.pdf Or, go to www.gilbertling.com, choose volume and article from the drop-down list and click.
- Ling, G.N. (2007b) Nano-protoplasm, the Ultimate Unit of Life. *Physiol. Chem. Phys. & Med. NMR* 39: 111–234. Also available via: http://www.physiologicalchemistryandphysics.com/pdf/PCP39-111_ling.pdf Or, go to www.gilbertling.com, choose volume and article from the drop-down list and click.
- Ling, G.N. and Gerard, R. W. (1949) The normal membrane potential of frog muscle fibers. *J. Cell. Comp. Physiol.* 34: 383.
- Ling, G.N. and Hu, W.X. (1988) *Physiol. Chem. Phys. & Med. NMR* 20: 293. Also available via: http://www.physiologicalchemistryandphysics.com/pdf/PCP20-293_ling_hu.pdf Or, go to www.gilbertling.com, choose volume and article from the drop-down list and click.
- Ling, G.N. and Negendank, W. (1970) Studies on the physical state of water in frog muscle. *Physiol. Chem. Phys.* 2: 15. Or go to: http://www.physiologicalchemistryandphysics.com/pdf/PCP2-15_ling_negendank.pdf Or, go to www.gilbertling.com, choose volume and article from the drop-down list and click.
- Ling, G.N. and Ochsenfeld, M. M. (1965) Studies on the permeability of muscle cells and their models. *Biophysical J.* 5: 777–807.
- Ling, G.N. and Ochsenfeld, M. M. (2008) A historically significant study that at once disproves the membrane (pump) theory and confirms that nano-protoplasm is the ultimate physical basis of life: yet so simple and low-cost that it could easily be reported in many high school biology classrooms worldwide. *Physiol. Chem. Phys. & Med. NMR* 40: 89–113. Also available via: http://www.physiologicalchemistryandphysics.com/pdf/PCP40-89_ling_ochsenfeld.pdf Or, go to www.gilbertling.com, choose volume and article from the drop-down list and click.
- Ling, G.N., Walton, C. and Ling, M. R. (1979) Mg^{++} and K^+ distribution in frog muscle and egg: a disproof of the Donnan Theory of membrane-equilibrium applied to the living cell. *J. Cell. Physiol.* 101: 261–278.
- McCutcheon, M. and Lucké, B.M (1932) The living cell as an osmotic system and its permeability of water. *Physiol. Rev.* 12: 68–139.
- McDonald, R.C. and Bangham, A. D. (1972) *J. Membr. Biol.* 7: 29.
- Michaelis, L. and Perlzweig, W. (1927) Studies on permeability of membranes and diffusion of ions across dried colloidion membrane. *J. Gen Physiol.* 10: 575–598.
- Mohl, H. von (1846) *Bot. Z.* 4: 73, 84.
- Mond, K. and Amson, K. (1928) Über die Ionenpermeabilität des querstreiften Muskels. *Pflügers Arch ges. Physiol.* 220: 67–81.
- Moore, B. and Roaf, H.E. (1908) On the equilibrium between the cell and its environment in regard to soluble constituents. *Biochem. J.* 3: 55–81.
- Morikawa, T. (2001) Model for teaching about electrical neutrality in electrolyte solutions. *J. Chem. Edu.* 78: 934.
- Nasonov, D.N. and Aizenberg, E.I. (1937) The effect of non-electrolytes on the water content of live and dead muscles. *Biol. zh.* 6: 165–183.
- Nernst, W.H. (1889) *Z. physik. Chem.* 4: 129.
- Nernst, W.H. (1892) *Z. Physik. Chem.* 9: 137.
- Netter, H. (1928) Über die Elektrolytegleichgewichte an elektiv ionenpermeablen Membranen und ihre Bedeutung. *Pflügers Arch ges. Physiol.* 220: 107–123.
- Nicolisky, B.P. ((1937) *Acta Physiochim.* 7: 595.

- Ohki, S. (1972) *Biochem. Biophys. Acta* 282: 55.
- Ostwald, Wilhelm (1890) *Z. physik. Chem.* 6:71.
- Pfeffer, W.F. (1877) *Osmotische Untersuchungen: Studien zur Zell-Mechanik*, Englemann, Leipzig.
- Ponder, E. (1948, 1971) *Hemolysis and Related Phenomena*. (Grune and Stratton, New York. pp. 119–121.
- Proctor, H.R. and Wilson, J. A. (1916) *J. Chem. Soc.* 109: 307.
- Rich, A.S. (1926) The place of H. Dutrochet in the development of the cell theory. *Bul. Johns Hopkins Hospital.* 39: 330.
- Schultze, M. (1861) *Arch. Anat. Physiol. Wiss. Med.* 1861: 1. English translation of part of this article can be found in Hall, 1951, pp. 449–455.
- Schwann, T. (1839) *Mikroskopische Untersuchungen über den Übereinstimmung in der Struktur and dem Wachstum der Thiere and Pflanzens.* Engelmann, Leipzig.
- Schwann, T. (1847) *Microscopical researches into the accordance in the structure and growth of animals and plants* (English translation by Henry Smith). Sydenheim Society, London.
- Sollner, K., Abrams, I. and Carr, C.W. (1941) *J. Gen. Physiol.* 24: 467.
- Tamagawa, H. and Nogata, F. (2004) Extension of Colacicco's experiment supporting the adsorption theory. *J. Coll. Interfac. Sci.* 275: 113–122.
- Traube, M. (1867) *Arch. Anat. Physiol. Wiss, Med.* 87: 128, 129–165.
- Troshin, A.S. (1966) *Problems of Cell Permeability* (Revised Ed.) (transl. by M.G.Hell, Editor for transl., W.F. Widdas) Pergamon Press, London, New York.
- Vries, H. de (1871) Sur la perméabilité protoplasmic de betteraves rouges. *Archnéerl. Sci.* 6: 117.
- Vries, H. de (1884) Eine Methode zur Analyse der Turgorkraft *Jahrb. wiss. Bot.* 14: 427–601.
- Wilson, T.H. (1954) *Science* 120: 104.

Received December 20, 2010;

accepted February 2, 2011.

Hydrazide Drugs that Inhibit Growth and Proliferation of Tuberculosis Bacteria

Ronald Bartzatt^{1*}, Suat L. G. Cirillo², Jeffrey Cirillo²

¹University of Nebraska, Department of Chemistry, Durham Science Center, Omaha, Nebraska 68182 USA

²Texas A & M, Health Science Center, Dept. of Microbial and Molecular Pathogenesis, College Station, Texas 77843 USA

*Author for correspondence: Email: rbartzatt@mail.unomaha.edu

Abstract: Four hydrazide drugs are shown to effectively and strongly inhibit the growth of *Mycobacterium bovis* BCG. The four compounds were found to be comparable to isoniazid for extent of growth inhibition. Similar to isoniazid, the four drug designs have a hydrazide functional group (-C(O)NHNH₂) that replaces a former carboxyl group (-C(O)OH). Important pharmaceutical properties were determined for all drugs including Log P, polar surface area, water solubility, and violations of the Rule of 5. Values of Log P for A, B, C, D, and isoniazid were determined to be 1.08, 1.26, 1.26, 1.06, and -0.70, respectively. The polar surface area for drugs A, B, and C were calculated to be 55.12 Angstroms², which is a value that suggests these drugs will effectively penetrate the central nervous system for targeting tuberculosis that infects that anatomical region. All drug designs and isoniazid show zero violations of the Rule of 5 indicating favorable drug bioavailability. Water solubility for all drugs varies from 1074 milligrams/liter to 16690 milligrams/liter. Growth inhibition of tuberculosis bacteria was greater than 50% for all novel drugs at concentrations of 62.5 micrograms/milliliter and higher. Cluster analysis determined that isoniazid is distinct from all new drug designs. For molecular descriptors, molecular volume is directly correlated to formula weight and polar surface area (Pearson $r > 0.8800$). The four novel drug designs show substantial efficacy for the clinical treatment of tuberculosis.

KEY WORDS: tuberculosis, isoniazid, TB, hydrazide

MYCOBACTERIUM IS a genus of Actinobacteria and a genus that includes dangerous pathogens known to cause deadly disease in mammals such as tuberculosis and leprosy (1, 2, 3). The family of *Mycobacterium* is *Mycobacteriaceae*, and all *Mycobacteria* have an unusual thick cell wall, which is thicker than that of many other types of bacteria, that is hydrophobic and consists of a hydrophobic mycolate layer and a peptidoglycan layer (1, 2, 3). This thick cell wall contributes to the hardness of the pathogens and the difficulty of clinical treatment.

The *Mycobacterium tuberculosis* complex (MTBC) includes members that are dangerous causative agents of both human and animal tuberculosis and include the following (4): *M. tuberculosis* (causative agent of human tuberculosis), *M. bovis*, *M. bovis* BCG, *M. africanum*, *M. canetti*, *M. caprae*, *M. microti*, and *M. pinnipedii*. *M. bovis* is transmitted to humans by infected milk and is still a cause of human tuberculosis (4). Individuals infected with pulmonary *M. tuberculosis* (TB) can spread the bacteria by cough, sneeze, or spit (1,2). The majority of individuals infected with *M. tuberculosis* have asymptomatic condition but which can progress to the full disease, killing more than 50% of victims (1, 2, 3). Of active disease, approximately 75% of cases are pulmonary with the remaining 25% causing extrapulmonary tuberculosis of the central nervous system (in meningitis), pleura, lymphatic system, bones and joints of the spine, intestines, and urogenital tuberculosis (5, 6). Treatment duration for tuberculosis is lengthened in cases of central nervous system and skeletal tuberculosis (5, 6).

Vaccination for tuberculosis is often accomplished with a live but attenuated strain of *Mycobacterium bovis* BCG (Bacillus Calmette-Guerin) (*M. bovis* BCG). Treatment of the disease requires a lengthy time period because the bacteria grow very slowly and have a thick cell wall that is a barrier to chemotherapeutics. Often a multiple drug regimen is followed to increase the efficiency of treatment and inhibit appearance of drug resistant organisms. During the course of treatment the type and/or administration of drugs will change according to the current laboratory results. Tuberculosis is still a major public health problem in the Western Pacific Region (WPR) where more than 20% of the global burden is located (7). Cambodia, China, Vietnam, and the Philippines account for more than 90% of the total incidence of cases in the WPR (7). In the WPR cases of multidrug resistant-TB (MDR-TB) occur to various levels depending on the location (7). Southern Africa is a region hard hit by drug resistant TB (8).

Emerging cases of MDR-TB have been observed in Europe, Russia, South America, China, and Asia, with extensively drug resistant-tuberculosis (XDR-TB) becoming observable (9, 10). Treatment regimens of at least four drugs are used for treating MDR-TB with fluoroquinolones applied in the majority of cases to ensure successful outcome (11, 12, 13, 14), however some resistance to fluoroquinolones have arisen in XDR-TB cases (12). Recently the identification of totally drug resistant (TDR-TB) cases has been revealed occurring in Iran (15).

To evaluate the bacterial inhibition of *Mycobacterium bovis* BCG, a member of the *Mycobacterium tuberculosis* complex, by four novel drug designs cultures having variation in drug concentration were monitored. It is found that the new drug designs were comparable to isoniazid in growth inhibition of this bacteria.

Materials and Methods

Reagents and Instrumentation

All solvents and reagents were analytical grade and obtained from Aldrich Chemical Company (P.O. Box 355, Milwaukee, WI USA). Fourier transform infrared spectroscopy (FTIR) was accomplished using a Mattson Galaxy with analytes dissolved in dimethyl-sulfoxide previously dried over molecular sieves.

Molecular Modeling and Multivariate Analysis

Modeling and property determination was accomplished by ChemSketch v. 5 (ACD, 90 Adelaide Street West, Toronto, Ontario Canada). Some properties were determined by EPISUITE v. 1.40 (US Environmental Protection Agency, Washington D.C., USA). Pearson's correlation coefficient determined by Microsoft Office Excel 2003 (copyright 1985–2003 Microsoft Corporation). Cluster analysis was performed by KyPlot version 2.0 beta 15 (copyright 1997–2001 Koichi Yoshioka).

Culture of Bacteria and Evaluation of Drugs

Strain: Mycobacterium tuberculosis var. bovis bacillus Calmette-Guerin (BCG) wild type carrying vector plasmid (BCG18) and BCG carrying the same vector expressing a codon-optimized click beetle red gene (CBR) (BCG47-CBR) were used. Both bacterial strains were grown to an optical density (OD) ~ 1.0. Bacteria were then diluted to OD = 0.5 in media for survival assays.

Media: Both BCG18 and BCG47-CBR were grown in Middlebrook 7H9 supplemented with albumin dextrose complex (M-ADC) (Difco), 0.05% Tween 80 (M-ADC-Tw) and hygromycin B at a final concentration of 80 µg/ml to select for plasmid maintenance in the strains.

Treatment with Compounds: All compounds were dissolved to a final concentration of 5mg/ml. Compounds A, B and E were dissolved in sterile water; compound C was dissolved in 15% ethanol; compound D was dissolved in 75% ethanol. Isoniazid (Sigma) was prepared in sterile water to a concentration of 625 µg/ml. Both isoniazid and compounds were sterilized by passage through 0.22 µm-syringe filters.

Survival by Optical Density: Four clear 96-well flat bottom plates were filled with 108µl per well of M-ADC-Tw media supplemented with 80 µg/ml hygromycin B. Each tested compound was added to duplicate wells of 72 µl per well at a final concentration of 2 mg/ml. Similar amount of isoniazid was added to the first two wells at a concentration of 250µg/ml. Two-fold serial dilutions were carried out six times for all compounds and isoniazid. The last row of wells was maintained without any antibiotic. 10 µl per well of BCG18 and BCG47-CBR was added to two 96-well plates per strain to give a final volume of 100 µl per well. Plates were incubated at 37°C for 7 days and 14 days. Bacteria survival was measured at 620 nm using a Mithras (Berthold) plate reader at day 0, 7 and 14 in the presence of compounds.

Survival by Luminescence: Two sets of eight solid white 96-well flat bottom plates were prepared as described above. One set consisted of BCG18 and the other of BCG47-CBR. Plates were incubated at 37°C for 2, 7 and 14 days. Luminescence measurements were taken for day 0, 2, 7, and 14 in the presence of compounds. Bacterial luminescence was measured 5 minutes after injection of 10µl of 5 mM D-luciferin in 0.45M sodium citrate buffer pH 5.0 (Gold Biotechnology) using a Mithras plate reader. Photon collection time was one second per well.

Synthesis of Compounds

Prior to use the hydrazine (NH_2NH_2) must be distilled over CaO and NaOH. The anhydrous NH_2NH_2 is collected at 113°C and is stored sealed at -20°C . Hydrazide derivatization: All compounds were treated similarly. Place 0.000727 moles of carboxylic acid compound into glass vessel, then add 0.035 to 0.060 mL of SOCl_2 and microwave for 2 to 4 minutes. Add Na_2CO_3 solid at mole ratio that is equal to that of SOCl_2 . Microwave Irradiation Synthesis of Compounds: All treated similarly. Place 150 mg of compound into pyrex open test tube with 50 μl of SOCl_2 . Microwave 3 to 5 minutes, then cool. Place about 20 mg of Na_2CO_3 into the mixture and mix. Add 50 μl of anhydrous NH_2NH_2 and microwave up to 1 minute. The NaCl formed can be removed by dissolving the preparation in minimal water and extracting with ethyl acetate or acetonitrile, which is pooled, dried over anhydrous magnesium sulfate then evaporated to obtain the final product residue. The presence of the hydrazine group can be confirmed by FTIR, peaks at 944 cm^{-1} for hydrazine and 1000 cm^{-1} to 1200 cm^{-1} for C-N stretch (3000 cm^{-1} to 3500 cm^{-1} N-H stretch).

Results and Discussion

The primary use of *Mycobacterium bovis* BCG (Bacille Calmette-Guerin) is as a vaccine against tuberculosis. When utilized for this purpose the bacillus is alive but in a weakened condition (16). This variant of *Mycobacterium* has been observed to provide some protective effect against leprosy ($> 20\%$) (17). The administration of BCG to immunocompromised individuals can produce serious infection. BCG is utilized successfully as a modulator for immunotherapy of superficial urothelial carcinoma of the bladder (18), that has provided outcome of greater efficacy than routine chemotherapy (19). Unfortunately a potential side effect does include the occurrence of a life-threatening or fatal infection (19), such as in AIDS patients, in which isoniazid and streptomycin are applied for treatment. Tuberculosis remains a worldwide threat for humans and animals. The BCG vaccine is also used in veterinary applications such as vaccination of cattle (20) and for oral vaccination of some wildlife (21).

In cases where infection results after BCG therapy for bladder carcinoma the use of tuberculostatics for up to six months, such as isoniazid, provide remedial treatment (22). In some cases of intravesical instillation therapy with BCG some difficulties have been recognized such as bacterial resistance to pyrazinamide and cycloserine (23). In such cases the use of fluoroquinolones has been beneficial (23), however the threat of a bacterial resistant infection strongly supports the further study of new drug designs such as the compounds presented in this study. The recognition of risk to immunodeficient children for BCG vaccination further supports the need for additional novel drugs that are shown to be effective inhibitors of bacterial growth of the BCG variant and the well known highly dangerous pulmonary *Mycobacterium tuberculosis* (24), particularly since BCG vaccination of newborns is a standard practice in developing countries (25). Existence of effective and suitable tuberculostatics will increase the efficacy of application of BCG strains for clinical vaccination and chemotherapy (26).

Substituents covalently bonded to a supporting framework of a pharmaceutical can significantly affect the druglikeness favorably or negatively (27). A judicious choice of sub-

stituents can be useful for improving pharmacodynamics and pharmacokinetics of a drug. Some structure components are vital for medicinal activity whereas others are amenable to alteration. It is possible for a molecular structure to have potential for multiple medicinal activities. Compounds A, B, C, and D are presented in Figure 1 alongside isoniazid for comparison. All drugs have the vital substituent hydrazide ($-C(O)NHNH_2$), which is the active functional group for isoniazid. Drugs A, B, and C have a roving bromine atom ($-Br$) covalently bonded to an aromatic ring moving from ortho-, to meta-, and para-position, respectively. Drug D is highly unique as the parent compound is ciprofloxacin, which is a broad spectrum antibiotic. To obtain drug D the former carboxyl group ($-C(O)OH$) of ciprofloxacin is converted to the hydrazide group ($-C(O)NHNH_2$). Previous studies have shown that metabolism of isoniazid involves conversion to acetylisoniazid, isonicotinic

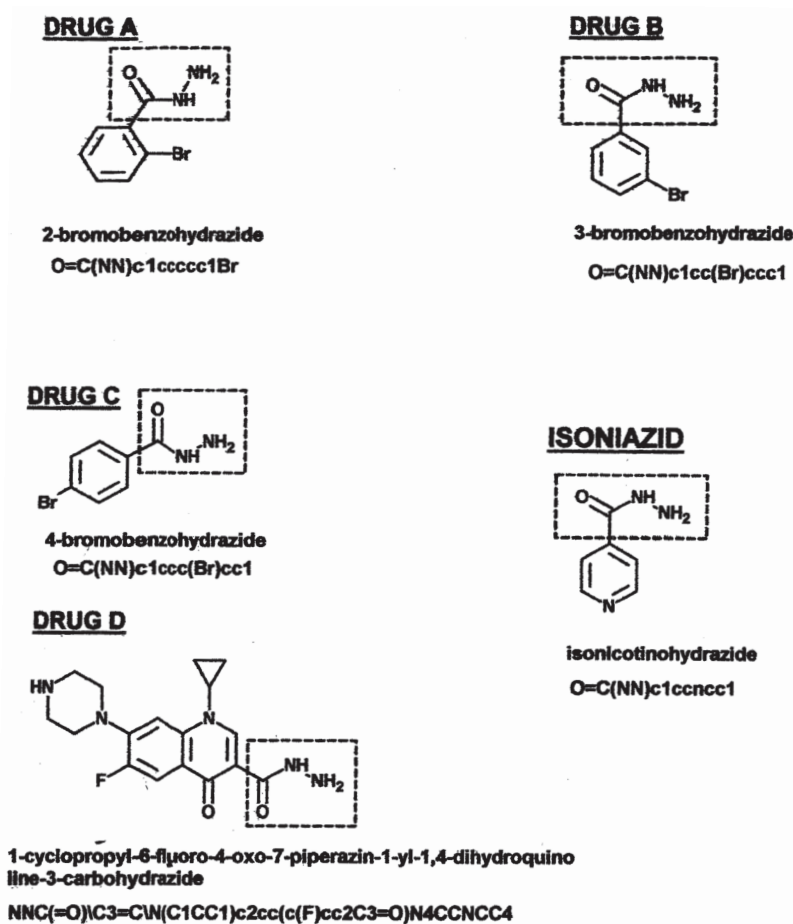


FIGURE 1. The molecular structures of novel drugs A, B, C, and D have each a hydrazide functional group as does isoniazid (see inset box). Drugs A, B, and C have a bromine atom at the ortho, meta, and para position to the hydrazide group, respectively. Drug D is a ciprofloxacin derivative with the former carboxyl group replaced by the hydrazide functional group. The SMILES designation and name is given for each compound.

acid, isonicotinylglycine, monoacetylhydrazine, and diacetylhydrazine, followed by excretion in the urine (28). The primary path of isoniazid metabolism is acetylation (28).

Various important pharmaceutical properties are presented in Table I that significantly affect the druglikeness value of compounds. These include water solubility, 1-octanol/water partitioning (Log P), polar surface area (PSA), formula weight, molecular volume, and Violations of the Rule of 5. The Rule of 5 was developed to estimate absorption and permeation attributes of a compound to enhance selection of highly potential drug candidates among a large population. The Rule of 5 states that poor absorption or permeation attributes exist in a drug candidate when (27): 1) There are more than 5 hydrogen bond donors (considered to be $-OH$ and $-NH_n$); 2) The formula weight is over 500; 3) The Log P is over 5; and 4) There are more than 10 hydrogen bond acceptors. Notably all drugs A, B, C, D, and isoniazid have zero violations of the Rule of 5. This outcome indicates these compounds should have favorable bioavailability (i.e., Favorable absorption/permeation).

Values of Log P have been interpreted as a qualitative indicator of permeation of cell membrane by-layers, an action important for the medicinal activity of a drug. The tuberculostatics presented here have Log P values varying from -0.70 (isoniazid) to 1.26 (drug B and C) (see Table I). A Log P value of -0.70 for isoniazid indicates a more hydrophilic agent which is accompanied by a much higher determined water solubility of 16690 mg/liter than A, B, C, and D. The Log P values for A, B, C, and D are greater than 1.0 , indicating a greater lipophilic (more hydrophobic) attribute than isoniazid. Among this group of compounds, isoniazid has the smallest molecular volume and formula weight. Pearson r correlation determination reveals trends within the data set of Table I. Essentially Log P is highly inversely correlated with water solubility having correlation of -0.9638 , however it is moderately directly correlated with formula weight having $r = 0.6002$. Molecular volume is highly correlated to formula weight ($r = 0.9442$) and polar surface area ($r = 0.8859$).

Polar surface area characteristic has been used for prediction of intestinal absorption post oral administration (29) and efficacy of brain-blood barrier (BBB) penetration for drug targeting the central nervous system (CNS)(30). Here, the PSA values of 55.12 Angstroms² for A, B, and C purports an intestinal absorption of approximately 90% or

TABLE I. Molecular Properties

DRUG	LOG P	Polar Surface Area (A ²)	Formula Weight	Violations of Rule of 5	Molecular Volume (A ³)	Water Solubility Mg/Liter
A	1.08	55.12	215.05	0	144.60	1074
B	1.26	55.12	215.05	0	144.60	3069
C	1.26	55.12	215.05	0	144.60	2950
D	1.06	92.39	345.38	0	301.13	817.5
Isoniazid	-0.70	68.01	137.14	0	122.56	16690

A³ is Angstroms³

higher, which is comparable to isoniazid. A qualitative estimate for drug D would be about > 50% intestinal absorption. All these values are favorable for clinical application.

In addition, the descriptor PSA is an indicator of potential central nervous system interpenetration. Previous studies of known CNS penetrating drugs show consistently that a PSA of less than 60 Angstroms² is a property that secures BBB penetration (30). Clearly then, drugs A, B, and C (PSA < 60 A²) would be useful for clinical treatment of extrapulmonary tuberculosis infection of the central nervous system. The outcome is a substantial affirmation of the potential efficacy of these novel tuberculostatics.

To ascertain the extent of growth inhibition of bacteria induced by A, B, C, and D, a comparable dosage administration *in vitro* was accomplished utilizing isoniazid. The outcome is presented in Figure 2, where percent survival is compared to concentration by a 2-way plot. Bacteria survival is below 20% at a concentration of isoniazid of about 31 micrograms/milliliter and greater. Isoniazid is widely used as a treatment for cases of *Mycobacterium tuberculosis*. Bacterial culture evaluation of drugs A and B were accomplished similarly to that of isoniazid with results presented in Figure 3. As with isoniazid tremendous reduction in bacterial survival was accomplished at very low concentrations of A and B. Less than 50% of bacterial survival is realized at a concentration of only 62.5 micrograms/milliliter for drug A and even 31.3 micrograms/milliliter for drug B. This profound and substantial reduction in bacteria survival by these two tuberculostatics is an extremely strong attribute supporting clinical application for the treatment of tuberculosis.

Outcome for similar *in vitro* evaluation of drugs C and D produced striking results presented in Figure 4. Again, there is tremendous reduction in bacterial survival at very low concentrations. At 62.5 micrograms/milliliter, drug C reduces bacterial survival to less than

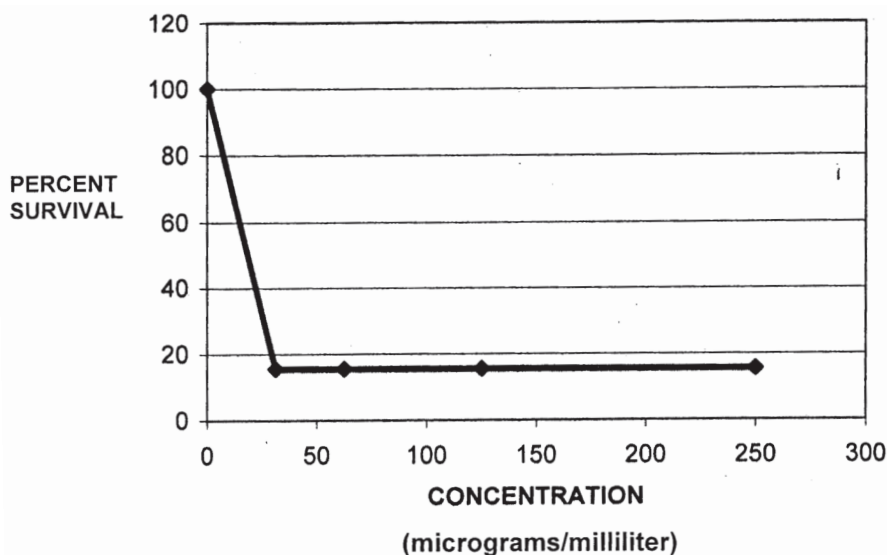


FIGURE 2. Growth inhibition of *M. bovis* BCG induced by isoniazid. The extent of bacterial growth drops precipitously at 25 micrograms/milliliter. The level of bacteria remains minimal at all concentrations above 25 micrograms/milliliter.

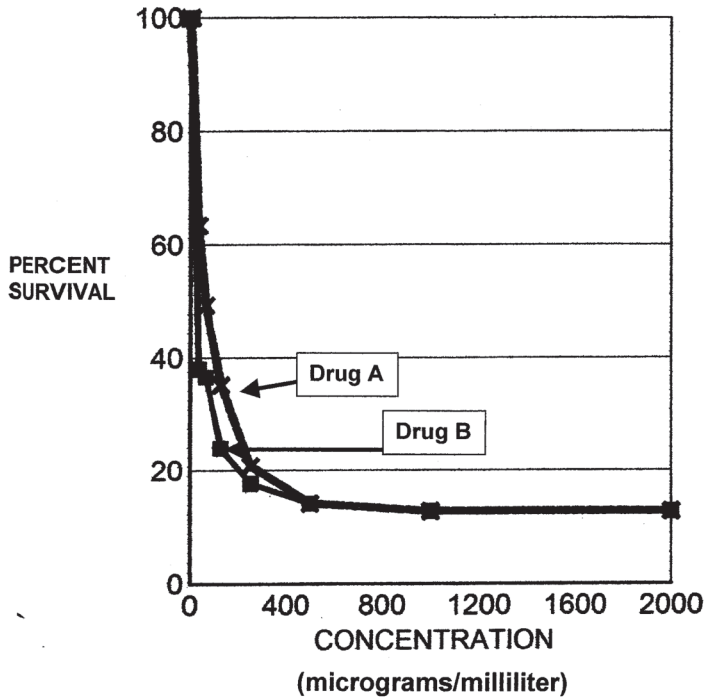


FIGURE 3. For drugs A and B the *M. bovis* BCG growth proliferation drops below 50% at a concentration of 62.5 micrograms/milliliter. Bacteria survival drops to 20% and below at concentrations of 250 micrograms/milliliter and greater.

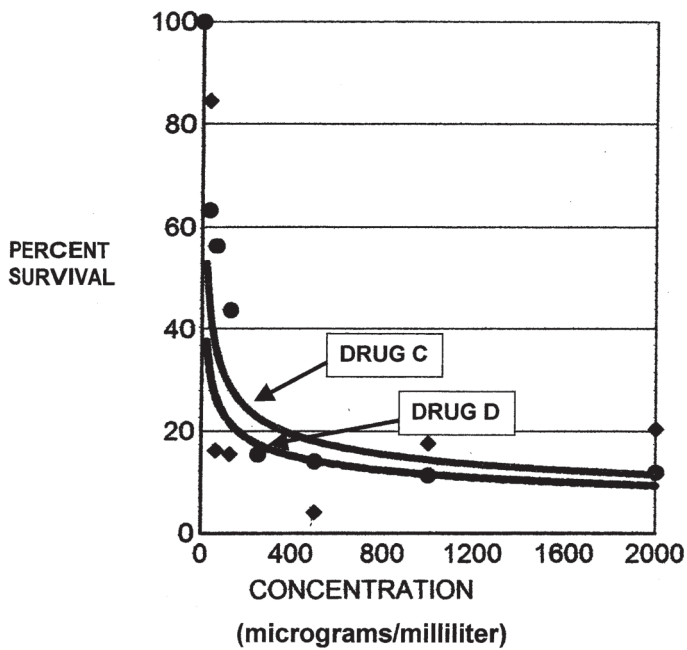


FIGURE 4. For drugs C and D the *M. bovis* BCG growth proliferation drops below 50% at a concentration of 125 micrograms/milliliter. The strongest inhibition is induced by drug D having greater than 80% inhibition at concentrations of 62.5 micrograms/milliliter and greater.

60%, whereas at this same concentration drug D reduces bacteria survival to less than 20%. This striking and profound bacterial inhibition is highly important and supportive of clinical efficaciousness of these tuberculostatics. Clearly the use of ciprofloxacin as a carrier agent for the hydrazide functional group is well chosen and well delivered. The MIC₅₀ concentration for A, B, C, and D are 63 micrograms/milliliter, 24 micrograms/milliliter, 75 micrograms/milliliter, and 46 micrograms/milliliter, respectively.

Cluster analysis is efficient and effective for discerning underlying relationships and interaction among descriptors within a multivariate data set such as Table I. This is a type of pattern recognition analysis that is very effective in finding hierarchical groupings in multivariate data sets. The hierarchical clustering routine produces a 'dendrogram' showing how subjects (drugs in this study) can be clustered based on similarity of molecular properties. A 2-way plot or dendrogram is presented in Figure 5, depicting the association of drugs A, B, C, D, and isoniazid to each other based on molecular properties. In this analysis single linkage or nearest neighbor clustering conditions were applied where clusters are joined based on the smallest distance between the two groups (31, 32). The Euclidean distance (shortest distance between two points) is a robust and widely applicable measure of distance. Interestingly, isoniazid is determined to be distinct (dissimilar) from all new designs A, B, C, D, and is placed into a cluster unique to itself. However, drugs A, B, C, and D are joined at super node 1 (see dendrogram), but separated into two sub-nodes 2 and 3. Sub-node 2 defines a cluster having drugs A and B, while sub-node 3 defines a cluster having C and D. Essentially drugs A and B are determined to have the highest similarity to each other. Likewise drugs C and D are most similar in this population. Isoniazid is determined to be dissimilar to A, B, C, and D. This outcome suggests that some differentiation in pharmaceutical activity may be anticipated and is actually observed in action with the *in vitro* antibacterial determination.

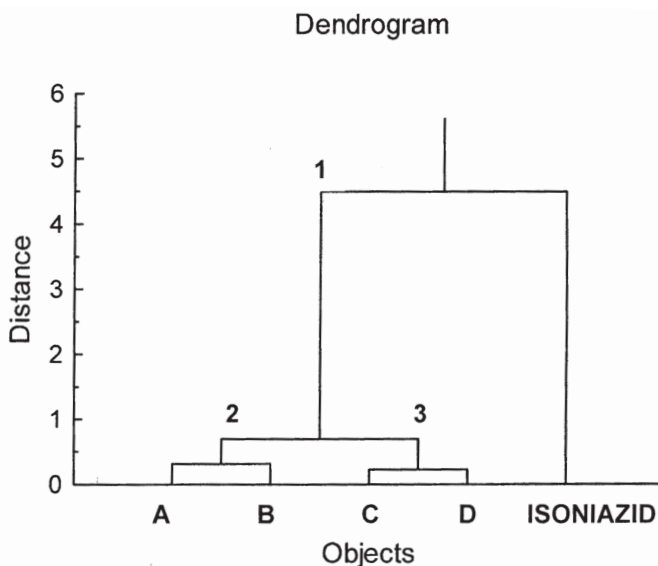


FIGURE 5. Cluster analysis of the multivariate data matrix of Table I shows that isoniazid is distinct from drugs A, B, C, and D. Drugs A and B are most similar. Drugs C and D are most similar to each other. Parameters for cluster analysis is standard Euclidean distance and single linkage clustering.

Conclusion

In summation, four novel drug designs were synthesized utilizing microwave irradiation synthesis techniques. Four new drug designs were produced that contained a hydrazide group replacing a carboxyl group of the initial parent compound. Drug D is a derivative of a broad spectrum antibiotic ciprofloxacin. Drugs A, B, and C have a PSA value of 55.12 Angstroms², indicating they would penetrate the BBB and target tuberculosis infections of the central nervous system. All drugs showed zero violations of the Rule of 5, which indicates these tuberculostatics would have favorable bioavailability (absorption and permeation). All drugs substantially inhibited growth of bacteria at concentrations of 31 micrograms/milliliter and higher. Bacterial inhibition was profound. Cluster analysis determined that isoniazid is distinct from drugs A, B, C, and D based on molecular properties. The drugs A, B, C, and D strongly inhibit growth of bacteria and possess molecular properties appropriate and advantageous for the clinical treatment of pulmonary and extrapulmonary tuberculosis.

This work was supported by the College of Arts & Sciences, Department of Chemistry, Durham Science Center, University of Nebraska.

References

1. Ryan, K.J., Ray, C.G. (2004) *Sherris Medical Microbiology* (4th edition). McGraw Hill.
2. Parish, T., Brown, A. (2009) *Mycobacterium: Genomics and Molecular Biology*. Caister Academic Press.
3. McMurray, D.N. (1996) *Mycobacteria and Nocardia, Baron's Medical Microbiology* (4th ed.). University of Texas Medical Branch.
4. O'Reilly, L.M., Daborn, C.J. (1995) *Tuber. Lung Dis.* 76(Suppl 1): 1–46.
5. Reider, H.L., Snider, D.E. Jr, Cauthen, G.M. (1990) *Am. Rev. Respir. Dis.* 141: 347–351.
6. Shafer, R.W., Kim, D.S., Weiss, J.P., Quale, J.M. (1991) *Medicine* (Baltimore) 70: 384–397.
7. van Maaren, P.J. (2010) *Kekkaku* 85(1): 9–16.
8. Grobuwch, M.P. (2010) *Curr. Opin. Pulm. Med.* 16(3): 180–185.
9. Migliori, G.B., Centis, R., Lange, C., Richardson, M.D., Sotgiu, G. (2010) *Curr. Opin. Pulm. Med.* 16(3): 171–179.
10. Zager, E.M., McNerney, R. (2008) *BMC Infect. Dis.* 8: 1–10.
11. Shigetoh, E., Murakami, I., Yokosaki, Y., Kurimoto, N. (2000) *Kekkaku* 76(12): 723–728.
12. Alcaide, F. (2008) *Santin M. Enferm. Infec. Microbiol. Clin. Suppl.* 13: 54–60.
13. Jassal, M., Bishai, W.R. (2009) *Lancet* 9(1): 19–30.
14. Jain, A., Mondal, R. (2008) *FEMS Immunol. Med. Microbiol.* 53(2): 145–150.
15. Velayati, A.A., Masjedi, M.R., Famia, P., Tabarsi, P., Ghanavi, J., Ziazarif, A.H., Hoffner, S.E. (2009) *Chest* 136(2): 420–425.
16. Comstock, G.W., Palmer, C.E. (1966) *Am. Rev. Resp. Dis.* 93(2): 171–183.
17. Setia, M.S., Steinmaus, C., Ho, C.S., Rutherford, G.W. (2006) *Lancet Infect. Dis.* 6(3): 162–170.
18. Kresowik, T.P., Griffith, T.S. (2009) *Immunotherapy* 1(2): 281–288.
19. Lamm, D.L., van der Meijden, P.M., Morales, A., Brosman, S.A., Catalona, W.J., Herr, H.W., Soloway, M.S., Steg, A., Debruyne, F.M. J. (1992) *Urol.* 147(3): 596–600.
20. Buddle, B.M., Parlane, N.A., Keen, D.L., Aldwell, F.E., Pollock, J.M., Lightbody, K., Andersen, P. (1999) *Clinical and Diagnostic Laboratory Immunology* 6(1): 1–5.

21. Cross, M.L., Lambeth, M.R., Aldwell. (2009) *Clinical and Vaccine Immunology* 16(9): 1378–1380.
22. Medicentrum, B., Ziekengasthuis, G. (1995) *Eur. Urol.* 27(Suppl 1): 23–28.
23. Durek, C., Rusch-Gerdes, S., Jocham, D., Bohle, A. (2000) *Eur. Urol.* 37(Suppl 1): 21–25.
24. Hesseiling, A.C., Rabie, H., Marais, B.J., Manders, M., Lips, M., Schaaf, H.S., Gie, R.P., Cotton, M.F., van Helden, P.D., Warren, R.M. (2006) *Clin. Infect. Dis.* 42(4): 548–558.
25. Monajemzadeh, M., Shahsiah, R., Zarei, A., Alamooti, A.A., Mahjoub, F., Mamishi, S., Khotai, g, Pazira, R., (2010) *Eram, N. Am. J. Clin. Pathol* 133(1): 102–106.
26. Shishido, Y., Mitarai, S., Otomo, K., Seki, M., Sato, A., Yano, I., Koyama, A., Hattori, T. (2007) *Int. J. Tuberc. Lung Dis.* 11(12): 1334–1338.
27. Lipinski, C.A., Lombardo, F., Dominy, B.W., Feeney, P.J. (1997) *Drug Delivery Reviews* 23: 3–25.
28. Ellard, G., Gammon, P. (1976) *Journal of Pharmacokinetics and Pharmacodynamics* 4(2): 83–113.
29. Palm, K., Stenberg, P., Luthman, K., Artursson, P. (1997) *Pharmaceutical Research* 14(5): 268–571.
30. Kelder, J., Grootenhuis, P.D.J., Bayada, D.M., Delbressine, L.P.C., Ploemen, J-P. (1999) *Pharmaceutical Research* 16(10): 1514–1519.
31. Harper, D.A.T. (1999) *Numerical Palaeobiology*. John Wiley & Sons.
32. Theodoridis, S., Koutroumbas, K. (2009) *Pattern Recognition*, (4th Edition). Academic Press.

Received March 28, 2010;

accepted June 7, 2010.

SHORT NOTE

Artifacts of Electron Microscopy in Cells

Harold Hillman

*Unity Laboratory of Applied Neurobiology, 76, Epsom Road, Guildford, Surrey, GU1 2BX, U.K.
Email: Harold.hillman@btinternet.com*

Abstract: With the exception of the Golgi apparatus, the main artifacts were first seen by electron microscopy. Those detected over the last 30 years, and the reasons for which they are artifacts, are summarised.

THE FOLLOWING structures are postulated, but rarely seen in light or electron micrographs of intact tissues (Table 1). Authors who have seen them are invited to send in micrographs or references (but not diagrams) showing them.

TABLE 1

Membrane receptors	Cisternae
Transmembrane molecules	Molecular motors
Membrane carriers	Presynaptic connections to dendrites
Uniporters, symporters and antiporters	T-tubules in muscles
Membranes around muscle fibres	Ion channels*
Microsomes	Membranes around astrocytes and oligodendrocytes
Liposomes	

Many of these have been isolated and sequenced, and their dimensions are within the resolution of the electron microscope, but they are not seen in micrographs. Ion channels*, the Na⁺ channel is the only one in the literature (Unwin and Zampighi, 1980).

The *images* of the following 'unit' membranes only appear in two dimensions, although the membranes exist. They must have arisen after the sections have been cut (Table 2).

TABLE 2

Cell membranes	} 'unit'	Tight junctions
Nuclear membranes		Gap junctions
Mitochondrial membranes		Intermediate junctions
Endoplasmic reticulum		Nuclear pores
Cytoskeleton		Mitochondrial cristae
Cisternae		Thick and thin muscle filaments
Myelin lamellae		Pre- and post-synaptic thickenings

The two-dimensionality has not previously been noted (Hillman and Sartory, 1980; Hillman, 2008).

Intracellular movements of particles occur in living cells. They include: Brownian movement, streaming, diffusion, convection, nuclear rotation, meiosis, mitosis, phagocytosis, pinocytosis and fertilisation. They are not compatible with the existence in life of the following apparent structures (Table 3). (Hillman and Sartory, 1980).

With this exception of the Golgi apparatus, all the above structures were first seen by electron microscopy (Porter, Claude and Fullham, 1945; Sjöstrand, 1953; Robertson, 1959), inter alia. Necessarily, these observations were made on the deposits of heavy metals on dead cells. It would seem desirable to prefer observations made in living unicellular organisms, tissue cultures and plant cells to those made on metal deposits on dead cells. The detailed evidence for the belief that these structures are artifacts has been published (Hillman and Sartory, 1977; 1980; Hillman, 1986; 2008). Only two publications have taken issue with our conclusions (Horne and Harris, 1981; Michell, Finean and Coleman, 1982), and we were allowed only a short letter to reply (Hillman, 1982). We are still willing to enter interdialogue on these questions.

TABLE 3

Endoplasmic reticulum	Lysosomes
Cytoskeleton	Sartoplasmic reticulum
Cisternae	Peroxisomes
Contractile systems	Microtrabeculae
Golgi apparatus	'Stress fibres'

This problems has not been addressed in the literature, although it has been suggested in personal communications, that the above structures dissolve or move out of the way when the particles approach them (Hillman, 2008).

References

- Hillman, H. (1982) Cell structure. Some questions not answered by the electron microscopists. *School Science Rev.*, 224, 173–177.
- Hillman, H. (1986) *The Cellular Structure of the Mammalian Nervous System*, M.T.P. Press, Lancaster, p. 127.
- Hillman, H. (2008) *Evidence-based Cell Biology with Some Implications for Clinical Research*. Shaker, Maastricht, pps. 262–263.
- Hillman, H. and Sartory, P. (1977) The unit membrane, the endoplasmic reticulum and the nuclear pores are artifacts. *Perception*, 6, 677–678.
- Hillman, H. and Sartory, P. (1980) *The Living Cell*. Packard Publishing, Chichester, pages 44–60.
- Horne, R.W. and Harris, J.R. (1981) The electron microscope in biology. *School Science Rev.*, 63, 434–441.
- Michell, R.H., Finean, J.B. and Coleman, R. (1982) Widely accepted modern views of cell structure are correct. *School Science Rev.*, 63, 434–441.
- Porter, K.R., Claude, A. and Fullam, E.F. (1945) A study of tissue cells by electron microscopy. *J. exp. Med.*, 81, 233–246.
- Robertson, J.D. (1959) The ultrastructure of the cell membrane and their derivatives. *Biochem. Soc. Symp.*, 16, 3–43.
- Sjöstrand, F.S. (1953) Systems of double membranes in cytoplasm of certain tissue cells. *Nature*, 17, 31–32.
- Unwin, P.N.T. and Zampighi, G. (1980) Structure of the junction between communicating cells. *Nature*, 283, 545–549.

*Received February 6, 2010;
accepted February 20, 2010.*

INDEX

- Abderhalden, Emil, 22
discoverer of low Na^+ in human rbc, 22
- Active living state, 34
- AI Cascade Mechanism (formerly indirect F-effect), 34
as fundamental mechanism of long-distance information and energy transfer in and among nano-protoplasmic units, 34
- Aizenberg, E.I., 24
- Amson, K., 23
- Arrhenius, S., 36
- Association-Induction (AI) Hypothesis, 31
AI Cascade Mechanism, 34
as heir to protoplasmic theory of Dujardin, von Mohl, 31
as only confirmed unifying theory of life, 31, 36
ATP as principal EWC, 34–35
the dead state, 34–35
the living state
resting living state, 34–35
active living state, 34–35
Nano-protoplasm, 32
successful interpretation of 4 classical cell physiological manifestations, 36–42
- Atomic sieve theory of cell membrane and models
by Traube, 23
by Boyle and Conway, 23
- BARTZATT, R., 49
- Basil vein of Rosenthal, 15
- Baur, E., 28
- Bernstein, Julius, 22
theory of membrane potential, 22
- Boltzmann, L., 31
inventor of statistical mechanics, 31
- Boltzmann distribution law, 31
in Ling's fixed charge hypothesis, 31
- Boyle, P. J., 23
- Carboxyl (e.g., β -, γ -) groups, 34, 35, 37–39, 42
- Cell artifacts in electron microscopy, 61
- Cellular electric potentials, 22
as adsorption potential by Baur, 28
as arrested diffusion potential by Bernstein, 22
as close-contact, one-on-one adsorption potential on surface β -, γ -carboxyl groups by Ling, 39–41
as membrane potential by Bernstein, 22–23
as phase-boundary potential by Nernst, 28
improved methods of measuring, 23
- Cell swelling and shrinkage, 41
- Cell water
POM, PM theory of, 31
- Cerebrospinal fluid (CSF)
antigenic proteins in CSF, 14
Dawson's fingers, 14
leakage into ventricles, 14–16
role of recumbent sleep, 11
- Cerebrospinal fluid (CSF) dynamics
cinematography, 2
flow obstruction, 10
inflow velocity, 3, 10
sharply reduced in upright position, 10, 11
imaging of, by upright MRI, 2
outflow velocity, 10
peak CSF velocity, 3, 10
posture dependency, 3, 10
quantitative flow measurements, 3–10
- Cerebrospinal fluid (CSF) flow imaging by MRI
in multiple sclerosis, 3, 13

- Cervical spine pathology
 anatomical abnormalities, 11, 12
 posture dependency, 11, 13
 visualized by Upright MRI, 13
- CG electrode
 close model of muscle cells, 39–40
- CHU, D. 1
- CIRILLO, J., 49
- CIRILLO, S.L.G., 49
- Close-contact, one-on-one adsorption
 vital to life and life activities, 36
 on β -, γ -carboxyl groups and backbone
 NHCO groups, 34
- Collodion membrane, 29
- Conway, E. J., 23
- Cranio-cervical trauma, 1, 12
 athletes, 15
 in the genesis of multiple sclerosis, 1
 motor vehicle whiplash injury, 12, 15
 MR imaging of, 3
- c-, and c' value, 35
- c-value and c' value analogue, 35
- DAMADIAN, R., 1
- Dead state, 34
- Debye, P., 36
- Deplasmolysis, 21
- deVries, H., 21
 osmotic method, 22
- Dissociation of ions, 35
 theory of, by van't Hoff, Arrhenius, Debye,
 35–36
- Donnan, Frederick G., 20
 early personal history, 20
- Donnan ratio (r), 20, 24, 25
 definition, 20
- Donnan's membrane theory
 fatal theoretical error, 26
 final experimental disproof, 24
 positive contribution, 30
 summary, 20
 theory of membrane equilibrium, 20
 early apparent supportive evidence, 21–24
- Drugs
 as cardinal adsorbents, 35
- Dujardin, Felix, 31
- Dutrochet, H., 21
- EDC, EIC, EWC, 35
- Electron-donating cardinal adsorbent (EDC),
 35
- Electron-indifferent cardinal adsorbent (EIC),
 35
- Electron-withdrawing cardinal adsorbent
 (EWC), 34, 42
- Electron microscopy
 artifacts of, in cells, 61
- Equilibrium distribution coefficient (q-, or ρ -
 value), 37
- Extracellular space in frog muscle, 24–25
 critical role of correct value, 25
- Fischer, M., 36
- Four classic cell physiological manifestations
 explanations in obsolete macroscopic
 membrane theory, 21–24
 explanations in up-to-date microscopic AI
 Hypothesis, 36–42
- Glass membrane, 28
- Glucose permeability, 38–39
- Guggenheim, E.A., 27
- HILLMAN, H., 61
- Höfler, K., 22, 25
- Horovitz, (aka Lark-Horovitz), K., 28
- Huxley, Thomas, 31
 protoplasm as physical basis of life, 32
- Hydrazide drugs
 effect on tuberculosis bacteria, 49
- Idealized NP system, 42
- Immunoreactive tau proteins, 15, 16
- Innovation, scientific, 19
- Ioniazid, as an inhibitor of tuberculosis
 bacterial growth, 49
- Ionic accumulation, 23, 36
 See selective ionic accumulation
- Intracranial pressure, 13–14
 possible role in multiple sclerosis, 15
 relationship with blood flow velocity, 15
 relationship with pressure gradient, 13
- K^+ , 25
 equilibrium distribution follows Troshin
 equation, 26
- Kamnev, I. Ye., 25
- KCl-induced swelling of muscle, 41
- Law of electric neutrality, 28
- Law of macroscopic electro-neutrality, 27
 fatal error by violating, 27
- LING, G.N., 19
- Ling's fixed charge hypothesis, 31
 enhanced counter-ion association due to site
 fixation, 36

- Living activity, 34–35
- Long-range attributes, 36
 identical in K^+ and Na^+ , 36
- Membrane equilibrium, 20
- Membrane models, 27–30
- Membrane permeability, 21
 glucose permeability, 38–39
 osmotic method assaying, 21–22
 to Na^+ , proved by radioactive tracer studies, 24
- Membrane potential theories (see also Donnan theory), 20
 refutation from in depth studies on four inanimate models (oil, glass, collodion, phospholipids), 28–30
- Membrane (pump) theory, 20
 Schwann as originator, 44
- Membrane theory, 20
 disproof of, 20
- Mg^{++} , 25
 equilibrium distribution follows Troshin equation, 26
- Michaelis, L., 29
 in theory of electrically charged membrane pores, 29
- Moore, B., 36
- Multiple sclerosis
 correlation with cranio-cervical trauma, 32
 origin, new understanding of, 13
 peri-ventricular distribution, 1
 plaque lesions, 1, 13
- Myelogenesis, 16
- Myobacterium bovi
 inhibition of growth by hydrazides, 49
- Na^+
 See Sodium ion
- $NaCl$ induced swelling of injured tissue, 42
- Nano-protoplasm, 32
 as microscopic protoplasm, 32
 two alternative states, folded and fully-extended, 34
 rbc cytoplasmic nano-protoplasm, 32–33
 molecular formula for, 33
 size of nano-protoplasmic unit, 33
 relation to “protoplasm” of Dujardin, von Mohl, Schultze, Huxley renamed
 macroscopic protoplasm, 32
- Nasonov, D.M., 24
- Nernst, W.H., 28
 original author of phase-boundary electric potential, 28
- Netter, H., 23
- Oil membrane, 28
- Osmotic method, 22
 disproof by Nasonov-Aizenberg-Kamnev, 34–35
 plasmolysis and deplasmolysis in, 21
- Osmometer, perfect
 definition, 22
 living cell as, 22
- Ostwald, Wilhelm, 21
 role in introduction of membrane potential, 21, 22
- Oxidized collodion-coated glass electrode (CG) electrode, 40
- PCG electrode, 40
- Phlogiston, 30
- Phospholipid membrane, 29
- Physical basis of life, 32, 36
- Plasmolysis, 21
- Polarized (oriented) multilayer (POM, PM)
 theory of cell water, 31
- Poly-lysine treated, collodion -coated glass electrode (PCG), 40
- Principle of enhanced association due to site fixation, 36
- Protoplasmic doctrine, 31
- Protoplasm of Dujardin, von Mohl, Schultze and Huxley
 as a specific macroscopic protoplasm (which is), 32
 an aggregate of similar microscopic nano-protoplasm, 32
- q-value (true equilibrium distribution coefficient), 37
- Radioactive tracer
 providing unique tool to assay permeability, 24
- Red blood cells (rbc), human, 22, 32
 Na^+ concentration in, 32
- Resting living state, 34
- Resting (injury) potential, 22
- ρ -value (apparent equilibrium distribution coefficient), 37
- Roaf, H.E., 36
- Schultze, M., 31
- Schwann, T., 44

- Selective ionic accumulation, 23
 K⁺ over Na⁺, 35, 37
 independence of K⁺ and Mg⁺⁺ distribution, 25
 in early protoplasmic theories by Fischer, Moore, Roaf, Troshin, 36
 in Ling's AI hypothesis (see also nano-protoplasm), 36
 in membrane theory of Donnan, 23–24
 in (sieve) membrane theory of Boyle and Conway, 23
- Semipermeable membrane, 20
- Semipermeability, 21
 accepted later definition, 21
 as an obsolete macroscopic concept, 30–31
 original definition by van't Hoff, 21
- Short-range attribute, 36
- Size rule, 37
- Sodium ion (Na⁺)
 exclusion, 37–38
 in rbc, 32
- Sodium pump hypothesis, 41, 43–44
- Sollner, C., 29
- Stahl, G., 30, 43
 failed phlogiston theory, 30
- Straight sinus, 15
- Swelling and shrinkage of living cells, 22
 explanation by membrane theory, 22
 explanation by AI Hypothesis, 41–42
- Teaching truth
 foundation for continued innovation, 43
- Treatment of multiple sclerosis
 non-invasive, 13
 relapse after treatment, 14–15
 stenting of cervica, 15
- Troshin, A.S., 36
- Troshin equation (from his Sorption Theory), 26, 36
- Tuberculosis bacteria
 effect of hydrazide drugs on growth of, 49
- Upright MR imaging, 1
 of multiple sclerosis patients, 1
- van't Hoff, J., 21
- von Helmholtz, L., 22, 28
- von Mohl, H., 31
- Water in nano-protoplasm, 33
 bulk-phase, *ad infinitum* polarization-orientation, 42
 bulk-phase, dissociated in active living and dead state, 34–35
 bulk-phase, polarized-oriented in resting living state, 34–35